

# **The Potential Therapeutic Effect of Manipulating the Extracellular Matrix in Idiopathic Pulmonary Fibrosis**

*Christopher John Philp BSc.*

Thesis Submitted to the University of Nottingham for the Degree of  
Doctor of Philosophy

May 2016



The University of  
**Nottingham**

UNITED KINGDOM • CHINA • MALAYSIA

***For Mum & Dad,***

## Abstract

**Background:** Idiopathic Pulmonary Fibrosis (IPF) is a physiologically devastating disease. The debilitating nature and high mortality rates make this one of the most lethal conditions, usually associated with median time to mortality of around 3 years. Increased deposition of extracellular matrix (ECM) and fibroblast accumulation are hallmarks of idiopathic pulmonary fibrosis (IPF). We hypothesise that the ECM in IPF is structurally abnormal by virtue of aberrant cross linking and promotes fibroblast accumulation. This study examined the structure and biological activity of IPF derived ECM and how this related to the expression of ECM cross linking enzymes as well as how inhibiting Transglutaminase 2 affects active fibrosis in the murine Bleomycin model.

**Methods:** Primary fibroblasts from 3 patients with IPF and 3 controls were isolated from biopsy samples and characterised by immunocytochemistry. ECM from these cells was deposited onto tissue culture plastic, cells removed using ammonium hydroxide and confirmed by electron microscopy (SEM). IPF and control cells were then grown on their own ECM or ECM derived from other cells. ECM was labelled with <sup>3</sup>H-proline and digested with recombinant proteases and tritium liberation counted by scintillation as a measure of collagen proteolysis. A pilot study was carried out where C57BL/5J mice received a single intratracheal instillation of Bleomycin (2mg/kg) and administered cystamine dihydrochloride by intraperitoneal injection (IP), once a day for ten consecutive days at 40mg/kg or 100mg/kg, at 3 different time points.

**Results:** IPF derived fibroblasts had more distinct organisation of fibrous matrix filaments on the cell surface and between adjacent cells by SEM. Both control and IPF lung fibroblasts expressed transcripts for lysyl oxidase (*LOX*), *LOXL1*, *LOXL2*, *LOXL3*, *LOXL4* and transglutaminase (TG) 2. IPF derived matrix increased expression of *LOXL3* and *TG2* transcripts, *LOXL3* protein and TGase activity. Other cross linking enzymes were unchanged.

To assess if IPF matrix affected fibroblast accumulation, I measured fibroblast adhesion, proliferation by MTT and EDU assays, and apoptosis

by cleaved caspase 3, cleaved PARP and TUNEL assay on the different matrices. IPF matrix enhanced proliferation over control matrix in response to PDGF-BB. To determine if this pro-proliferative effect was dependent upon aberrant cross-linking we generated ECM from normal and IPF fibroblasts treated with cystamine dihydrochloride (TG2 inhibitor) or  $\beta$ -amino-proprionitrile (LOX family inhibitor). The enhanced fibroblast proliferation seen on IPF matrix was reduced close to levels of normal matrix by each cross link inhibitor. There was no effect on apoptosis induced by either FAS ligand or staurosporine when cells were seeded onto IPF or control matrix suggesting IPF ECM does not protect seeded fibroblasts from apoptosis.

Bleomycin showed a trend towards increasing total lung hydroxyproline at day 24, 34 and 44 post administration however this was not statistically significant. Administration of cystamine at 40mg/kg/day showed no effect on total lung hydroxyproline. At day 34 post Bleomycin, cystamine administration showed a trend towards decreasing total lung hydroxyproline however again this was not statistically significant.

**Conclusions:** The data supports the hypothesis that IPF derived matrix is structurally and functionally different from normal matrix. This results in enhanced fibroblast proliferation, adhesion and increased cross linking activity by effects on gene transcription. Inhibition of matrix cross-linking reduced this enhanced fibroblast adhesion and proliferation. Administration of cystamine dihydrochloride via IP injection for ten consecutive days at 100mg/kg/day in the Bleomycin model showed a trend towards decreasing total lung hydroxyproline.

## **Acknowledgements**

My greatest thank you goes to my supervisors Prof. Simon Johnson and Dr. Gisli Jenkins who have guided me throughout this entire project. All the feedback and guidance has been invaluable, and most appreciated.

I'd also like to thank Dr. Ivonne Siebeke, Dr. Alison John, Dr. Amanda Tatler and Mr. Anthony Habgood for their technical expertise, training and guidance in running the animal work contained in this thesis. Furthermore I'd like to thank all the staff of the Bio Support Unit for their time and assistance.

Thank you Dr. Debbie Clements for training me in the laboratory; and the entire research group for your support, time and patience. My gratitude also to Dr. Christine Grainger-Boulton for imaging the Scanning Electron Microscopy samples and the Advanced Microscopy Unit for training me to process the samples.

Finally to my family; Thank you mum for always believing in me, and helping me through the times when it got difficult. And to Liza; for putting up with me throughout my PhD, I know it hasn't been easy but you've always supported me through the good times, and the bad. You both have my sincere gratitude. Si & Evie also, for reminding me that no matter what, there is always a silver lining.

# Table of Contents

<b>ABSTRACT .....</b>	<b>III</b>
<b>ACKNOWLEDGEMENTS .....</b>	<b>V</b>
<b>LIST OF FIGURES .....</b>	<b>XI</b>
<b>1 CHAPTER 1: THE ROLE OF THE EXTRACELLULAR MATRIX IN THE HEALTHY LUNG AND IDIOPATHIC PULMONARY FIBROSIS .....</b>	<b>2</b>
1.1 THE HUMAN RESPIRATORY SYSTEM.....	2
1.2 IDIOPATHIC PULMONARY FIBROSIS.....	3
1.2.1 <i>Introduction</i> .....	3
1.2.2 <i>Epidemiology</i> .....	5
1.2.3 <i>Current Theories on Pathogenesis</i> .....	8
1.2.4 <i>Current Therapies</i> .....	14
1.2.5 <i>In vivo models of IPF</i> .....	16
1.3 COMPOSITION OF THE EXTRACELLULAR MATRIX.....	21
1.3.1 <i>Extracellular Matrix Constituents</i> .....	21
1.4 EXTRACELLULAR MATRIX TURNOVER .....	27
1.4.1 <i>Deposition of Type I Collagen in the ECM</i> .....	29
1.4.2 <i>Stabilisation</i> .....	32
1.4.3 <i>Tissue Transglutaminases</i> .....	36
1.4.4 <i>The Lysyl Oxidase Family</i> .....	41
1.5 SUMMARY.....	44
1.6 HYPOTHESES.....	45
1.7 AIMS.....	45
.....	<b>47</b>
<b>2 CHAPTER 2: MATERIALS AND METHODS .....</b>	<b>48</b>
2.1 REAGENTS AND PLASTICWARE .....	48

2.2	ANTIBODIES.....	48
2.3	RECOMBINANT PROTEINS.....	50
2.4	DRUG COMPOUNDS.....	50
2.5	CELL CULTURE REAGENTS.....	51
2.6	PRIMARY CELLS & CELL LINES.....	52
2.7	Human TISSUE SECTIONS .....	53
2.8	PATIENT COHORT SERUM SAMPLES.....	53
2.9	MAMMALIAN CELL CULTURE .....	53
2.10	TOTAL RNA EXTRACTION.....	54
2.11	CDNA SYNTHESIS .....	55
2.12	REAL TIME PCR .....	55
2.13	DATA ANALYSIS, STATISTICS AND GRAPHICAL SOFTWARE .....	56
2.13.1	<i>Power Calculations for Animal Work .....</i>	<i>56</i>
2.14	SENESCENCE ASSAY.....	57
2.15	EXTRACELLULAR MATRIX PREPARATION .....	57
2.16	RADIO-LABELLING OF ECM.....	58
2.17	ECM EXTRACTION .....	58
2.18	ECM PROTEOLYTIC DIGESTS.....	59
2.19	LIQUID SCINTILLATION COUNTING.....	60
2.20	BIO RAD TOTAL PROTEIN ASSAY.....	60
2.21	BCA TOTAL PROTEIN ASSAY .....	60
2.22	ACID HYDROLYSIS OF COLLAGEN.....	61
2.23	TOTAL COLLAGEN ASSAY .....	61
2.24	COLLAGEN SYNTHESIS ASSAY .....	62
2.25	SDS PAGE.....	62
2.26	WESTERN BLOTTING .....	62
2.27	ECL DETECTION .....	64
2.28	DENSITOMETRY .....	64

2.29	SILVER STAINING OF SDS-PAGE GELS .....	64
2.30	PROTEOME PROFILER .....	65
2.31	ELISAs.....	67
2.32	TRANSGLUTAMINASE ACTIVITY ASSAY .....	67
2.33	COLLAGEN COATING OF CELL CULTURE VESSELS .....	67
2.34	ADHESION ASSAY.....	68
2.35	MTT PROLIFERATION ASSAY.....	68
2.36	EDU PROLIFERATION ASSAY .....	69
2.37	TUNEL ASSAY FOR APOPTOSIS .....	69
2.38	IMMUNOFLUORESCENCE .....	70
2.39	IMMUNOHISTOCHEMISTRY.....	71
2.40	SCANNING ELECTRON MICROSCOPY .....	74
2.41	ETHICAL STATEMENT FOR ANIMAL USE .....	75
2.42	ANIMALS AND HUSBANDRY .....	75
2.43	<i>Ex Vivo</i> TG2 ACTIVITY IN BLEOMYCIN INJURED TISSUE.....	76
2.44	BLEOMYCIN MODEL OF FIBROSIS .....	77
2.45	MURINE EXPERIMENTAL PROCEDURES .....	77
2.46	TERMINAL ANAESTHESIA .....	82
2.47	PLASMA PREPARATION FROM WHOLE BLOOD .....	83
2.48	LUNG PROCESSING.....	83
2.49	PROTEIN EXTRACTION FROM MOUSE LUNG .....	84
2.50	HYDROXYPROLINE ASSAY.....	84
<b>3</b>	<b>CHAPTER 3: CHARACTERISATION OF PRIMARY HUMAN LUNG FIBROBLASTS.....</b>	<b>87</b>
3.1	INTRODUCTION .....	87
3.1.1	<i>Background.....</i>	<i>87</i>
3.1.2	<i>Aims &amp; Objectives.....</i>	<i>89</i>
3.2	RESULTS.....	90

3.2.1	<i>Senescence associated <math>\beta</math>-Galactosidase staining</i> .....	90
3.2.2	<i>Immunocytochemical detection of fibroblast markers</i> .....	91
3.2.3	<i>Real Time PCR analysis of ECM stabilising enzyme messenger RNA</i> .....	93
3.2.4	<i>Extracellular matrix cross linking enzyme expression in the IPF lung</i> .....	95
3.2.5	<i>ECM &amp; conditioned media collagen content of IPF fibroblasts</i> .....	99
3.2.6	<i>Cell proliferation of normal and IPF derived fibroblasts</i> .....	103
3.2.7	<i>Extracellular protease expression of primary fibroblasts</i> .....	104
3.2.8	<i>Scanning electron microscopy of primary IPF cultures &amp; biosynthesised matrix</i> .....	108
3.3	DISCUSSION .....	114
3.4	CONCLUSIONS .....	119
<b>4</b>	<b>CHAPTER 4 - IMPACT OF IPF ECM ON FIBROBLAST FUNCTION</b> .....	<b>121</b>
4.1	INTRODUCTION .....	121
4.1.1	<i>Background</i> .....	121
4.1.2	<i>Aims &amp; Objectives</i> .....	123
4.2	RESULTS .....	124
4.2.1	<i>Real Time PCR analysis of ECM stabilising enzyme messenger RNA during matrix interchange</i> .....	124
4.2.2	<i>Analysis of conditioned media LOXL3 during matrix interchange</i> .....	128
4.2.3	<i>Analysis of TG2 activity during matrix interchange</i> .....	129
4.2.4	<i>Cell proliferation of normal and IPF derived fibroblasts during matrix interchange</i> ....	130
4.2.5	<i>Manipulating adhesion and proliferation during matrix interchange</i> .....	132
4.2.6	<i>IPF ECM does not enhance protection against induced apoptosis</i> .....	135
4.2.7	<i>Immunohistochemistry of cross-linking enzymes and N-Epsilon-Gamma-Glutamyl Lysine in Control and IPF lung tissue</i> .....	139
4.2.8	<i>Optimisation of ECM proteolysis assays</i> .....	141
4.2.9	<i>Manipulation of proteolysis through cross link enzyme inhibitors</i> .....	143
4.3	DISCUSSION .....	148

4.4	CONCLUSIONS.....	152
<b>5</b>	<b>CHAPTER 5 - FACILITATION OF EXCESS ECM REMOVAL BY CROSS LINKING ENZYME</b>	
	<b>INHIBITION IN THE MURINE BLEOMYCIN FIBROSIS MODEL.....</b>	<b>154</b>
5.1	INTRODUCTION .....	154
5.1.1	<i>Background.....</i>	<i>154</i>
5.1.2	<i>Aims &amp; Objectives.....</i>	<i>157</i>
5.2	RESULTS.....	158
5.2.1	<i>Ex Vivo analysis of TG2 activity in Bleomycin treated mouse tissue.....</i>	<i>158</i>
5.2.2	<i>Bodyweight of mice post Bleomycin administration .....</i>	<i>161</i>
5.2.3	<i>Bodyweight of 40mg/kg treated mice.....</i>	<i>164</i>
5.2.4	<i>Bodyweight of 100mg/kg treated mice.....</i>	<i>166</i>
5.2.5	<i>Total lung hydroxyproline of 40mg/kg treated mice.....</i>	<i>168</i>
5.2.6	<i>Total lung hydroxyproline of 100mg/kg treated mice.....</i>	<i>170</i>
5.3	DISCUSSION.....	172
5.4	CONCLUSIONS.....	177
<b>6</b>	<b>GENERAL DISCUSSION .....</b>	<b>179</b>
6.1	GENERAL DISCUSSION .....	179
6.2	FUTURE WORK.....	190
<b>7</b>	<b>REFERENCES.....</b>	<b>194</b>

## List of Figures

<i>Figure 1.1 Haematoxylin and eosin staining of normal lung and IPF lung tissue at 10x magnification showing destruction of the lung architecture.....</i>	4
<i>Figure 1.2. Crude incidence rate of IPF diagnosis between 2000 and 2008 showing an increase in IPF diagnosis.....</i>	6
<i>Figure 1.3 Crude incidence rate of IPF diagnosis based on sex.....</i>	7
<i>Figure 1.4 Schematic representation of ECM turnover in normal and IPF lung tissue.....</i>	28
<i>Figure 1.5 Schematic representation of the collagen synthesis pathway.....</i>	31
<i>Figure 1.6 Schematic representation of the effect of ECM stiffness on proliferation, migration and differentiation of cell populations.....</i>	34
<i>Figure 1.7 The process of transamidation of collagen by TG2.....</i>	36
<i>Figure 1.8 The potential role of TG2 in the pathogenesis of IPF.....</i>	38
<i>Figure 1.9 The potential role of the LOXL family in the accumulation of ECM in IPF.....</i>	43
<i>Figure 2.1 Schematic diagram of treatment of mice in Time Course 1 (40mg/kg).....</i>	81
<i>Figure 2.2 Schematic diagram of treatment of mice in Time Course 2 (100mg/kg).....</i>	82
<i>Figure 3.1. 8-Galactosidase staining of primary lung fibroblasts.....</i>	90
<i>Figure 3.2 Images of stained primary human airway smooth muscle (ASM) cells.....</i>	91
<i>Figure 3.3 Expression of cross-linking enzyme transcripts in control and IPF derived fibroblasts....</i>	93
<i>Figure 3.4. ECM cross-linking enzymes and transglutaminase mediated cross-links are expressed in IPF tissue at x20 magnification.....</i>	96
<i>Figure 3.5. Isotype control images of ECM cross-linking enzymes and transglutaminase mediated cross-links are expressed in IPF tissue at x20 magnification.....</i>	97
<i>Figure 3.6 Characterisation of fibroblast derived ECM.....</i>	99
<i>Figure 3.7 Collagen Type I-V mRNA expression does not vary between IPF and control fibroblasts.....</i>	101
<i>Figure 3.8 Proliferation of primary lung fibroblasts in response to foetal bovine serum.....</i>	103
<i>Figure 3.9 Optical density of ADAM family and Cathepsin proteases in IPF and control fibroblast conditioned media.....</i>	105

<b>Figure 3.10 Optical density of Matrix Metalloproteinases and Urokinase in IPF and control fibroblast conditioned media.</b> .....	106
<b>Figure 3.11 Scanning electron microscopy of primary control and IPF derived fibroblasts at X750 magnification.</b> .....	108
<b>Figure 3.12 Scanning electron microscopy of primary IPF derived and control fibroblast cultures at x10,000 magnification.</b> .....	110
<b>Figure 3.13 Scanning electron microscopy of primary control and IPF derived fibroblast ECMs at X750 magnification.</b> .....	111
<b>Figure 3.14 Scanning electron microscopy of primary IPF derived and control fibroblast ECMs at x10,000 magnification.</b> .....	112
<b>Figure 4.1 Cross-linking enzyme mRNA expression of control and IPF fibroblasts on control and IPF matrices showing donor effect.</b> .....	125
<b>Figure 4.2 Cross-linking enzyme mRNA expression of control and IPF fibroblasts on control and IPF matrices showing donor effect.</b> .....	127
<b>Figure 4.3 LOXL3 content of fibroblast conditioned media during matrix interchange.</b> .....	128
<b>Figure 4.4 Total TGase activity of fibroblast conditioned media during matrix interchange.</b> .....	129
<b>Figure 4.5 Proliferation of control fibroblasts seeded onto control and IPF matrices and exposed to FBS and PDGF-bb.</b> .....	130
<b>Figure 4.6 Average well fluorescence of Cell-Tracker dye labelled fibroblasts seeded into Type I collagen coated wells.</b> .....	132
<b>Figure 4.7 Control fibroblast adhesion and proliferation on control and IPF ECM treated with cross-linking inhibitors.</b> .....	133
<b>Figure 4.8 Three control and three IPF derived fibroblasts were cultured on three control and three IPF derived ECM preparations and apoptosis induced by (A) staurosporine (1<math>\mu</math>M) or (B) fas ligand (100ng/ml).</b> .....	136
<b>Figure 4.9 Western blotting of three control and IPF derived fibroblasts cultured on control and IPF derived ECM and treated with staurosporine (1<math>\mu</math>M) or fas ligand (100ng/ml), shows no difference in cleaved PARP or caspase 3 between ECM types.</b> .....	138

<b>Figure 4.10 Immunohistochemistry of primary IPF and non-IPF lung tissue stained for smooth muscle actin and Thy1(CD90) as markers of fibroblast populations. ....</b>	<b>139</b>
<b>Figure 4.11. Tritiated hydroxyproline release from normal human lung fibroblast synthesised ECM .....</b>	<b>142</b>
<b>Figure 4.12 Tritiated hydroxyproline release from control and IPF synthesised ECM. ....</b>	<b>144</b>
<b>Figure 4.13 Tritiated hydroxyproline release from control and IPF synthesised ECM and digested with recombinant catalytic domain of MMP1.....</b>	<b>145</b>
<b>Figure 4.14 Tritiated hydroxyproline release from IPF synthesised ECM or IPF ECM synthesised with TG2 inhibitor; and digested with recombinant catalytic domain of MMP1.. .....</b>	<b>146</b>
<b>Figure 5.1 Bleomycin and CyM treatment of ex vivo (A) liver and (B) lung samples from 8 week C57BL/6 mice. (A) .....</b>	<b>159</b>
<b>Figure 5.2 Body weight of PBS control and Bleomycin treated mice. ....</b>	<b>161</b>
<b>Figure 5.3 Percentage of initial bodyweights of mice treated with 40mg/kg CyM during Bleomycin induced fibrosis at day 24, 34 and 44. ....</b>	<b>165</b>
<b>Figure 5.4 Bodyweights of mice treated with 100mg/kg CyM during Bleomycin induced fibrosis at day 24, 34 and 4. ....</b>	<b>167</b>
<b>Figure 5.5 Total lung hydroxyproline levels during bleomycin induced fibrosis, treated with CyM; .....</b>	<b>168</b>
<b>Figure 5.6 Total lung hydroxyproline levels during bleomycin induced fibrosis, treated with CyM; .....</b>	<b>170</b>

## List of Tables

<b>Table 1.1 The major collagens and their structural features adapted from Lodish .....</b>	<b>23</b>
<b>Table 2.1 List of primary antibodies used for immunohistochemistry, immunofluorescence and western blotting within this project with the respective host species and suppliers.....</b>	<b>49</b>
<b>Table 2.2 List of secondary antibodies used in this project for immunohistochemistry, immunofluorescence and western blotting with the list of suppliers.....</b>	<b>50</b>
<b>Table 2.3 Primary and commercial cell types using in this project with descriptions of derivation methods for primary cells obtained from biopsy.....</b>	<b>52</b>
<b>Table 2.4. Ex Vivo culture conditions of C57BL/6 lung and liver .....</b>	<b>76</b>
<b>Table 2.5: Experimental groupings of mice for Time Course 1 (40mg/kg). .....</b>	<b>79</b>
<b>Table 2.6 Experimental groupings of mice for Time Course 2 (100mg/kg). .....</b>	<b>80</b>

## Abbreviations

AA	Amino Acid
AB-G	Anaesthetic Code (General)
Abs.	Absorbance
AC	Anaesthetic Code (Terminal)
ADAMTS2	A Disintegrin and Metalloproteinase with Thrombospondin Motifs 2
AECII	Type 2 Alveolar Epithelial Cells
ANOVA	Analysis of Variance
APMA	Aminophenylmercuric Acetate
ASM	Airway Smooth Muscle Cells
ASPA	Animals in Scientific Procedures Act
ATF-4	Activating Transcription Factor 4
ATF-6	Activating Transcription Factor 6
AWERB	Animal Welfare and Ethical Review Board
BLM	Bleomycin
BMP-1	Bone Morphogenic Protein 1
BSA	Bovine Serum Albumin
CD90	Thy1 Cell Surface Antigen
CMAC	Cell-Matrix Adherence Complex

COPD	Chronic Obstructive Pulmonary Disease
CT	Computed Tomography
CY-3	Cyanine Fluorophore 3
CyM	Cystamine Dihydrochloride
DAPI	6-Diamidino-2-Phenylindole Dihydrochloride
DMEM	Dulbecco's Modified Eagles Medium
DMSO	Dimethyl Sulphoxide
DPM	Disintegrations per Minute
dsDNA	Double Stranded DNA
ECL	Enhanced Chemiluminescent
ECM	Extracellular Matrix
EDTA	Ethylenediaminetetraacetic Acid
EdU	5-ethynyl-2'-deoxyuridine
ELISA	Enzyme Linked Immunosorbent Assay
EMT	Epithelial-Mesenchymal Transition
ER	Endoplasmic Reticulum
FAP- $\alpha$	Fibroblast Activation Protein Alpha
FBS	Foetal Bovine Serum
FCS	Foetal Calf Serum
FF	Fibroblast Foci

FGF	Fibroblast Growth Factor
GAG	Glycoaminoglycan
GRP78	78 kDa Glucose-Regulated Protein
Gy	Gray Units
HASM	Human Airway Smooth Muscle Cell
HIF-1	Hypoxia Inducible Factor 1
HPF	Human Pulmonary Fibroblasts
HRCT	High-Resolution Computed Tomography
HRP	Horseradish Peroxidase
HYP	Hydroxyproline
IHC	Immunohistochemistry
IL-1	Interleukin 1
IL-6	Interleukin 6
ILD	Interstitial Lung Disease
IP	Intraperitoneal Injection
IPF	Idiopathic Pulmonary Fibrosis
IRE-1	Inositol-Requiring Enzyme 1
ITS	Insulin-Transferrin-Selenium
IU	International Units
IV	Intravenous Injection

IVC	Individually Vented Cage
LAP	TGF- $\beta$ Latency Associated Peptide
LASA	Laboratory Animal Science Association
LOX	Lysyl Oxidase
LOXL	Lysyl Oxidase Like Protein
LRR	Leucine Rich Repeat
LTBP	Latent TGF- $\beta$ Binding Protein
MC3T3-E1	Mouse Osteoblast Cell Line
MMP	Matrix Metalloproteinase
MRC-5	Normal Human Lung Fibroblast Cell Line
MSC	Microbiological Safety Cabinet
MTT	3-(4,5-dimethylthiazol-2-yl)-2,5-diphenyltetrazolium bromide
MWCO	Molecular Weight Cut-Off
NHLF	Normal Human Lung Fibroblasts
NTCO	Named Training and Competency Officer
NVS	Named Veterinary Surgeon
OP	Oropharyngeal Administration
P50	Nuclear Factor Kappa-B p105 Subunit
PBS	Phosphate Buffered Saline

PBST	Phosphate Buffered Saline with Tween 20
pCP	Procollagen C-Proteinase
PCR	Polymerase Chain Reaction
PDGF	Platelet Derived Growth Factor
PDGFR	Platelet Derived Growth Factor Receptor
PERK	Protein Kinase R-Like Endoplasmic Reticulum Kinase
pNPI	Procollagen Type I N-Proteinase
PPV	Positive Predicted Value
RCF	Relative Centrifugal Force
RER	Rough Endoplasmic Reticulum
RIPA	Radio Immunoprecipitation Assay
RNA	Ribonucleic Acid
S100A4	S100 Calcium Binding Protein A4
SABG	Senescence Associated $\beta$ -Galactosidase
SC	Subcutaneous Injection
SD	Standard Deviation
SEM	Scanning Electron Microscopy
SFPTC	Surfactant Protein C
SPF	Specific Pathogen Free
ssDNA	Single Stranded DNA

SD	Standard Deviation
STAT6	Signal Transducer and Activator of Transcription 6
TC	Time Course
TG2	Tissue Transglutaminase 2
TGF- $\beta$	Transforming Growth Factor Beta
TGase	Transglutaminase
TGM2	Tissue Transglutaminase 2 Transcript
TNF- $\alpha$	Tumour Necrosis Factor Alpha
TP	Time Point
TUNEL	Terminal Deoxynucleotidyl Transferase dUTP Nick-End Labeling
UPR	Unfolded Protein Response
$\alpha$ -SMA	Alpha Smooth Muscle Actin
$\beta$ APN	Beta Aminopropionitrile

## **CHAPTER 1**

# Extracellular Matrix in the Healthy Lung and Idiopathic Pulmonary Fibrosis

# **1 CHAPTER 1: The Role of the Extracellular Matrix in the Healthy Lung and Idiopathic Pulmonary Fibrosis**

## **1.1 The Human Respiratory System**

Contained within the pleural cavities of the thorax in humans, is the machinery necessary for breathing. The lung alone cannot perform the tasks of inhalation and exhalation without the diaphragm, ribs & the thoracic cavity. It involves the alteration of the internal volume of the thoracic cavity by anterior/posterior movement of the diaphragm, and the dorsal expansion/contraction of the ribcage that makes a person breathe. This manipulation of the internal structure draws air in when the lung is expanded, and pushed out when returned to its resting volume. Pulmonary compliance is the measurement of the lung's ability to exhibit elastic-like properties when breathing. A simple method of assessing this is with lung function testing using the formula (  $Compliance = \frac{\Delta V}{\Delta P}$  ) where  $\Delta V$  is the change in volume of the lung and  $\Delta P$  is the change in intrapleural pressure. In fibrotic lung disease, such as Idiopathic Pulmonary Fibrosis (IPF), compliance is decreased due to the reduced ability of the lung to expand easily. This is a result of deposition of large amounts of extracellular matrix proteins and destruction of the normal lung tissue.

## **1.2 Idiopathic Pulmonary Fibrosis**

### 1.2.1 Introduction

Idiopathic Pulmonary Fibrosis (IPF) is a physiologically devastating disease. The debilitating nature and high mortality rates make this one of the most lethal conditions, usually associated with median time to mortality of around 3 years (Dempsey, 2006). To put this in perspective, this is a worse prognosis than most cancers.

IPF is histologically characterised by fibroblast foci (FF) within the periphery of the lung. These are comprised of dense clusters of activated fibroblasts which stain positive for defined  $\alpha$ -smooth muscle actin ( $\alpha$ -SMA) stress fibres in culture (Visscher and Myers, 2006) and thus can be termed myofibroblasts. Furthermore it is these activated fibroblasts in the IPF lung which are responsible for the majority of the interstitial collagen deposition which is theorised to ultimately lead to dysfunction of the extracellular architecture. However, it is not known exactly how these fibroblasts come to be situated in such large numbers within the lung.

IPF is hallmarked by a large increase in the quantity of extracellular matrix (ECM) within the lung. This net increase in ECM results in reduced pulmonary compliance through stiffening of the lung tissue, making normal respiration extremely difficult for the afflicted. This aggressive & progressive fibrosis ultimately leads to severely impaired gas exchange within the lung (Agusti et al., 1991), due to destruction of the normal lung architecture and alveolar loss (Chilosi et al., 2006). Figure 1.1 below illustrates the destruction of normal lung tissue in IPF with the characteristic FF shown in the tissue.

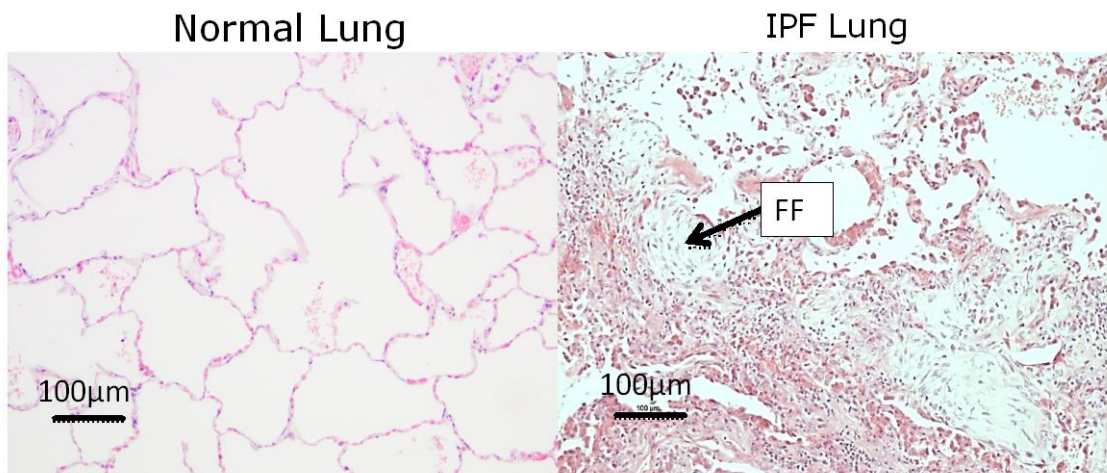


**Figure 1.1 Haematoxylin and eosin staining of normal lung and IPF lung tissue at 10x magnification showing destruction of the lung architecture.** Haematoxylin (purple) shows nuclei and eosin (pink) shows the cytoplasm. FF – Fibroblast focus. Normal lung image courtesy of Dr. Suzanne Miller and IPF lung image courtesy of Dr. Amanda Tatler (Division of Respiratory Medicine, School of Medicine, University of Nottingham, UK).

### 1.2.2 Epidemiology

In 2011, the international consensus on diagnosing IPF was established (Raghu et al., 2011). It was stated that a case may only be termed IPF if there is progressive fibrosing interstitial pneumonia with an unknown cause and/or a high resolution computed tomography (HRCT) pattern similar to usual interstitial pneumonia. This can further be confirmed by histology of surgical biopsy. Previous to this publication, but after some of the first descriptions from a pathological perspective of interstitial pneumonia, IPF was often combined, along with other conditions such as desquamative interstitial pneumonia, into the interstitial pneumonia classification. In 2012 5,292 people in the UK died from Pulmonary Fibrosis, which accounts for 4.6% of deaths from lung disease or 0.9% of all deaths in that year (British Lung Foundation, UK).

The prevalence of IPF is around 7 per 100,00 people per year in the UK (Navaratnam V, et al, 2011) however this does vary significantly depending on criteria such as diagnostic method, case definition and study design (Nalysnyk et al., 2012). Nalysnyk continued to explain the variability of incidence based on both broad and narrow case definitions, which brings to light the need for defined guidelines for a common consensus when diagnosing and managing the condition. Raghu *et al.* (2011) has outlined the diagnosis guidelines and clinical management of the disease; however it is the adoption of this into clinical practice on a global scale that will provide maximum benefit to patients.

### 1.2.2.1 Incidence and risk factors

Data suggests that the incidence of IPF is on the rise. Figure 1.2 is a graphical representation of the crude incidence rate as reported by Navaratnam *et al.* (2011). Incidence over time has shown a trend towards an increase over the 9 years until 2008 from 5-6 per 100,000 people to 8 per 100,000.

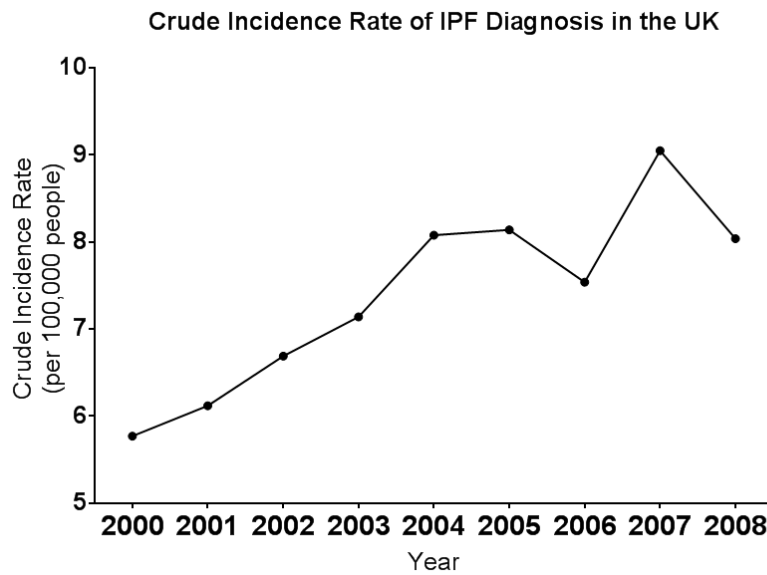


**Figure 1.2. Crude incidence rate of IPF diagnosis between 2000 and 2008 showing an increase in IPF diagnosis.** Data was obtained and graphed from Navaratnam *et al.* (2011).

IPF is more common in males than females with a crude incidence rate of 9.46 compared to 5.46 respectively (**Figure 1.3**). This may be due to a number of risk factors that have been identified due to occupation and lifestyle.

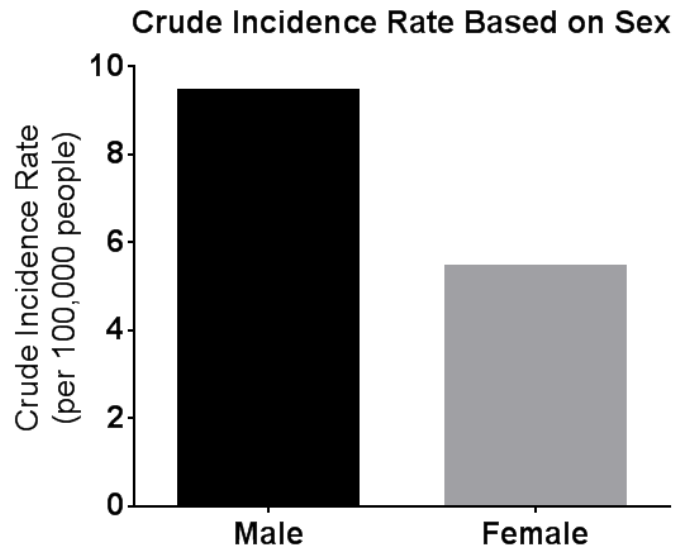


**Figure 1.3 Crude incidence rate of IPF diagnosis based on sex.** Data was obtained and graphed from Navaratnam et al. (2011).

IPF is most common in men over the age of 75 compared to any other age group (Raghu et al., 2006). This study also defined the disparity between broad and narrow case definitions and how validating the initial diagnosis of IPF, with such other techniques as HRCT or surgical biopsy, can both increase accuracy of the diagnosis itself, as well as impact the epidemiological studies.

There is a large amount of evidence suggesting that certain occupations have higher risk ratios for IPF, than others such as agriculture, stonecutting and hairdressing (Baumgartner et al., 2000, Awadalla et al., 2012). Exposures to certain occupational agents including, but not limited to, vegetable and animal dust (dander), magnesium silicate dust (talc) and

metal dusts also increases the odds ratio. Therefore, it seems most plausible that continuous microinjury to the lung epithelium from inhaled particulates is a route of pathogenesis.

### 1.2.3 Current Theories on Pathogenesis

There have been a number of theories surrounding the route of pathogenesis. Indeed it may be multifactorial, which is highly likely considering the complexity of the disease itself. Repetitive alveolar epithelial injury and the subsequent epithelial/mesenchymal cross talk is the most plausible explanation for the initiation of the pathogenesis of IPF with the previously described possible risk factors. This sustained injury may cause a number of responses which can lead to fibrosis such as TGF- $\beta$  activation, epithelial-mesenchymal transition and ECM accumulation through an attenuated wound repair response. These processes drive the generation of excess ECM and destruction of the lung parenchyma as seen in IPF (Katzenstein and Fiorelli, 1994). Furthermore the large increase in ECM protein synthesis as a result of the aberrant wound repair response has the potential to cause endoplasmic reticulum stress.

### 1.2.3.1 *Endoplasmic Reticulum Stress*

Situated within the cytoplasm of all eukaryotic cells is the endoplasmic reticulum (ER). This organelle is responsible for both lipid and protein synthesis among its highly complex network of microtubules and in the ER lumen. ER stress can be caused by a variety of factors including elevated protein synthesis, calcium store depletion, reduced energy stores and metabolic stress (Schonthal, 2012). This deviation from the normal homeostasis prevents the normal folding of immature polypeptide chains into their resolved 3D protein structures. When the ER is under stress, improperly folded protein aggregation may interfere with basic cell function such as forcing growth arrest or apoptosis. Cells that have high metabolic activity and secretory cells in particular rely on this mechanism due to the high protein synthesis rate.

In IPF it is hypothesised that an abundance of misfolded protein causes a response within the cell known as the unfolded protein response (UPR). In normal tissue, this response is mediated by the protein GRP78. Unstressed, GRP78 is immobilised and bound to transmembrane proteins such as PERK, ATF-6 and IRE-1. When nascent, immature polypeptides build up within the cell, GRP78 is released from its anchor and the downstream cascades promote an increase in apoptosis, expression of additional protein folding chaperones, and expression of proteolytic components. This tightly regulated mechanism serves to maintain a delicate balance between protein synthesis and maturation. Evidence for this is found predominantly in the type II alveolar epithelial cells (AECII) (Korfei et al., 2008). In IPF tissue explants, levels of ER stress mediator proteins such as p50, ATF-4 and 6 were significantly elevated over controls and non-IPF ILD cases in both whole lung homogenates and AECII's. Furthermore it was concluded from this study that this ER stress mechanism may be the cause of the loss of the AECII's apparent in the IPF lung.

The reason for the build-up of nascent protein is still not fully understood. However, mutation within the *SFTPC* gene, encoding surfactant protein C, has been hypothesised to be a cause of immature protein aggregation and the subsequent UPR (Kropski et al., 2013, Tanjore et al., 2012). Surfactant protein C is a highly hydrophobic protein which is secreted by alveolar epithelial cells to aid in reducing surface tension of fluids that coat the lung to aid in tissue stability (Nogee, 2002). Due to the nature of surfactant

protein C, it is highly hydrophobic (Murray and Mason, 2010) which means that the ER is essential for correct protein maturation and secretion. A study conducted by Lawson *et al.* found that by expressing a mutant SFTPC where a glutamine residue is substituted for a leucine at position 188 (L188Q) caused ER stress in stably transfected mouse lung epithelial cells (Lawson *et al.*, 2008).

#### 1.2.3.2 *Epithelial-Mesenchymal Transition*

Epithelial-mesenchymal transition (EMT) is the process by which epithelial cells are redifferentiated into mesenchymal cells such as myofibroblasts, chondrocytes and smooth muscle cells. As the exact origin of the abundance of fibroblasts in the IPF lung is still unclear, the transition of epithelial cells to mesenchymal cells presents a potential therapeutic target for the treatment of IPF. Currently, lineage tracing of fibroblasts in IPF have questioned the findings that both epithelial and mesenchymal markers in IPF lung tissue are co-localised (Kim *et al.*, 2006, Willis *et al.*, 2005). In animal models of kidney fibrosis, the major source of myofibroblasts has been shown to be recruitment from circulating pericytes (Humphreys *et al.*, 2010). The contribution of EMT to IPF may not be as great as once thought, however the anti-apoptotic effects of EMT and the phenotypic changes associated with EMT following epithelial damage may provide insight into the mechanism of IPF initiation or progression as a surrogate marker for epithelial damage (Kage and Borok, 2012).

### 1.2.3.3 *TGF-β*

TGF-β is known to be a key signalling molecule in IPF (Khalil and Greenberg, 1991, Bergeron et al., 2003, Cao et al., 2000) affecting the activation of fibroblasts, transformation to myofibroblasts & alteration of specific gene expression associated with fibrotic disease states. TGF-β has been extensively reviewed in IPF and the 'fibrotic response' evaluated (Leask and Abraham, 2004, Annes et al., 2003). It has been suggested that TGF-β may be the 'master switch' in controlling fibrosis within the lung (Bienkowski and Gotkin, 1995).

TGF-β functions in normal tissue can be altered through a variety of transcriptional regulation changes, interactions of the TGF-β protein itself, or through a protein that directly binds to it such as the latency associated peptide. An important concept in IPF is that of TGF-β activation via interaction with integrins. The aberrant accumulation of ECM in IPF provides a key structure through which increased activation of latent TGF-β can occur. Mechanical tension within the ECM can alter mature TGF-β levels available to adjacent cells through covalent attachment of the αvβ6 integrin and the latency complex to the latent TGF-β binding protein. Mechanical tension then opens the latency associated peptide, rendering the TGF-β available to bind to the TGF-β receptor on adjacent epithelial cells. It has been shown in IPF that αvβ6 levels in lung tissue correlate with mortality (Saini et al., 2015) and degree of fibrosis in the Bleomycin model (John et al., 2013). Interestingly, no current small molecule inhibitors of TGF-β activity, such as Pirfenidone, N-acetyl cysteine and Nintedanib,

inhibit  $\alpha\beta6$  mediated TGF- $\beta$  activation (Porte and Jenkins, 2014). This concept of local propagation of increased TGF- $\beta$  binding to adjacent epithelial cells may be a part of the propagation of IPF which is supported by the hypothesised excessively cross-linked ECM. This stiffer ECM could provide a mechanical tension which leads to consistent TGF- $\beta$  activation via the  $\alpha\beta6$  integrin.

Another mechanism of TGF- $\beta$  activation *in vitro* is cleavage of the latency complex by MMP-14, a member of the matrix metalloproteinase family. This has been shown to occur during binding of the TGF- $\beta$  latency complex to the  $\alpha\beta8$  integrin. Through this mechanism, mature TGF- $\beta$  is released into the ECM, unlike with  $\alpha\beta6$  activation. This enables paracrine signalling to nearby epithelial cells. Integrins play a vital role within TGF- $\beta$  signalling. The  $\alpha\beta3$ ,  $\alpha\beta5$ , and  $\alpha\beta6$  integrins allow TGF- $\beta$  activation through deformation of the latency complex to provide a proteolysis independent mechanism of TGF- $\beta$  activation in response to mechanical stress (Clarke et al., 2013). This is in contrast to the  $\alpha\beta8$  mechanism of proteolytic liberation of mature TGF- $\beta$  (Mu et al., 2002).

TGF- $\beta1$  inhibition is currently under investigation in a phase I clinical trial in patients with IPF using antibody targeted therapy to inactivate TGF- $\beta$ . This antibody has been shown to effectively reduce TGF- $\beta$  activity in a variety of diseases (Lacouture et al., 2015, Morris et al., 2014, Stevenson et al., 2013) and as reviewed previously, TGF- $\beta$  is thought to be a key molecule in the development of IPF.

#### 1.2.4 Current Therapies

No efficacious therapy exists to date which prolongs life expectancy in IPF patients. Many classes of drug have been trialled in response to observations in patients such as anti-inflammatory agents, anti-fibrotic agents and immune modulators (Rafii et al., 2013). Corticosteroids have been proven to reduce the presenting 'ground glass' opacities on high resolution CT (Gross and Hunninghake, 2001) however the characteristic alteration of the lung architecture remains unchanged (Lee et al., 1992).

Pirfenidone may be administered in the treatment of IPF for its combination of anti-inflammatory and anti-fibrotic properties and was approved for use by the European Medicines Agency in March 2011 (Azuma, 2012, Cottin, 2013, Potts and Yogaratnam, 2013). Still incompletely understood, the main mechanism of action is believed to be a suppression of activity and production of TGF- $\beta$ . Bleomycin induced animal models of IPF have shown that oral administration of Pirfenidone reduced TGF- $\beta$  mRNA by 33% (Iyer et al., 1999b) plus a reduction in procollagen I & III transcripts (Iyer et al., 1999a). Furthermore, the Phase III clinical trial (Clinicaltrials.gov, number NCT01366209) showed that when compared to placebo, Pirfenidone was successful in reducing disease progression through improved exercise tolerance; and a caused a 32.5% reduction in the degree of lung function decline in the population that previously presented a >10% drop in FVC (King et al., 2014).

Another drug recently described for IPF therapy is Nintedanib. This is a small molecule inhibitor of intracellular tyrosine kinases. The phase 3 trials, known as INPULSIS1 (ClinicalTrials.gov number NCT01335464) and 2 (ClinicalTrials.gov number NCT01335477), assessed primarily the decline in FVC over 12 months. Side effects included diarrhoea which led to around 5 % of patients failing to complete the study. However, patients receiving Nintedanib reduced the decline in lung function over 12 months which is associated with a slowed progression of the disease (Richeldi et al., 2014).

Currently it is a pressing necessity that new lines of enquiry be followed in the continuing effort to understand the pathogenesis and progression of IPF with respect to new and novel therapies (Selman et al., 2011) and to improve diagnostic, prognostic and theranostic biomarkers.

### 1.2.5 *In vivo* models of IPF

The complexity and heterogeneity of IPF have led to a number of animal models for studying the pathogenic mechanisms underlying the condition. With respect to IPF, a true isomorph model would not be technically plausible, as we are yet to identify the exact mechanism of disease progression. However, a number of useful *in vivo* techniques, in animals, can be employed to produce pulmonary fibrosis with characteristics similar to the disease of the human lung. Here presented are three of the most commonly utilized models, with the rationale for experimental use in this project.

#### 1.2.5.1 *Bleomycin*

The most commonly used mouse model for IPF is the single intratracheal administration Bleomycin model. Bleomycin (BLM) is a chemotherapeutic agent for the treatment of squamous cell and testicular carcinomas (Maiche, 1983), as well as pleural effusion (Nikbakhsh et al., 2011) and ovarian cancer (Pautier et al., 2008). The drug itself is a water soluble molecule of 1500Da and derived from *Streptomyces Verticillus* which is usually supplied as bleomycin sulphate.

Intratracheal administration of a dose of 1-2mg/kg in phosphate buffered saline (PBS) to C57BL/6 mice creates an initial period of inflammation, lasting approximately 7-10 days with subsequent fibrosis. The inflammation stage is predominantly characterised by an increase in pro-

inflammatory cytokines such as TNF- $\alpha$ , IL-1 and 6, and interferon- $\gamma$ . Bleomycin achieves this through chelation of metallo-ions and the formation of superoxide and hydroxide free radical compounds. These cleave both ssDNA and dsDNA (Claussen and Long, 1999) resulting in cytotoxicity and cell death (Chen et al., 2008).

The Bleomycin model is the most widespread model of lung fibrosis in publication currently. Using search terms 'bleomycin, fibrosis and mouse' in the search string ("mice"[MeSH Terms] OR "mice"[All Fields] OR "mouse"[All Fields]) AND ("bleomycin"[MeSH Terms] OR "bleomycin"[All Fields]) AND ("fibrosis"[MeSH Terms] OR "fibrosis"[All Fields]) on PubMed on the 14.09.2015 returns 5092 publications. This does not however include *in vitro*, *ex vivo* and *in silico* modelling. Furthermore this will not encompass articles with these search terms omitted.

The reason that the Bleomycin model is so widely used is that it is relatively cheap, requiring little technical expertise in inducing fibrosis. Intratracheal instillation produces a greater degree of fibrosis compared to intravenous (IV) injection (Lindenschmidt et al., 1986), and may produce a pathogenic effect more similar to IPF through AEC II damage when compared to IV. However, there are disadvantages to the Bleomycin mouse model. The main characteristic of IPF is that there is no reverting of progressive fibrosis. In the Bleomycin model, without intervention, it has been noted that there is a slow regression of the fibrosis without intervention which is not representative of the human disease (Izbicki et al., 2002) however

there is a disparity in reports as it has been shown that persistent changes still are present up to 6 months after Bleomycin administration (Limjunyawong et al., 2014).

In summary, the Bleomycin model is the most accessible, best documented and most commonly used model for IPF in rodents with good reproducibility. However, the limitations must be realised in that it does not truly model the pathophysiology of IPF, and therapeutic intervention study design must take into consideration the predominant inflammatory phase of the model time-course which is not representative of the human disease, but more of an acute lung injury (Goodman et al., 2003). The Bleomycin model presents a simple yet powerful tool for the rapid screening of antifibrotic compounds over a relatively short timescale.

#### 1.2.5.2 *Silica*

From the odds ratios described earlier in 1.2.2.2, and the aerosolised inhaled particulates associated with those professions, an inhaled particulate which damages the alveolar epithelium in the lung would mimic the theorised route of pathogenesis of IPF. The silica model is another frequently reported animal model of lung fibrosis (Davis et al., 1998, Moore and Hogaboam, 2008). Drug intervention studies utilising this model describe a persistent progression of fibrosis in the chronic phase, exhibiting a pattern of fibrosis that is similar to that of occupational silicosis (Degryse and Lawson, 2011, Oberdorster, 1996). However, the limitations to using this method are that administration of particulate silica requires expensive

equipment and technical expertise that other models such as Bleomycin do not. Another limitation to the silica model, is the timescale involved in producing a fibrotic phenotype in the mouse. Studies range from reporting a persistent fibrosis within 30 days post administration (Lakatos et al., 2006, Lardot et al., 1998) up to 60 days (Barbarin et al., 2005). Extended periods of experimentation will result in a more expensive study which may exclude initial drug pilot studies, which more readily adopt the Bleomycin model, regardless of the phenotypic advantages of the silica model. In this project, the technical expertise in running this model within is limited, whereas the Bleomycin model has been optimised and conducted with low mortality and good reproducibility.

#### 1.2.5.3 *Irradiation*

Radiation is another method for inducing pulmonary fibrosis in animal models. It is characterised by both pneumonitis and pulmonary fibrosis, however the timescale involved is much more extensive than the Bleomycin model. The pneumonitis can be observed from the third week for several months prior to fibrosis which persists from around 20 weeks (Morgan and Breit, 1995). This model involves the administration of 10 to 20 Gy (Gray Units) of ionising radiation which is cheap to administer, however the husbandry of the animals over the subsequent 6 months can lead to this model being expensive to conduct. One of the major features of this model is that fibrosis is induced through free radical mediated DNA damage and an increase of TGF- $\beta$  signalling (Moore and Hogaboam, 2008) similar to that of Bleomycin administration. A common feature of this

model is pulmonary arterial hypertension (PAH), which is associated with vascular remodelling (Ghobadi et al., 2012). In IPF it is noted that PAH complicates the course of disease progression in between 32%-85% of IPF cases (Nathan et al., 2007). The time scale involved in producing fibrosis using radiation is prohibitive in this project, requiring around 20 weeks to establish (McDonald et al., 1993).

### **1.3 Composition of the Extracellular Matrix**

The mammalian matrisome consists of around 300 individual proteins (Hynes and Naba, 2012). In addition to this there are many modifying/stabilising enzymes, growth factors and receptors. The complexity of the matrisome allows for highly coordinated and controlled cell function through signalling within the ECM. Modifying the extracellular environment in; structure, pH, growth factor content, cytokine content, polarity of cells, and much more, the matrisome is implicated in nearly all cellular function, even if indirectly. The role of the ECM can be seen through the diversity of ECM proteins and their interaction with each other and native cell populations.

#### **1.3.1 Extracellular Matrix Constituents**

ECM is a key feature of multicellular organisms. It provides structure and organisation to the cell populations and can be divided into 5 distinct categories when concerned with specific protein function:-

1. Collagens
2. Proteoglycans
3. Glycoproteins
4. Signal Molecules
5. Modifying and Stabilising Enzymes

### 1.3.1.1 *Collagens*

The Collagens represent the most abundant protein group in the human body (Di Lullo et al., 2002) with around 85% being of type I, II or III (Lodish, 2000). They provide strong, structural components of the ECM where their strength can be seen via the content of collagen in structures such as tendon and skin. These proteins form triple helices comprised of two  $\alpha 1(I)$  and one  $\alpha 2(I)$  chains in type I collagen. Each chain of 1050 amino acids (AA) triple helix complex measures 300nm in length, known as fibrils. The major collagen molecules are shown in **Table 1.1** consisting of structural features, and in which tissues they are commonly found.

<b>Type</b>	<b>Subunit Composition</b>	<b>Structural Features</b>	<b>Representative Tissues</b>
<b>Fibrillar Collagens</b>			
I	$[\alpha 1(I)]_2[\alpha 2(I)]$	300nm long fibrils	Skin, tendon, bone, ligaments, dentin, interstitial tissues
II	$[\alpha 1(II)]_3$	300nm long fibrils	Cartilage, vitreous humor
III	$[\alpha 1(III)]_3$	300nm long fibrils; often with type I	Skin, muscle, blood vessels
V	$[\alpha 1(V)]_3$	390nm long fibrils with globular N-terminal domain; often with type I	Similar to type I; also cell cultures, foetal tissues
<b>Fibril-Associated Collagens</b>			
VI	$[\alpha 1(VI)][\alpha 2(VI)]$	Lateral association with type I; periodic globular domains	Most interstitial tissues
IX	$[\alpha 1(IX)][\alpha 2(IX)][\alpha 3(IX)]$	Lateral association with type II; N-terminal globular domain; bound glycosaminoglycan	Cartilage, vitreous humor
<b>Sheet-Forming Collagens</b>			
IV	$[\alpha 1(IV)]_2[\alpha 2(IV)]$	Two-dimensional network	All basal laminae

**Table 1.1 The major collagens and their structural features adapted from Lodish (Lodish, 2000). In IPF, collagens I and III are the most commonly observed in abundance.**

### 1.3.1.2 Proteoglycans

Proteoglycans offer little in the way of structural support. Basic composition of the proteoglycans are glycoprotein bound, repeating polymers of disaccharides with additional sulphate and carboxyl groups, also known as glycoaminoglycans (GAG's). The major feature of the proteoglycan component in the ECM is the ability to be hydrophilic and attract divalent ions through the relatively high negative molecular charge. The GAG unit may also bind secreted signalling molecules within the ECM, and along with water, create a fluid environment. The leucine rich repeat (LRR) domains of proteoglycans bind to a diverse range of collagens forming large linked complexes. Furthermore the hyalectan members bind to glycoprotein components of the ECM. The large amount of variation in

complex constituent components performs an important role in the regulation and turnover of the ECM.

#### 1.3.1.3 *Glycoproteins*

Comprising of around 200 complexes, the glycoproteins within the matrisome provide a hugely diverse range of functions, from regulation of growth factors including TGF- $\beta$  through binding into a latency complex, to providing structural integrity similar to collagens. Their basic structure consists of an oligosaccharide or glycan chain, covalently bound to polypeptide side chains. The process of glycosylation (addition of glycan groups) may happen at either an asparagine residue containing an amide nitrogen (N-glycosylation) or at the hydroxyl oxygen in the side chain of hydroxylysine, hydroxyproline, serine or threonine. Furthermore they form many cellular receptors and integral membrane proteins as the hydrophobic amino acid domain inserts into the phospholipid bilayer of cell membranes.

Another group of glycoproteins of note is the fibrillins. It has been shown that TGF- $\beta$  is closely associated with the fibrillins within the ECM in a latent form, bound to Latency Associated Peptide (LAP) and Latent TGF- $\beta$  Binding Protein (LTBP) (Hynes et al., 2012).

#### 1.3.1.4 *Signalling Molecules*

From the early embryogenesis, signalling within the ECM is essential. For cells to communicate across any significant distance, a chemical mediator must be passed through the ECM. The myriad of protein, glycoprotein & proteoglycan complexes that reside here have been shown to initiate & alter cell signalling. Morphogen gradients in development are essential for proper formation of offspring especially during polarization of the embryo to allow such structures as limb formation (Benazet and Zeller, 2009). The release of a signal molecule from one region or group of cells may affect the cell lineage of surrounding cells in a dose dependent manner (Gurdon and Bourillot, 2001).

Recently it has been noted that microarray data from IPF derived primary cells in short term cultures shows distinct patterns of gene expression, similar to that of during lung development (Selman et al., 2008). Indeed these transcription patterns are highly similar to those activated during lung development (Studer and Kaminski, 2007). This distinct signature of IPF gene expression is however observed in lung biopsy samples (Selman et al., 2006) whereas the major components of the ECM itself, as stated earlier are secreted from fibroblasts.

#### 1.3.1.5 *Stabilising and Modifying Proteins*

The ECM is a complex network of interconnected macromolecules which forms a biological scaffold as a structure on which cells adhere and grow (Burgess, 2009). The human lung contains over 40 distinct cell types (Fernandez and Eickelberg, 2012) however excess ECM deposition in IPF is attributed to just 1 of these.

Contained within the characteristic fibroblastic foci, the activated myofibroblasts deposit large amounts of collagen. The control of this ECM turnover is extremely complex, involving many different cytokines and growth factors. However, excess deposition of ECM (Martinet et al., 1996, Vaillant et al., 1996, Zhang and Phan, 1996) is the net result of both positive and negative processes. It is dysfunction within this balance of deposition and degradation that leads to an increase in ECM and a reduction in pulmonary compliance (Karlinsky and Goldstein, 1980).

The theory stands as abnormal wound repair response in IPF, causes a result similar to that of repeated alveolar epithelial injury from multiple sites within the lung (Plataki et al., 2005, Selman and Pardo, 2006, Uhal, 2003) contributing to a net increase in ECM, yet MMP levels are known to be elevated in IPF (Craig et al., 2015, Dancer et al., 2011, Hayashi et al., 1996, Ramos et al., 2001a). Therefore, other processes which impair normal endogenous proteolysis may be altered. This may be through formation of proteolytically resistant cross-links such as formed by

Transglutaminase 2 or lack of recognition of their substrates by proteases known to be in abundance in IPF.

#### **1.4 Extracellular Matrix Turnover**

ECM is a very dynamic environment comprising of a delicate balance of synthesis, stabilisation and degradation. The cross talk between the cell populations within and ECM itself orchestrates a multitude of cellular functions including but not limited to proliferation, apoptosis and differentiation. Fibrotic diseases are characterised by excessive accumulation of ECM resulting in tissue stiffening, organ function impairment and ultimately organ failure. The potential routes of pathogenesis of IPF discussed previously in section 1.2.3 outline potential mechanisms of disease initiation and propagation; however currently, there are very limited treatment options for patients with IPF.

ECM turnover can be thought of as a balance between deposition and degradation, with stabilisation enhancing the stability of the deposited ECM proteins as shown in Figure 1.4. This would render degradation by normal endogenous proteolysis more difficult through the formation of TG2 and LOXL family mediated cross linking of the ECM proteins.

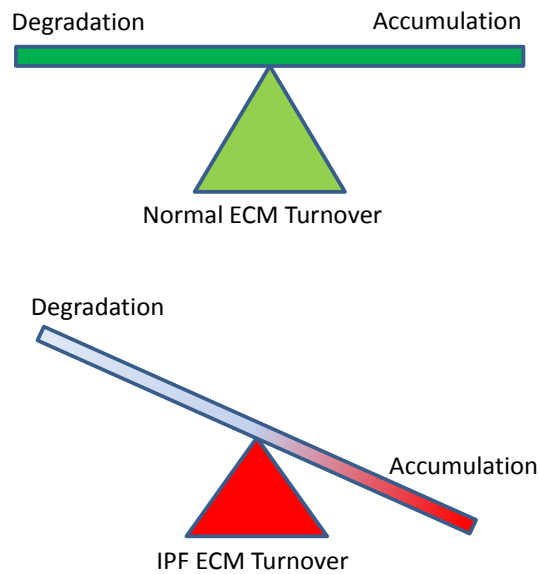


**Figure 1.4 Schematic representation of ECM turnover in normal and IPF lung tissue.** Normal ECM turnover shows a balance between accumulation and degradation, whereas in IPF lung tissue this balance is skewed towards excess accumulation of ECM.

Furthermore, this balance of increased ECM accumulation is almost paradoxical. It is well characterised that the MMP's are one of the most upregulated gene families in IPF (Gadek et al., 1979, Pardo et al., 2005, Zuo et al., 2002), however the microenvironment within the IPF lung appears to be non-collagenolytic and profibrotic which is still incompletely understood.

#### 1.4.1 Deposition of Type I Collagen in the ECM

The ECM in each tissue has specific biochemical, biophysical and component content (Kleinman et al., 2003). The components of the ECM were discussed earlier in section 1.3 however the current project will focus on collagen types I deposition and degradation. The majority of collagen is transcribed and secreted by mesenchymal cells, predominantly fibroblasts. With the addition of the described EMT in IPF as described in section 1.2.3, fibroblasts have an increased capacity to migrate and increase production of ECM components and MMP's.

The collagen biosynthesis pathway involves synthesis and processing of collagen precursor molecules. mRNA translation begins in the rough endoplasmic reticulum (RER) where membrane bound ribosomes translate collagen mRNA into  $\alpha$ -chains in the lumen of the ER. These  $\alpha$ -chains are hydroxylated at specific prolyl and hydroxyl residues, which enables the self-assembly into the collagen triple helix, during which glucosyl and galactosyl residues are added to hydroxylysine residues. Furthermore, oligosaccharide chains are attached to the C-terminal propeptide. This procollagen unit is transferred to the Golgi where it is packaged into secretory vesicles for exocytosis as shown in Figure 1.5. Once in the extracellular space, the cleavage of the N and C-terminal propeptides occurs via procollagen type I N-proteinase (pNPI), or more commonly known as ADAMTS2 (Colige et al., 1999), and Procollagen C-proteinases (pCP) respectively (Pischon et al., 2005, Prockop et al., 1998) The cleavage of the C terminal is performed by bone morphogenic protein-1.

This enzyme has been identified to be a shorter splice variant of the mammalian tolloid (mTld) (Hartigan et al., 2003). This form of collagen is known as tropocollagen (Obrink, 1973). Pischon *et al.* further notes that specific BMP-1 inhibitor addition to MC3T3-E1 cells derived from C57BL/6 mice, dose dependently inhibits LOX activation during the aggregation and fibril formation stages of collagen processing. This suggests that the proteolytic domain of pCP (BMP-1) plays a role in tropocollagen processing and LOX activation for stabilisation of the fibril.

Following pro-peptide cleavage the tropocollagen aggregates and polymerises into fibrils, and is stabilised by LOX in the extracellular space. Formation of the stabilising cross links through reactive aldehyde production on the tropocollagen units is exclusively an extracellular process through LOX only being present in the extracellular environment.

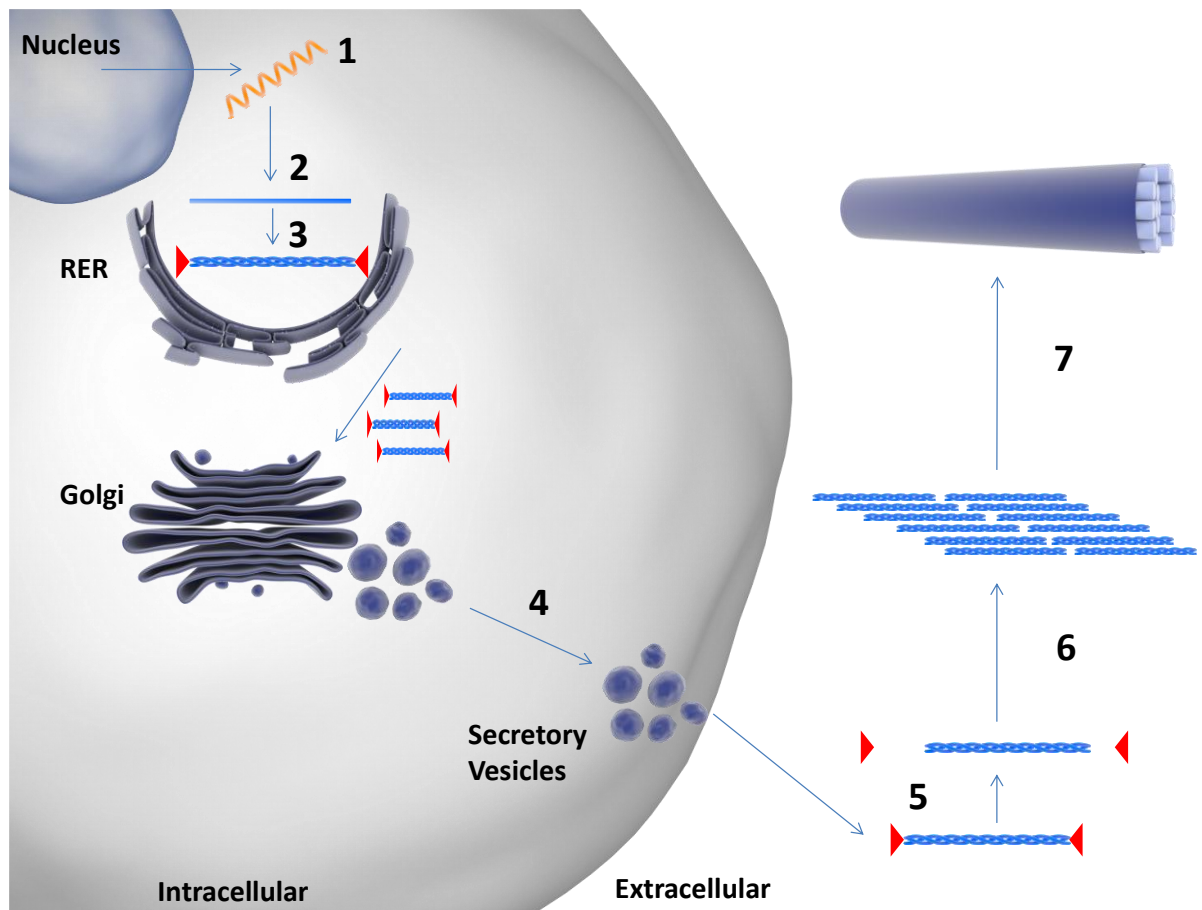


**Figure 1.5 Schematic representation of the collagen synthesis pathway.** mRNA is transcribed (1) and translocated to the rough endoplasmic reticulum (RER) where it is translated to the propeptide alpha chains (2) These alpha chains then undergo hydroxylation of specific prolyl and lysyl residues with further attachment of galactosyl and glucosyl groups to these hydroxylysyl units. These modified alpha chains are assembled into the procollagen triple helical structure (3) and transferred the golgi for packaging and exocytosis (4). In the extracellular space, the signal peptides are cleaved from the procollagen helices to form tropocollagen (5), which aggregates (6) and self assembles into fibrils (7) which is subsequently stabilised by ECM cross linking enzymes; predominantly the LOX family.

The mechanism of procollagen signal peptide cleavage functions as a negative feedback loop to regulate collagen synthesis in that addition of N and C-terminal procollagen peptides to human lung fibroblast cultures diminishes collagen synthesis as assayed with tritiated proline incorporation (Wu et al., 1986). Following the hypothesis that IPF is propagated by an aberrant wound repair response mediated by an increase in TGF- $\beta$ , it would be expected that activation of the TGF- $\beta$  receptors (type I and II) and downstream signalling through the SMAD superfamily, would

increase collagen type I synthesis (Leask and Abraham, 2004). Furthermore, it is not only the TGF- $\beta$  superfamily that can induce collagen synthesis. Transcription of collagen type I mRNA can be mediated by numerous cytokines from inflammatory cells including tumour necrosis factor- $\alpha$  (TNF- $\alpha$ ), interferon- $\gamma$  (INF- $\gamma$ ) and the interleukin family. Interleukin-4 (IL-4) has been shown to signal through induction of the transcription factor STAT6, which binds to the promoter sequences within the *COL1A1* and *COL1A2* genes to increase *COL1A1* and *COL1A2* mRNA in MRC-5 fibroblasts (Buttner et al., 2004). Initiation of collagen synthesis is a hugely complex system, relying on a balance between negative and positive cues from the surrounding extracellular environment, multiple cell types and various cytokines which indicates that the process is tightly regulated at both transcriptional and protein levels.

#### 1.4.2 Stabilisation

ECM is known to regulate cell fate through complex interactions of the cell with the mechanical properties, composition and structural organisation of the ECM. Through research in the tissue engineering field, and stem cell lineage tracing, it has been demonstrated that the transduction of mechanical factors plays an important role in cell phenotype (Guilak et al., 2009, Kshitiz et al., 2012).

#### 1.4.2.1 *Collagen Cross Linking*

Initial stabilisation of the collagen fibril as described in 1.4.1 occurs through the LOX family of enzymes. The importance of these lysine derived cross links are demonstrated in the rat, showing administration of  $\beta$ -aminopropionitrile ( $\beta$ APN), an inhibitor of the LOX family (Bondareva et al., 2009, Mammoto et al., 2013, Martinez-Martinez et al., 2016), reduced aorta ECM strength and stiffness (Bruehl et al., 1998). Due to the blood pressure within the aorta, this resulted in distention of the aorta wall. This study indicates the importance of normal LOX family function in mature collagen formation. Furthermore,  $\beta$ APN administration as a tool to study collagen maturation has shown that chronic inhibition of the LOX family results in lathyrism (Yeager et al., 1985). Malformation of mature collagen cross links, in the extracellular environment can cause severe disruption to tissue and organ function through both mechanical compromise of the extracellular protein integrity and through differential signalling to the cell populations residing within.

#### 1.4.2.2 *Effects of Collagen Cross Linking on tissue function*

Recently, the influence on cell behaviour of cell scaffold stiffness and composition has come to be a prominent research interest in regenerative medicine. Cells transduce mechanical forces from their adhered substrate through integrin binding in focal adhesions and transduction through the cytoskeleton, which in turn, regulate cell behaviour (Liu et al., 1999). Most

of this work has been conducted using polyacrylamide gels, which enable

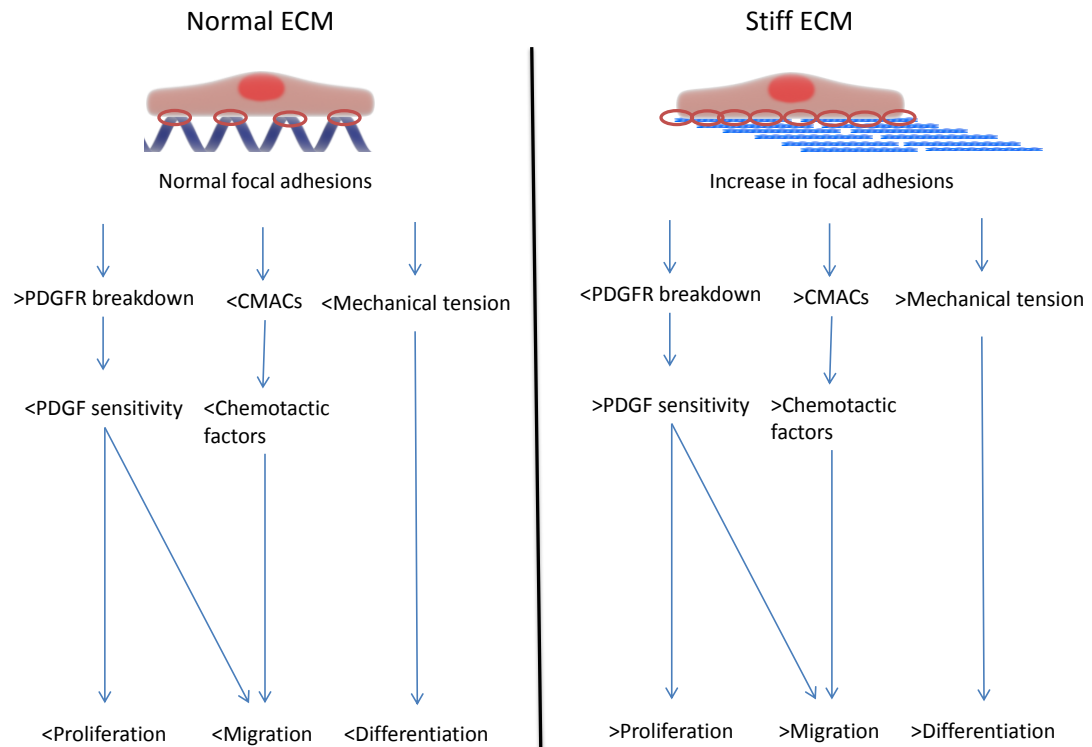


**Figure 1.6 Schematic representation of the effect of ECM stiffness on proliferation, migration and differentiation of cell populations.** Stiff ECM results in increased number of focal adhesions. This feeds back to the cell through mechanical transduction of the cytoskeleton and numerous pathways to increase cell proliferation, migration and differentiation. Reduced PDGFR breakdown results in increased sensitivity to PDGF-bb, increasing proliferation. Mechanical tension in the cytoskeleton may result in differentiation along with an increase migration capacity. CMAC=cell matrix adhesion complex. ECM=Extracellular Matrix; PDGF=Platelet Derived Growth Factor; PDGFR=Platelet Driven Growth Factor Receptor

very accurate adjustment of stiffness, similar to that of ECM *in vivo* (Beningo and Wang, 2002, Pelham and Wang, 1997, Wang and Pelham, 1998).

Mechanical tension created by cell adherence to stiff ECM has been shown to be a key factor in differentiation of fibroblast to the myofibroblast phenotype (Li et al., 2007). In IPF it is known that the abundance of ECM creates a much stiffer tissue, leading to increased difficulty in breathing. This stiff extracellular environment may push both resident and recruited

fibroblasts to differentiate down the myofibroblast lineage. Furthermore, it is also known that the majority of interstitial collagen in IPF comes from the myofibroblast populations. Therefore this abnormal propagation of a profibrotic microenvironment may create opportunities for therapeutic intervention in IPF, during ECM maturation and stabilisation.

Cell-matrix adherence complexes (CMACs) are the protein complexes that are present at focal adhesions of cell contact with the ECM. They allow interaction and mediation of communication between the cell and its environment (Delon and Brown, 2007). These complexes are mostly comprised of integrins, which allow transduction of extracellular signals into cell behaviours (Lock et al., 2008). Increased numbers of focal adhesion in IPF (Lagares and Kapoor, 2013), due to increased ECM stiffness may produce an increased migrative capacity, thus increasing fibroblast invasion into the profibrotic environment. Targeting matrix stiffness and cross linking may therefore be a possible therapeutic target in IPF to reduce the increased proliferation, migration and differentiation associated with increased ECM stiffness.

### 1.4.3 Tissue Transglutaminases

The family of transglutaminases are a highly complex family of enzymes that have a wide variety of functions. These calcium dependent enzymes catalyse the post-translational transamidation of free glutamine residues (Greenberg et al., 1991). In IPF TG2 has been noted to be a potential therapeutic target by a number of studies due to the high expression in IPF tissue and its contribution to ECM stabilisation (Clarke et al., 2013, Oh et al., 2011, Olsen et al., 2014, Olsen et al., 2011).

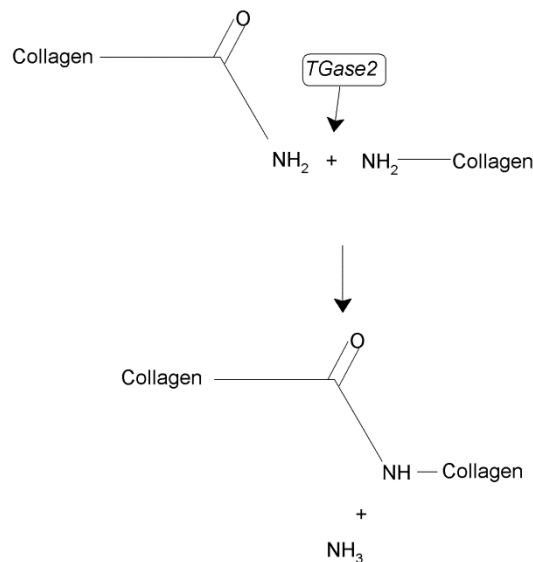


**Figure 1.7 The process of transamidation of collagen by TG2.** Formation of  $n$ - $\epsilon$ - $\gamma$  glutamyl lysine cross links in ECM proteins provide mechanical stability and grant proteolytic resistance.

#### 1.4.3.1 Tissue Transglutaminase 2

The *TGM2* gene (chr20q11.23) encodes the protein Tissue Transglutaminase-2. This well characterised protein has a large variety of functions both within the cell and in the ECM, which range from intracellular signal transduction (Mhaouty-Kodja, 2004) to modulating apoptosis (Jang et al., 2010, Yuan et al., 2005). Most notable of its

functions is creating mechanical & proteolytic resistance of the ECM through transamidation. Formation of amide bonds between glutamine and  $\epsilon$ -amino groups of lysine residues result in cross linked protein complexes which are highly resistant to mechanical challenge and endogenous proteolysis (Griffin et al., 2002).

The role of TG2 outside the cell is still poorly understood however it is known that localisation of protease inhibitors and cytokines within the ECM is due to the action of TG2 in the stabilisation phase (Larreta-Garde and Berry, 2002, Nakane et al., 2002, Verderio et al., 2004). Many other functions exist for this enzyme in a wide number of clinical pathologies (Lai and Greenberg, 2013).

### 1.4.3.2 Potential role of TG2 in IPF

The normal function of TG2 can be thought of as a biological suturing enzyme in the context of IPF. Acting as one of nature's 'biological glues' (Griffin et al., 2002) it plays a role in normal wound healing through the formation of proteolytic resistant cross links as described previously in section 1.4.3. However this process is potentially propagated by an increase in TGF- $\beta$  signalling through integrin mediated activation in IPF and cell surface TG2/plasmin-mediated latent TGF- $\beta$  activation (Kojima et

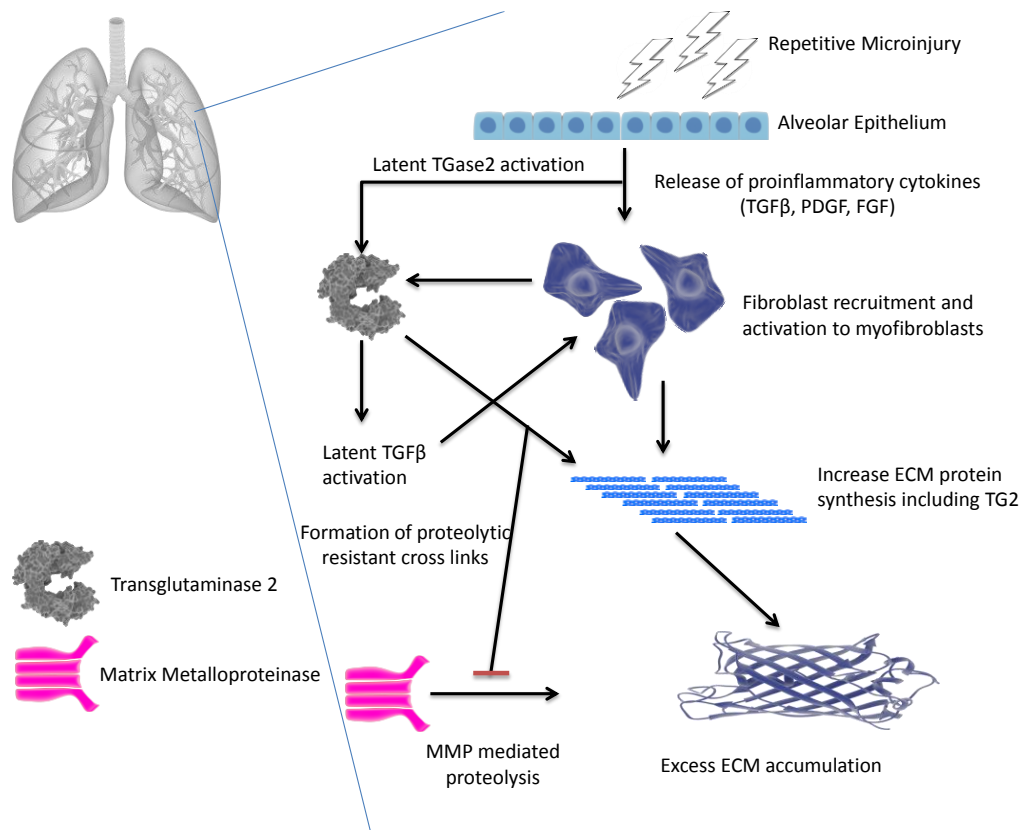


**Figure 1.8 The potential role of TG2 in the pathogenesis of IPF.** Repetitive damage to the alveolar epithelium is hypothesised to cause latent TG2 activation and TG2 synthesis. The TG2 then catalyses formation of proteolytically resistant cross links within the ECM leading to reduced MMP mediated proteolysis in the IPF lung.

al., 1993).

During inflammation immediately following the initial injury, TG2 mRNA expression is up-regulated by cytokines released from damaged cells

including TGF- $\beta$ , TNF- $\alpha$ , IL-1 & IL-6 (Suto et al., 1993, Skill et al., 2004, Nieder et al., 2005, Le et al., 2001, Johnson et al., 2003, George et al., 1990). These inflammatory cytokines also attract inflammatory cells to the site of injury. Latent TGF- $\beta$  stored within the ECM has been shown to be cleaved to its active form and released by the activity of TG2 in articular cartilage (Le et al., 2001), therefore increasing amplitude of the TGF- $\beta$  signal from the damaged cell population, creating a much larger response (Mohan et al., 2003). In this manner, the release of latent matrix bound TGF- $\beta$ , and the subsequent stimulation of expression of TG2 can be a positive feedback loop. Excessive expression of TG2 may lead to aberrant cross linking of ECM substrates and creation of a microenvironment within the tissue which propagates cell proliferation and promotes fibrosis, including  $\alpha\beta 6$  integrin mediated TGF- $\beta$  signalling. This area of ECM would exhibit a distinct increase in proteolytic resistance (George et al., 1990, Haroon et al., 2002) compared to normal ECM where TG2 was not overexpressed.

TG2 null mice have been shown to present no abnormal phenotype at baseline (Nanda et al., 2001), which is surprising considering the constitutive expression of the enzyme itself and its diversity of functions. There is robust evidence of that reducing TG2 activity results in a decreased level of fibrogenesis in other organ systems (Huang et al., 2009, Johnson et al., 2007, Qiu et al., 2007). Most TG2 knockout mice have furthermore been shown to develop a reduced pulmonary fibrosis following Bleomycin instillation (Olsen et al., 2011) through a proposed mechanism

of reducing TGF- $\beta$  activation. TGF- $\beta$  itself is known to increase cell surface expression of TG2 which in turn can anchor the latency complex to the cell membrane, and rendering it susceptible to mechanical tension induced maturation as described previously. This is supported by work from Schweke *et al.* (2008) in that TG2 null mice exhibit attenuated renal fibrosis through a reduction in TGF- $\beta$  activation which is the same mechanism as proposed here (Shweke et al., 2008).

#### 1.4.4 The Lysyl Oxidase Family

The *LOX* gene (chr5q23.2) encodes the enzyme Lysyl Oxidase (LOX). This copper dependant protein is responsible for catalysing the covalent cross linking of elastin and collagen, which stabilises the ECM. In healthy tissue these extracellular enzyme aid the formation of hydroxylysine-derived cross links of collagens and the lysine-derived cross links between elastin (Maki et al., 2005). The elastic like properties of elastin within the ECM are due to these cross links and along with the tensile strength of collagens, give rise to the functional integrity of connective tissue (Kagan and Li, 2003, Myllyharju and Kivirikko, 2004). Furthermore, LOX is known to play a role in cancer progression and metastasis (Gao et al., 2010, Erler et al., 2006). There are 5 currently characterised members of the LOX family; LOX, LOXL1, LOXL2, LOXL3, LOXL4. Each member of this family contains the conserved C-Terminal functional domain for amine oxidase activity directed towards collagen and elastin (Kim et al., 2009).

##### 1.4.4.1 *Lysyl Oxidase*

Increased LOX mRNA in IPF may be a combined result of the SMAD3 signalling but also the crosstalk of Hypoxia Inducible Factor-1 (HIF-1), which is the major transcription factor that responds to a hypoxic cellular environment (Semenza, 2001). In IPF, HIF-1 is has been shown to be localised to the alveolar epithelial cells which directly overlay highly proliferative fibroblast populations within FF (Tzouvelekis et al., 2007). This indicates possible signalling between both the AECs and the

underlying fibroblasts, with potential for injury to the epithelial cells, resulting in a direct upregulation in gene expression of LOX family. Suggestion of HIF-1 contributing to an early event in the fibrogenic cascade has also been noted.

#### 1.4.4.2 *Potential roles of the LOX family in IPF*

In Bleomycin animal models and human cell culture models of IPF, LOX expression is shown to increase (Chen et al., 2010, Li et al., 2012a, Yamaguchi et al., 2012, Blaisdell and Giri, 1995). Aberrant expression of LOX could, at least in part, be responsible for the increased rigidity of pulmonary tissue and reduced lung compliance through increased formation of covalent collagen and elastin bonds (Gao et al., 2010, Levental et al., 2009). The exact mechanism of monocyte recruitment in the IPF lung is still not fully understood however LOX acts as a strong chemoattractant for monocytes (Li et al., 2000, Lazarus et al., 1995). Overexpression of LOX as shown in Figure 1.9 may be a part of the process of excess ECM accumulation in IPF.

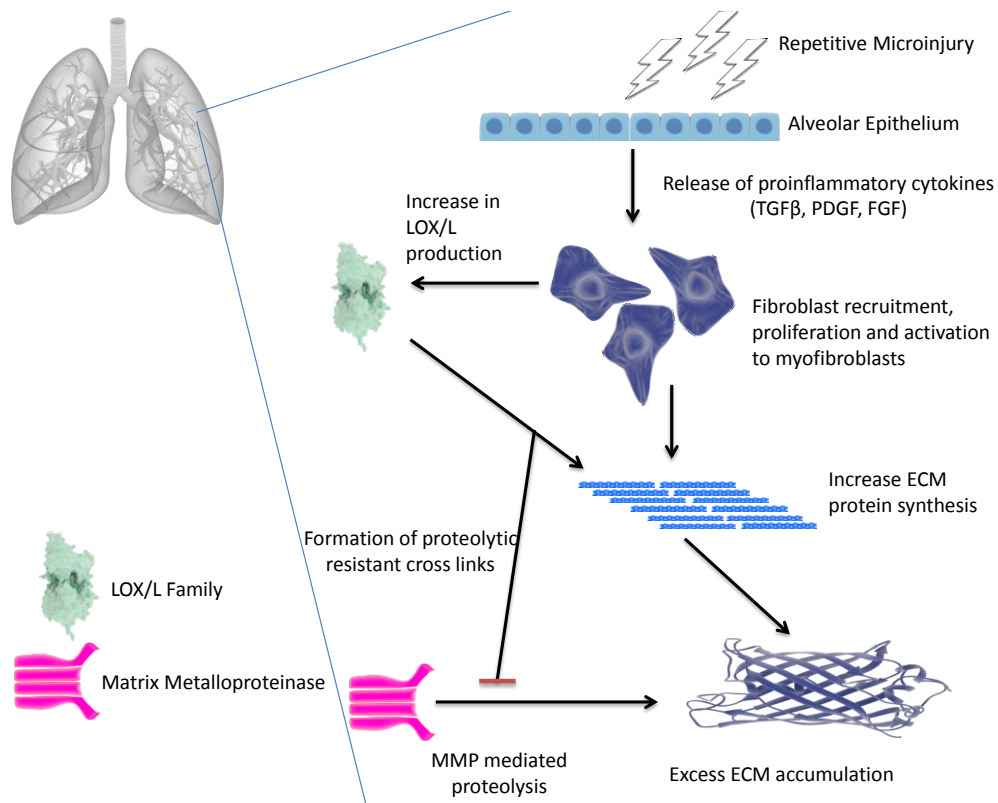


**Figure 1.9 The potential role of the LOXL family in the accumulation of ECM in IPF.** LOX mediates the cross linking of collagen during collagen maturation. Increased LOX/L family expression as described in the literature is hypothesised to increase collagen stabilisation, leading to relative proteolytic resistance compared to normal ECM in IPF.

The mechanism of hydroxylysine cross link formation mediated by the LOX family, may give an insight into the accumulation of ECM in IPF. Furthermore, the elastin lysine cross links could result in impaired pulmonary compliance. In IPF it is plausible that the combination of alveolar epithelial injury, HIF-1 signalling and increased collagen synthesis could all contribute to collagen deposition that is excessively stabilised compared to healthy lung tissue. This mechanism may feed forward into the profibrotic environment described in 1.4.2.2.

## 1.5 Summary

The potential for therapeutic intervention in matrix stabilisation during ECM deposition presents a yet unexplored opportunity in the treatment of IPF. Inhibiting ECM cross linking may allow for increased ECM removal by normal endogenous proteolysis, leading to a decreased decline in lung function of patients.

TG2 in IPF has the potential for formation of  $\alpha$ - $\epsilon$ - $\gamma$  glutamyl lysine cross links which are known to exhibit strong mechanical and proteolytic resistance under normal conditions. Therefore, the increased TG2 expression seen in IPF may contribute to excessive ECM stabilisation and the inability of normal proteolytic cleavage by the MMP family. This would lead to a net increase in ECM, as seen in abundance in the IPF lung.

Excess collagen accumulation is a hallmark of IPF. The LOX family contribution to collagen and elastin stabilisation during deposition may be another therapeutic target. Furthermore, both animal models and IPF fibroblast and epithelial cell cultures show an increase in transcription of LOX. Therefore, increased LOX expression may contribute to excessive stabilisation of extracellular collagen and elastin, resulting in impaired pulmonary compliance and a decrease in lung function.

## **1.6 Hypotheses**

We hypothesise that ECM accumulation in IPF is contributed to by excessive cross-linking of the ECM by Transglutaminase 2 and the LOX family which leads to increased proteolytic resistance, resulting in the impaired proteolysis mechanisms such as MMP's. This reduction in extracellular matrix proteolysis may contribute to the observed net increase in extracellular matrix in the IPF lung.

Inhibiting TG2 or the LOX family of cross-linking enzymes during the formation of IPF matrix may reduce the accumulation of extracellular matrix through a relative increase in proteolysis of extracellular proteins.

## **1.7 Aims**

- To characterise primary IPF derived fibroblast expression of ECM cross linking enzymes through PCR and protein expression levels by ELISA and activity assays.
- To generate control and IPF ECMs suitable for seeding new fibroblast populations
- To analyse the effect of ECM cross linking inhibitors on seeded fibroblast population proliferation, adhesion and apoptosis
- To quantify ECM proteolysis of IPF and normal ECM and assess the influence of cross linking enzyme inhibitors on the rate of proteolysis through radiolabelled hydroxyproline liberation

- To determine the effectiveness of cross linking enzyme inhibitors on reducing total lung collagen levels in the Bleomycin mouse model of fibrosis

## **CHAPTER 2**

### Materials and Methods

## **2 CHAPTER 2: Materials and Methods**

### **2.1 Reagents and Plasticware**

Unless otherwise stated, all following reagents were obtained from Sigma Aldrich (Dorset, UK). All cell culture vessels and assay plates were obtained from Corning/Costar UK Ltd. (High Wycombe, UK).

### **2.2 Antibodies**

Table 2.1 displays the anti-bodies used and their respective suppliers.

<i>Primary Antibodies</i>					
<b><u>Antigen</u></b>	<b><u>Monoclonal/ Polyclonal</u></b>	<b><u>Host</u></b>	<b><u>Isotype</u></b>	<b><u>Product Code</u></b>	<b><u>Supplier</u></b>
S100A4	Monoclonal	Mouse	IgG1	ab93283	Abcam, Cambridge, UK
FAP- $\alpha$	Polyclonal	Rabbit	IgG	ab53066	Abcam, Cambridge, UK
$\alpha$ -Smooth Muscle Actin	Monoclonal	Mouse	IgG2a	A2547	Sigma Aldrich, Dorset, UK
Isotype	Monoclonal	Mouse	IgG1	MAB002	R&D Systems, MN, USA.
Isotype	Monoclonal	Mouse	IgG2a	ab18413	Abcam, Cambridge, UK
Isotype	Monoclonal	Rabbit	IgG	sc-3888	Santa Cruz Biotechnology Inc., CA, USA.
N-Epsilon- Gamma Glutamyl Lysine	Monoclonal	Mouse	IgM	ab424	Abcam, Cambridge, UK
Isotype	Monoclonal	Mouse	IgM	ab18401	Abcam, Cambridge, UK
LOXL3	Polyclonal	Rabbit	IgG	ab122263	Abcam, Cambridge, UK
TG2	Monoclonal	Rabbit	IgG	ab109200	Abcam, Cambridge, UK
CD90 (Thy1)	Monoclonal	Rabbit	IgG	ab92574	Abcam, Cambridge, UK
Anti-Actin $\alpha$ - Smooth Muscle - Cy3™	Monoclonal	Mouse	IgG2a	C6198	Sigma Aldrich, Dorset, UK

**Table 2.1** List of primary antibodies used for immunohistochemistry, immunofluorescence and western blotting within this project with the respective host species and suppliers.

A range of secondary antibodies were also used and their details displayed in Table 2.2. below.

<i>Secondary Antibodies</i>				
<b><u>Antibody</u></b>	<b><u>Isotype</u></b>	<b><u>Conjugate</u></b>	<b><u>Product Code</u></b>	<b><u>Supplier</u></b>
Goat Anti-Mouse	IgG	Alexa 488	ab150117	Abcam, Cambridge, UK
Goat Anti-Rabbit	IgG	Alexa 488	ab150077	Abcam, Cambridge, UK
Goat Anti-Rabbit	IgG	HRP	A0545	Sigma Aldrich, Dorset, UK
Goat Anti-Mouse	IgM	HRP	A-10668	Life Technologies, CA, USA

**Table 2.2** *List of secondary antibodies used in this project for immunohistochemistry, immunofluorescence and western blotting with the list of suppliers.*

### **2.3 Recombinant Proteins**

Human recombinant LOXL3, MMP1, MMP2 and MMP7 were obtained from R&D Systems (MN, USA). Subsequent MMP activation was conducted as described by the manufacturer. Purified TG2 from guinea pig liver was purchased from Sigma Aldrich (Dorset, UK).

### **2.4 Drug Compounds**

Cystamine Dihydrochloride (CyM) was obtained from Tocris Bioscience (Abingdon, UK) for cell culture experiments and for animal studies from Sigma Aldrich (Dorset, UK).  $\beta$ -aminopropionitrile ( $\beta$ APN) was obtained from Sigma Aldrich (Dorset, UK). Bleomycin Sulphate was obtained

through the Clinical Pharmacy, University of Nottingham Hospitals Trust, Queens Medical Centre, Nottingham from Kyowa Kirin Limited, UK.

## **2.5 Cell Culture Reagents**

Dulbecco's modified Eagle medium (DMEM), Dimethyl Sulphoxide, Penicillin-Streptomycin x100 solution and Dulbecco's phosphate buffered saline were obtained from Sigma Aldrich (Dorset, UK). DMEM/F12 nutrient mix, phenol red free media and foetal bovine serum (FBS) was obtained from Life Technologies (CA, USA). Fibroblast Growth Medium was obtained from Promocell (Heidelberg, Germany).

## 2.6 Primary Cells & Cell Lines

Details of all cells used can be found in the table below.

<u>Cell Type</u>	<u>Cell ID</u>	<u>Derivation</u>
Human Airway Smooth Muscle cells	HASM (D0501)	Extracted from human tracheal rings of non-asthmatic patients and characterised by >95% actin staining by immunofluorescence, by Dr. Bo Liu (Division of Respiratory Medicine, University Of Nottingham, UK) according to a previously described method (Daykin et al., 1993).
Normal Human Lung Fibroblasts Control	NHLF (CC-2512)	Obtained from LONZA (MD, USA) These are a commercially available fibroblast cells line from a human adult lung.
Human Pulmonary Fibroblasts Control	HPF (C-12360)	Obtained from Promocell GmbH (Germany). Commercially available pulmonary fibroblasts from a pre-menopausal female.
Human Lung Fibroblasts Control	RS10005	Derived by Nottingham University Hospital, BRU from lung biopsies of patients without IPF.
	ALS09004	
	RS11010	
IPF Derived Human Lung Fibroblasts	RS12020	IPF derived cell lines were donated by Dr. Amanda Tatler (Division of Respiratory Medicine, University Of Nottingham, UK). Lung biopsies were grown out in tissue culture from patients with histopathologist confirmed IPF.
	RS09001	
	RS09004	

**Table 2.3 Primary and commercial cell types using in this project with descriptions of derivation methods for primary cells obtained from biopsy**

## **2.7 Human Tissue Sections**

IPF tissue sections were kindly donated by Dr. Amanda Tatler (Division of Respiratory Medicine, University of Nottingham, UK). Control lung, positive controls and optimisation tissue was donated by Dr. Suzanne Miller (Division of Respiratory Medicine, University of Nottingham, UK) which was collected from the Nottingham Health Science Biobank (Nottingham, UK) with the required ethical approval (08/H0407/1).

## **2.8 Patient Cohort Serum Samples**

Written and informed consent was taken before all procedures were carried out in accordance with the declaration of Helsinki (World Medical, 2013). Samples analysed were those as previously described by Navaratnam et al., of which a total of 45 IPF and 45 age and sex matched controls were assayed (Navaratnam et al., 2014).

## **2.9 Mammalian Cell Culture**

Unless otherwise stated, all cells were cultured in Dulbecco's Modified Eagles Medium (DMEM) (Sigma Aldrich, Dorset, UK) supplemented with 10% v/v foetal calf serum (FCS) (Life Technologies, CA, USA). Cells were incubated in a humidified atmosphere with 5% CO<sub>2</sub> at 37°C. When passaging, cells were detached from culture vessels by trypsinization with Trypsin-EDTA solution 1x (Sigma Aldrich, Dorset, UK), and the trypsin deactivated by addition of DMEM + 10% FCS in equal volume to the trypsin solution. Cell counts were conducted using a Neubauer haemocytometer

and cells stained with 0.4% trypan blue solution (Sigma Aldrich, Dorset, UK) in PBS. Drug treatments were supplemented into the media where stated. CyM was used at a final concentration of 0.5mM,  $\beta$ APN at 1mM or PXS-5120A (Pharmaxis, UK) at 0.02 $\mu$ M in DMEM + 10% FBS. For long term storage cells were frozen at  $\sim 7.5 \times 10^6$  cells/ml in a solution of 10% v/v Dimethyl Sulphoxide (DMSO) in FBS. Vials were cooled at  $-1^\circ\text{C}/\text{min}$  to  $-80^\circ\text{C}$  in the freezer and left for 24 hours before transfer to liquid nitrogen. Recovery of cryopreserved cells was performed by warming frozen cryovials in a water bath at  $37^\circ\text{C}$  until thawed. The cell suspension was transferred to warmed DMEM + 10% FCS and spun at 200g for 5 minutes to form a pellet, then resuspended in DMEM + 10% FCS and seeded into a T75 culture vessel. This was transferred to a humidified atmosphere incubator with 5%  $\text{CO}_2$  at  $37^\circ\text{C}$  overnight to allow cells to adhere. The following morning, media was aspirated and replaced with fresh DMEM + 10% FCS.

## **2.10 Total RNA Extraction**

Total RNA was extracted from cultures at approximately 80% confluence in 6 well plates ( $\sim 1 \times 10^6$  cells) using the GenElute™ Mammalian Total RNA Miniprep Kit (Sigma Aldrich, Dorset, UK). On-Column DNase I Digestion Set (Sigma Aldrich, Dorset, UK) was used during RNA extraction to remove genomic DNA contamination and prevent false positive PCR traces. RNA was eluted in 30ul of the elute solution and analysed on a NanoDrop (Fisher Scientific, UK) for quantity and quality.

## **2.11 cDNA Synthesis**

cDNA was synthesised using Superscript First-Strand Synthesis System (Invitrogen, UK) to the manufacturers specifications.

## **2.12 Real Time PCR**

Quantitative RT-PCR was conducted to assess the relative abundance of gene transcripts. Brilliant III SYBR Green QPCR Master Mix (Agilent Technologies Ltd., USA) or SensiFAST SYBR No-ROX Master Mix (Bioline Reagents Ltd., UK) were used as master mixes when plating out PCR reactions. Specific details regarding master mix will be represented in results sections where appropriate. Reactions were run using the Mx3005P qPCR System with MxPro Software (Agilent Technologies, CA, USA). Predesigned KiCqStart SYBR Green primers were obtained from Sigma Aldrich (Dorset, UK). PCR data was analysed using the  $2^{-\delta_{ct}}$  method (Livak and Schmittgen, 2001, Rao et al., 2013) which provides normalisation to an endogenous reference in differing cDNA added to the reaction mixture. As total copy number is not a goal of these experiments, relative quantification is suitable as no standard curve is needed. Internal controls were validated to show what there was little variation of housekeeping gene expression with experimental protocols.

## **2.13 Data Analysis, Statistics and Graphical Software**

Unless otherwise stated, all data were processed using Microsoft Excel 2010 (Microsoft, USA) and graphed and analysed using Prism V6 (GraphPad Software, USA). Unless otherwise stated, n=3 experimental data are presented with  $\pm$  standard deviation (SD). Statistics were performed on data using Prism V6 (GraphPad Software, USA). Normality testing was conducted where appropriate to ensure the correct parametric or non-parametric test was conducted. When comparing two groups either a Students t-test (parametric) or Mann Whitney test (non-parametric) was conducted using the 'Analyse' function in Prism.

The two-way ANOVA was also used to determine the main contributory effect of the experimental design through classifying data in two categories such as dose and time. This also allowed for analysis of interaction between the independent variables. Post-hoc tests were carried out in one-way ANOVAs in order to identify the groups that power the significant variance within the analysed population. These consisted of either Tukey's post-hoc test, where all columns were compared to each other or Dunnet's when columns were compared to a selected control column.

### **2.13.1 Power Calculations for Animal Work**

Power calculations were performed using PS version 3.1.2 (Dupont and Plummer, 1990). Previous work from the Jenkins group (University of Nottingham, UK) was used to calculate the values for  $\alpha$  at 0.001,  $\delta$  at 500,

$\sigma$  at 200 with a power of 0.95. This yielded a sample size of 8 for animal work with a standard deviation assumed of 200ug hydroxyproline and the difference of the group means of 500ug hydroxyproline. This enables us to study 8 pairs of subjects to be able to reject the null hypothesis that this response difference is zero with probability (power) 0.95. The Type I error probability associated with this test of this null hypothesis is 0.001.

### **2.14 Senescence Assay**

Cell cultures were stained using the  $\beta$ -Galactosidase Staining Kit (Cell Signalling Technology, Inc., USA) and imaged on a Nikon Diaphot 300 Inverted Microscope (Nikon UK Limited, UK)

### **2.15 Extracellular Matrix Preparation**

Cultures were grown in complete media to confluence and for a further 3 days to ensure sufficient matrix deposition. Culture media was aspirated and frozen at  $-20^{\circ}\text{C}$  for later analysis. Cultures were washed with Phosphate Buffered Saline (PBS). Decellularization was adapted from a previously described method (Lu et al., 2012).

Cultures were incubated at room temperature with 50mM  $\text{NH}_4\text{OH}$  + 0.05% Triton X-100 (Sigma Aldrich, Dorset, UK) in PBS for 15 minutes or until cells were no longer visible under 10x magnification on a Nikon Diaphot 300 Inverted Microscope (Nikon UK Limited, UK). Ammonium hydroxide and triton solution was aspirated and the cultures briefly washed with

50mM NH<sub>4</sub>OH. Following this, all plates were washed 3 times with PBS. Upon completion, all liquid was aspirated and all dishes were incubated at 37°C with 20 U/mL DNase I (Sigma Aldrich, Dorset, UK) to remove DNA contamination for 1 hour then washed 3 times with PBS before further experimentation.

### **2.16 Radio-labelling of ECM**

Culture medium was supplemented with L-[2,3,4,5-<sup>3</sup>H]-Proline to a final activity of 1 µCi/ml (Perkin Elmer, MA, USA) during matrix synthesis to enable incorporation of proline to collagen and subsequent conversion to hydroxyproline by prolyl hydroxylase. Matrix labelling was confirmed by matrix extraction and liquid scintillation counting as described in 2.17 and 2.19 respectively.

### **2.17 ECM Extraction**

Due to the variation in solubility of matrix proteins (Ngoka, 2008), a 2 stage extraction process was used as described by Ngoka (2008). However, reagents were modified slightly to allow more rapid processing.

#### *Extraction Buffer 1*

*Radioimmunoprecipitation Assay Lysis Buffer (modified)*; Base Ingredients (PBS, pH 7.4, SDS, 0.1%, Na-deoxycholate, 0.25%) Complete Mini Protease Inhibitor Cocktail + EDTA (1 tablet per 10ml extraction buffer).

#### *Extraction Buffer 2*

*Urea Lysis Buffer* (PBS, pH 7.4, 5.0 M Urea, 2.0 M Thiourea, 50 mM DTT, 0.1% SDS).

Buffer 1 was applied to the matrix preparations at 1ml per 9.5cm<sup>2</sup> (single well of 6 well plate) and incubated at room temperature for 5 minutes on a platform rocker. The liquid was then aspirated and collected in 1.5ml eppendorf tubes. To minimise loss of protein, buffer 2 was directly applied following aspiration of buffer 1 with no wash stage in between. This was applied at 1 ml per 9.5cm<sup>2</sup> plate and incubated for 5 minutes at room temperature on a platform rocker. The plate was scraped with a cell scraper and liquid was then aspirated and collected in 1.5ml eppendorf tubes. Each matrix extract was subject to dialysis using Slide-A-Lyzer G2 0.5mL/2K MWCO cassettes (Thermo Fisher Scientific Inc., USA) in PBS for 16 hours. All samples were stored at -20°C until further use.

### **2.18 ECM Proteolytic Digests**

Radio labelled ECMs were exposed to a range of proteases to determine the rate of degradation. This is a method for determining matrix collagen stability in relation to the amount of cross linking present. Cultures were supplemented as in section 2.1.16 and decellularized as described in 2.1.15. Following processing, activated recombinant human MMP-1, 2 and 7 were diluted in serum free DMEM/F12 to various concentrations and added to the matrices. Serum free DMEM with p-aminophenylmercuric acetate (APMA) (Sigma Aldrich, Dorset, UK) was used as a vehicle control and serum free DMEM with complete Mini Protease Inhibitor (Roche, USA)

as a negative control. ECM's were incubated at 37°C to various time points to allow the protease mediated digestion of the radio labelled extracellular proteins. Quantification of proteolysis was conducted through measuring the radioactivity of the digest solution using liquid scintillation counting.

### **2.19 Liquid Scintillation Counting**

Following incubation, ECM digest plates were gently agitated for 15 seconds and the assay buffer transferred to scintillation vials. 10mls of Ultima Gold XR Scintillation fluid (Perkin Elmer, MA, USA) was added to each vial and the radioactivity read on an LKB Wallac 1214 Rackbeta Liquid Scintillation Counter (Perkin Elmer, MA, USA) set for tritium and counted for 1 minute per vial.

### **2.20 BioRad Total Protein Assay**

Total protein assays were carried out using the protein-dye binding method as described by Bradford (Bradford, 1976). The Bio-Rad Total Protein Assay Kit was used to detect total protein levels in samples. The kit was used to the manufactures specifications with bovine serum albumin used for the standard curve. Assay plates were read using the Flexstation 3 (Molecular Devices, USA).

### **2.21 BCA Total Protein Assay**

Similar to section 2.20, the BCA uses a colourimetric detection method for the quantification of total protein levels in biological samples. The Pierce BCA Protein Assay Kit (Thermo Fisher Scientific Inc., UK) was used to

manufacturers specifications and the assay plates were read using the Flexstation 3 (Molecular Devices).

### **2.22 Acid Hydrolysis of Collagen**

ECM samples and mouse lung homogenates were subjected to acid hydrolysis for the quantification of hydroxyproline residues as an indicator of total collagen levels. Samples and the collagen standard from the kit mentioned in section 2.24 were diluted 1:1 (v/v) with 12M HCl (final concentration 6M HCl) and incubated for 20 hours at 95 °C in a thermoblock. Following incubation, samples were cooled to room temperature and spun in a centrifuge for 10 minutes at 13,000 x g. The supernatant was collected in Eppendorf tubes and kept for further analysis.

### **2.23 Total Collagen Assay**

The total collagen assay functions on the basis of colourimetric detection of hydroxyproline residues. The formation of hydroxyproline requires a proline residue bound into a collagen or elastin molecule. Prolyl hydroxylase does not affect unbound proline. This post translational modification is only found in collagen and elastin in mammals and measuring it is a direct, quantitative way of determining total collagen levels. The acid hydrolysed samples were assayed using the Total Collagen Assay Kit (Quickzyme Biosciences, NL) and performed to the manufacturers specification.

## **2.24 Collagen Synthesis Assay**

Medium was supplemented with tritiated proline as described in section 2.16 and decellularized as described in 2.15. ECM was then extracted as described in section 2.17. Samples were transferred to scintillation vials. 10mls of Ultima Gold XR Scintillation fluid (Perkin Elmer, MA, USA, MA, USA) was added to each vial and the radioactivity read as in section 2.19.

## **2.25 SDS Page**

Samples of 100ng total protein were mixed 1:1 with 2x Western Blot loading dye (3.2ml 1M Tris-HCl (pH 6.8), 8ml 10% SDS, 4ml 100% glycerol, 2ml  $\beta$ -mercaptoethanol, 160 $\mu$ l 5% bromophenol blue solution (in distilled water) and 2.8ml distilled water) and denatured at 95°C for 5 minutes.

Prepared samples were transferred to Mini-PROTEAN TGX Gels with polyacrylamide percentages of either 10% or Any kD™ (Biorad, UK). Kaleidoscope Prestained Standard (Biorad,UK) was used as a ladder to approximate molecular weights. Gels were resolved at 200 volts until the dye front reached the bottom of the gel.

## **2.26 Western Blotting**

A Mini-PROTEAN (Biorad, UK) tank was filled with transfer buffer (25mM Tris base; 192mM glycine) at 4°C and placed into a basin containing ice. An ice pack was further added into the tank to keep the solution cold during transfer. Gel cassettes were opened, the stacking gel removed and the

gels equilibrated in transfer buffer for 15 minutes. Hybond-P PVDF membrane (GE Healthcare Life Sciences, UK) was cut to size and submerged in 100% methanol for 5 minutes, prior to being placed in transfer buffer for 10 minutes, along with the transfer cassette sponges. Transfer cassettes were assembled and placed into the tank containing chilled transfer buffer, and submerged. The transfer was run at 100V, 350mA for 1 hour. Upon completion, membranes were removed and washed with 0.01% PBS-T for ten minutes.

Membranes were blocked with 5% non-fat dry milk in 0.01% PBS-T for 1 hour at room temperature on a platform rocker. Following this, primary antibodies were diluted in blocking solution, the block removed from the membranes and the antibody solutions added. This was left overnight at 4°C.

The following morning, the primary antibody solution was removed and the membrane washed 3 times with 0.01% PBS-T for 10 minutes. Secondary HRP conjugated antibodies were diluted in block solution and added to the membrane following the final wash. This was incubated at room temperature on a platform rocker for 1 hour. Following incubation the membrane was washed a further 3 times as described above.

## **2.27 ECL Detection**

Amersham ECL Western Blotting Detection Reagents (GE Healthcare Life Sciences, UK) were used to manufacturers specifications with a total volume of 1ml per membrane in a dark room. Membranes were then sealed in a light tight cassette with Amersham Hyperfilm (GE Healthcare) for exposure. Blots were exposed for optimal band density while maintaining a low background.

ECL film was then developed using sequential Carestream® Kodak® autoradiography GBX developer/replenisher (Sigma Aldrich, Dorset, UK). Followed by a wash in dH<sub>2</sub>O, then submerged in Carestream® Kodak® Fixer (Sigma Aldrich, Dorset, UK) until the film became transparent. This was followed with a final wash in dH<sub>2</sub>O before hanging to dry.

## **2.28 Densitometry**

Blots were scanned and imported into GIMP 2.8 and band density determined using the histogram function. All bands were normalised to an average background signal for each membrane. Data was then processed as stated in 2.13

## **2.29 Silver Staining of SDS-PAGE gels**

Gels were silver stained using the Silver Stain Plus Kit from Biorad (UK). All reagents were reconstituted as per manufacturer's instructions and a 5% (v/v) acetic acid stop solution was premade. Resolved gels were

trimmed of the stacking gel and placed in a fixative solution of 40% methanol & 10% acetic acid (v/v) in PBS. This was incubated for 30 minutes at room temperature on a rocker platform. Following this the fixative was removed and the oxidiser reagent was added. This was incubated for a further 5 minutes at room temperature.

Oxidiser was removed and the gels washed with 500ml deionised water, 6 times for 2 minutes per wash. The wash was then removed and the gels submerged in the silver reagent for 20 minutes under gentle agitation on the platform rocker. This was removed and the gels washed with 500ml deionised water for 30 seconds. 250mls of supplied developer reagent was added to the gels. This was incubated for 30 seconds until a brown precipitate appeared. At this point the developer was changed and the gels continued developing until the desired intensity of staining was reached. Developer was removed and the stop solution was added and left for 15 minutes before being removed and the gels washed prior to imaging on GeneGenius Gel Doc using the GeneSnap software (Syngene, UK).

### **2.30 Proteome Profiler**

To efficiently screen a diverse range of proteases in conditioned media samples, the Proteome Profiler Human Protease/Protease Inhibitor Array (R&D Systems, UK) was used. This dot blot based assay enables efficient screening of a large number of proteases from a single sample using antibody capture on pre-printed membranes. All reagents below are contained within the kit supplied.

Prior to beginning the assay, all reagents were reconstituted as detailed in the manufacturer's protocol. 2mls of blocking buffer was added to each membrane and incubated for 1 hour at room temperature. Samples were prepared by adding 1ml of fibroblast conditioned serum free media to 500µl of assay buffer. To this mixture, 15µl of detection antibody cocktail was also added. This mixture was incubated for 1 hour at room temperature while the membranes were blocking. After 1 hour, blocking agent was aspirated from the membranes and the 1.5mls of sample/antibody mixtures were added and incubated overnight at 4°C on a rocking platform.

The following morning, each membrane was removed from the container and placed into a clean one containing 20mls of wash buffer and placed on a platform rocker for 10 minutes. This wash process was repeated 3 times. The HRP-Streptavidin was diluted to a working concentration in assay buffer as directed in the manufacturer's protocol and 2mls added to the membranes. This was incubated for 30 minutes at room temperature before the membranes being washed 3 more times in wash buffer.

ECL was carried out as detailed 2.27 the same as a western blot. Densitometry was performed as described in 2.28 and each duplicate of antigens averaged. The average background was subtracted from the pixel densities of samples. The reference spots on the membranes serve as a positive control.

### **2.31 ELISAs**

Human TG2 ELISAs were obtained from Cloud Clone Corps (USA). Human LOXL3 ELISAs were obtained from Cusabio. The sample volume used was 100ul undiluted cell culture conditioned media with the standard curve standard ranging from 20ng/ml to 0.156ng/ml and including a substrate only blank. Life Science (China). The LOXL3 ELISA's sample volumes were 100ul of undiluted conditioned media from tissue culture, and the standard range set between 2000pg/ml and 31.25pg/ml by serial dilution along with a substrate only blank. Plates were read on a Flexstation 3 (Molecular Devices, USA) with standard curves set and sample concentrations back calculated in the SoftMax Pro version 5.4 software (Molecular Devices, USA). All ELISA's were carried out to their respective manufacturer's protocols

### **2.32 Transglutaminase Activity Assay**

Total transglutaminase activity was determined using the Transglutaminase Assay Kit (Sigma Aldrich, Dorset, UK). The kit was performed to manufactures specification.

### **2.33 Collagen Coating of Cell Culture Vessels**

Type I human placental collagen (Sigma Aldrich, Dorset, UK) was reconstituted in sterile 0.02M acetic acid to a stock concentration of 50ug/ml. This was diluted in sterile 0.02M acetic acid to a working concentration of 32ug/ml and 50ul pipetted into each well of a 96 well plate

and incubated at room temperature for 1 hour. Following incubation, the collagen solution was gently aspirated and the wells washed three times with 100ul of sterile PBS. Plates were left to air dry in the MSC overnight before seeding with cell populations.

### **2.34 Adhesion Assay**

Medium was aspirated from a flask of P4 NHLF's and replaced with CellTracker Green CMFDA Dye (Life Technologies, CA, USA) at 5µM final concentration in DMEM+10%FCS for 30 minutes. Cells were then trypsinised and resuspended in serum free DMEM and seeded onto the prepared matrices and incubated for 2 hours at 37°C. Following incubation, media and unadhered cells were aspirated and the plate washed once with PBS, before adding 200µl per well PBS and reading the average fluorescence of each sample at Abs. 492nm/517nm using flexstation 3 (Molecular Devices).

### **2.35 MTT Proliferation Assay**

$0.1 \times 10^6$  cells were plated out into 12 well plates and left to recover overnight as described in section 2.9. After adhesion, cells were growth arrested in serum free DMEM for 24 hours. Treatments were then applied for the designated experimental time. Following treatment a solution of 0.5mg/ml Thiazolyl Blue Tetrazolium Bromide (MTT) (Sigma Aldrich, Dorset, UK) was prepared in the DMEM/F12 phenol red free media (Life Technologies, CA, USA). Existing culture media was aspirated and replaced with 1ml of MTT solution and returned to the incubator for 6 hours.

Following incubation, MTT solution was gently aspirated and 1ml of isopropanol added to each well to dissolve the formazan crystals. Each sample was then aliquoted into 200ul triplicates in a 96 well plate and the absorbance read at 595nm, with background subtraction at 690nm, in the Flexstation 3 (Molecular Devices, CA, USA).

### **2.36 EdU Proliferation Assay**

To determine the number of proliferating cells through an independent method, a DNA synthesis approach was taken. Cells were plated for EdU assays the same as described for MTT assays in section 2.32. To directly measure new DNA synthesis the Click-iT® EdU Microplate Assay was used (Life Technologies, CA, USA) to manufacturers specifications with a final concentration of 10µM EdU and incubation time of 24 hours. The 96 well plate was read with excitation/emission of 568/585nm using the Flexstation 3 (Molecular Devices).

### **2.37 TUNEL Assay for Apoptosis**

DNA fragmentation was determined using the In Situ Cell Death Detection Kit (fluorescein) from Roche Diagnostics (UK). DNA fragmentation is determined using fluorescein-dUTP. The number of cells which stain positive under confocal microscopy are expressed as a percentage of the total cells in a fixed field of view. Slides were then imaged using the Improvision spinning disc confocal microscope using Volocity 3D image analysis software V6.3 (Perkin Elmer, MA, USA).

### **2.38 Immunofluorescence**

Cultures were grown to ~70-80% confluence then medium was aspirated and the contents of each well of the chamber slide washed 3 times with PBS. Cells were then fixed with 3.75% Formaldehyde (Sigma Aldrich, Dorset, UK) by incubation at room temperature for 15 minutes. Formaldehyde was then aspirated and the wells were washed 3 times with PBS. Cells were then permeabilised to expose the intracellular antigens by incubating with 0.15% Triton X-100 (Sigma Aldrich, Dorset, UK) in PBS for ten minutes, followed by aspiration and washing 3 times with PBS.

Cells were blocked with 10% Goat Serum (Sigma Aldrich, Dorset, UK) in 1% BSA/PBS overnight at 4 °C. Antibody dilution for all antibodies used was 1:250, with the antibody being diluted in the blocking agent. Isotype controls were also diluted to the same concentrations and carried out in the same method as the primary antibodies. Antibodies used are shown in Table 2.1 and Table 2.2.

Blocking agent was aspirated and the wells washed a further 3 times with PBS. The primary antibodies were added to the chamber slides and incubated at room temperature for 1 hour. This was then aspirated and slides washed 3 times with PBS. Secondary fluorophore-conjugated antibodies were added at a dilution of 1:250 and left to incubate for 1 hour at room temperature on a platform rocker, protected from light.

The secondary antibody was aspirated and the chambers washed 3 times with PBS. At this point, Cy-3 directly conjugated anti  $\alpha$ -SMA (Sigma Aldrich, Dorset, UK) was added to the cells at a dilution of 1:250.

This was further incubated for 1 hour as described for the secondary antibodies before aspiration and washing with PBS 2 times. 4, 6-diamidino-2-phenylindole dihydrochloride (DAPI) (Sigma Aldrich, Dorset, UK) at a stock concentration of 1mg/ml in dH<sub>2</sub>O was added to the PBS at 1:1000 dilution to allow visualisation of the nuclei, and left for 10 minutes before aspirating and washing 3 times with PBS.

Chamber sections of the slides were removed and slides were mounted with a cover slip using Dako Fluorescent Mounting Medium (Dako, Denmark). Slides were then imaged using the Improvion spinning disc confocal microscope using Volocity 3D image analysis software V6.3 (Perkin Elmer, MA, USA).

### **2.39 Immunohistochemistry**

All antibodies for Immunohistochemistry (IHC) were obtained from Abcam, Cambridge, UK and shown in table 2.1.1. 2.5% horse serum, citrate antigen unmasking solution and secondary antibody kits; Impress Anti-Mouse and Impress Anti-Rabbit were obtained from Vector Laboratories (CA, USA). Paraffin embedded tissue was obtained as described in 2.7.

Slides were placed into a coplin jar containing HistoClear (National Diagnostics, USA) for 5 minutes and transferred to another jar with fresh

Histoclear for a further 5 minutes. Slides were rehydrated in a graded alcohol series; 2 minutes in 100% ethanol, 2 minutes in 95% ethanol; 2 minutes in 70% ethanol. Finally slides were washed twice for 5 minutes each in dH<sub>2</sub>O, then PBS.

Antigen retrieval was conducted using a steamer and low pH Citrate based Antigen Unmasking Solution. Antigen unmasking solution was prewarmed in a microwave to 100°C. Also the same solution was added to a Breville ITP181 steamer and heated. Slides were placed into heated antigen unmasking solution in a rack and the rack wrapped in cling film. This was then placed into the preheated steamer and left at 100°C for 15 minutes. When this time had elapsed, the steamer was turned off and left to cool for 10 minutes.

Following this, slides were removed and washed two times for 5 minutes each in dH<sub>2</sub>O before being placed in a solution of 3% hydrogen peroxide for 10 minutes to quench endogenous peroxidases. When this time had elapsed, slides were washed two times each for 5 minutes in PBS.

Slides were then blocked using 2.5% horse serum in for 1 hour at room temperature. Following incubation slides were wiped using a tissue avoiding the tissue section to remove the blocking agent. Primary antibodies were diluted in 2.5% horse serum and pipetted onto the tissue section and incubated for 1 hour at room temperature. Slides were washed 3 times in 0.01% PBST for 5 minutes each.

Vector ImmPress HRP polymer detection kits were used as premade anti-mouse and anti-rabbit secondary antibody solutions (Vector Laboratories, CA, USA). 3 drops were added to each slide to cover the tissue section and incubated for 1 hour at room temperature. Slides were then washed 3 times for 5 minutes each in 0.01% PBST. ImmPACT DAB Peroxidase (HRP) Substrate kit (Vector Laboratories, CA, USA) was prepared by adding 30  $\mu$ l of ImmPACT DAB Chromogen concentrate to 1 ml ImmPACT DAB diluent. This HRP substrate was pipetted onto the tissue sections and incubated at room temperature for 5 minutes before washing 3 times in distilled water. Slides were counterstained for 30 seconds with haematoxylin solution according to Mayer (Sigma Aldrich, Dorset, UK). After the 30 seconds slides were placed into a bath containing a constant flow of tap water for 10 minutes.

Slides were dehydrated through an alcohol series; 2 minutes in 70% ethanol; 2 minutes in 95% ethanol; 2 minutes in 100% ethanol. Slides were placed into histoclear for a further 2 minutes and wiped carefully avoiding the tissue.

2 drops of VectaMount Permanent Mounting Medium (Vector Laboratories, CA, USA) was placed onto the slide and a cover slip lowered carefully over the tissue, removing all air bubbles. Edges of the slide were then wiped and left to set for 24 hours at room temperature. Slides were imaged on Nikon Diaphot 300 Inverted Microscope (Nikon UK Limited, UK).

## **2.40 Scanning Electron Microscopy**

Cell cultures were grown in 12 well plates with a glass cover slip in the base of the well in conditions as stated in 2.9. and decellularization conducted as described in 2.15 Unless otherwise stated all reagents were obtained from Sigma Aldrich (Dorset, UK) and all processing was conducted in a fume hood.

Media was aspirated and cultures gently washed with PBS. Wash was aspirated and replaced with a 1ml of 3% glutaraldehyde and plates placed in a sealed container overnight at room temperature. The following morning, the glutaraldehyde was removed and samples washed three times, each for 15 minutes with PBS. When the final wash was aspirated, it was replaced with 1ml of 1% Osmium Tetroxide and incubated in the fume hood for 2 hours. When incubation time had elapsed, samples were washed three times, each for 15 minutes with dH<sub>2</sub>O.

Samples were then dehydrated through an ethanol gradient; 25%, 50%, 70%, 90% and 95% each for ten minutes; and finally 100%, three times each for 5 minutes. Samples were transferred to the Histopathology Department, Queens Medical Centre, University of Nottingham, NG7 2UH. There they underwent critical point drying using liquid CO<sub>2</sub> to remove any remaining moisture and they were gold coated using a sputter coater before being transferred back for imaging. Samples were imaged on a JEOL 6060LV variable pressure scanning electron microscope (Jeol Ltd, UK).

## **2.41 Ethical Statement for Animal Use**

All animal work was approved by the Animal Welfare and Ethical Review Board (AWERB) of the University of Nottingham (UK) and conducted in accordance with all terms of the Establishment, Project and Personal Licences issued by the Secretary of State for the Home Office. Consistent with all national and international law, studies were carried out as detailed in the Animal [Scientific Procedures] Act 1986 (Amended Regulations 2012) (ASPA), Animal Welfare Act 2006, Directive 2010/63/EU, the LASA guidelines and in respect to the 3 R's. Work was performed under licence number RGJ 40/3709 using the 19b3 protocol.

## **2.42 Animals and Husbandry**

C57BL/6 Mice were obtained from Charles River Laboratories (Wilmington, Mass. USA.) at age 6 – 8 weeks old. Animals were housed in a Specific Pathogen Free (SPF) environment in the Bio Support Unit, University of Nottingham, UK. Mice were randomly divided into a maximum of 4 mice per cage. Cages used were Techniplast GR500 Individually Vented Cages (IVC) at 21 °C and 50% humidity with environmental enrichment. Bedding consisted of Nestpak grade 5 sawdust (Datesand Ltd., UK) and Sizzle-Nest (Scanbur, Denmark). Mice were fed *ad libitum* 2018S Teklad Global 18% Protein Rodent Diet (Harlan Laboratories, UK) with constant access to fresh, filtered water and maintained on a 12 hour light, 12 hour dark cycle. Food and bedding was sterilised by autoclaving prior to use. Following

<b><u>Condition</u></b>	<b><u>Liver</u></b>	<b><u>Lung</u></b>
Control	Untreated	Untreated
Control+CyM	CyM 0.5mM	CyM 0.5mM
Bleomycin	Bleomycin (15ug/ml)	Bleomycin (5ug/ml)
Bleomycin+CyM	Bleomycin+CyM	Bleomycin+CyM
Bleomycin+CyM t+23	Bleomycin+CyM for 1 hour	Bleomycin+CyM for 1 hour

receipt of the animals, they were left in their new environment for 5 days to acclimatise before any experimental work began.

### **2.43 Ex Vivo TG2 activity in Bleomycin injured tissue**

Lung and liver was harvested from three 8 week old C57BL/6 mice and dissected into 3mm cubes. These were placed into 6 well plates in serum free DMEM overnight. The following morning media was aspirated and media containing DMEM + 1% Insulin-Transferrin-Selenium (Gibco) + 100U/ml penicillin + 0.1mg/ml streptomycin (Sigma Aldrich, Dorset, UK). Bleomycin was added to non-control samples at 5ug/ml on the lung samples and 15ug/ml on liver samples. This was chosen as liver samples were approximately three times heavier per cube than lung tissue CyM was added to a final concentration of 0.5mM to one of the non-Bleomycin treated samples and to one of the Bleomycin treated. Samples were incubated in humidified atmosphere with 5% CO<sub>2</sub> at 37°C for 23 hours. CyM was added to a further tissue sample at t+23 hours. Incubation was resumed for another hour before all media was harvested for assay. Final conditions for the experiment are shown in Table 2.4 below.

**Table 2.4. Ex Vivo culture conditions of C57BL/6 lung and liver.** Lung and liver samples were cultured in technical triplicates per mouse. Untreated media base ingredients; DMEM + 1% Insulin-Transferrin-Selenium (Gibco) + 100U/ml penicillin + 0.1mg/ml streptomycin; subsequent conditions include addition of CyM to a final

concentration of 0.5mM, Bleomycin to either 15µg/ml in liver samples and 5µg/ml for lung samples. Bleomycin+CyM t+23 denoted addition of CyM to Bleomycin treated tissue at 23 hours post Bleomycin exposure.

Transglutaminase activity was assayed immediately following harvest as described in 2.40. Data were normalised per mg of tissue.

#### 2.44 Bleomycin Model of Fibrosis

All mice were anaesthetised with 2.5% inhaled isoflurane in a stream of oxygen (AB-G), weighed and ear marked. All mice received a single oropharyngeal administration of 60 IU Bleomycin (2mg/kg) in 50ul 0.9% sterile PBS or PBS only. All mice were closely monitored for full recovery and checked for health and weight loss exceeding 25% of starting weight once daily for 7 days and thereafter as required but minimum twice weekly. Bleomycin dose is based on a weight of 30g mouse. Day 0-14, during the inflammation stage, mice were observed for any deterioration in health before administration of experimental CyM.

#### 2.45 Murine Experimental Procedures

Mice were randomly allocated to each treatment group as shown in Table 2.5 and

Time Course 2 (100mg/kg)			
Time point	Group	Treatment	Number of animals
TP1	1	Saline + Saline (11x ip start d14)	2
	2	Saline + CyM (11x ip start d14)	2

	3	Bleomycin + Saline (11x ip start d14)	4
	4	Bleomycin + CyM (11x ip start d14)	4
TP2	1	Saline + Saline (11x ip start d24)	2
	2	Saline + CyM (11x ip start d24)	2
	3	Bleomycin + Saline (11x ip start d24)	4
	4	Bleomycin + CyM (11x ip start d24)	4
TP3	1	Saline + Saline (11x ip start d34)	2
	2	Saline + CyM (11x ip start d34)	2
	3	Bleomycin + Saline (11x ip start d34)	4
	4	Bleomycin + CyM (11x ip start d34)	5

**Table 2.6.** Two separate time course experiments were conducted both using the model as stated in section 2.44. Two doses of CyM were administered by IP injection at 40mg/kg and 100mg/kg respectively. To allowed us to study the effect of CyM at both early, active and late fibrosis as well as the effect of two different doses.

Time Course 1 (40mg/kg)			
Time point	Group	Treatment	Number of animals
TP1	1	Saline + Saline (10x ip start d14)	2
	2	Saline + CyM (10x ip start d14)	2
	3	Bleomycin + Saline (10x ip start d14)	4
	4	Bleomycin + CyM (10x ip start d14)	5
TP2	1	Saline + Saline (10x ip start d24)	2
	2	Saline + CyM (10x ip start d24)	2
	3	Bleomycin + Saline (10x ip start d24)	3
	4	Bleomycin + CyM (10x ip start d24)	4
TP3	1	Saline + Saline (10x ip start d34)	2
	2	Saline + CyM (10x ip start d34)	2
	3	Bleomycin + Saline (10x ip start d34)	5
	4	Bleomycin + CyM (10x ip start d34)	5

**Table 2.5: Experimental groupings of mice for Time Course 1 (40mg/kg).** IP=Intraperitoneal injection; CYM=Cystamine Dihydrochloride; d=day post Bleomycin.

Time Course 2 (100mg/kg)			
Time point	Group	Treatment	Number of animals
TP1	1	Saline + Saline (11x ip start d14)	2
	2	Saline + CyM (11x ip start d14)	2
	3	Bleomycin + Saline (11x ip start d14)	4
	4	Bleomycin + CyM (11x ip start d14)	4
TP2	1	Saline + Saline (11x ip start d24)	2
	2	Saline + CyM (11x ip start d24)	2
	3	Bleomycin + Saline (11x ip start d24)	4
	4	Bleomycin + CyM (11x ip start d24)	4
TP3	1	Saline + Saline (11x ip start d34)	2
	2	Saline + CyM (11x ip start d34)	2
	3	Bleomycin + Saline (11x ip start d34)	4
	4	Bleomycin + CyM (11x ip start d34)	5

**Table 2.6 Experimental groupings of mice for Time Course 2 (100mg/kg).** IP=Intraperitoneal injection; CYM=Cystamine Dihydrochloride; d=day post Bleomycin.

Following bleomycin installation mice received intraperitoneal (IP) injection of 100µl saline or CyM once daily for 10 consecutive days during time course (TC) 1 and 11 for time course 2, starting at various time points (TP), precisely d14, d24 and d34 (**Figure 2.1** and **Figure 2.2** respectively). The final IP in time course 2 was administered 90 minutes before sacrifice to allow determination of the longevity of biological activity of CyM. The day after the last IP (TC1) or 90 minutes after (TC2), mice were sacrificed by terminal anaesthesia (AC), described in section 2.46, for tissue and blood collection as specified in the diagram, precisely on d24, d34 and d44. The dose of CyM was calculated based on an average

weight of bleomycin treated mice at the starting point of each IP treatment series.

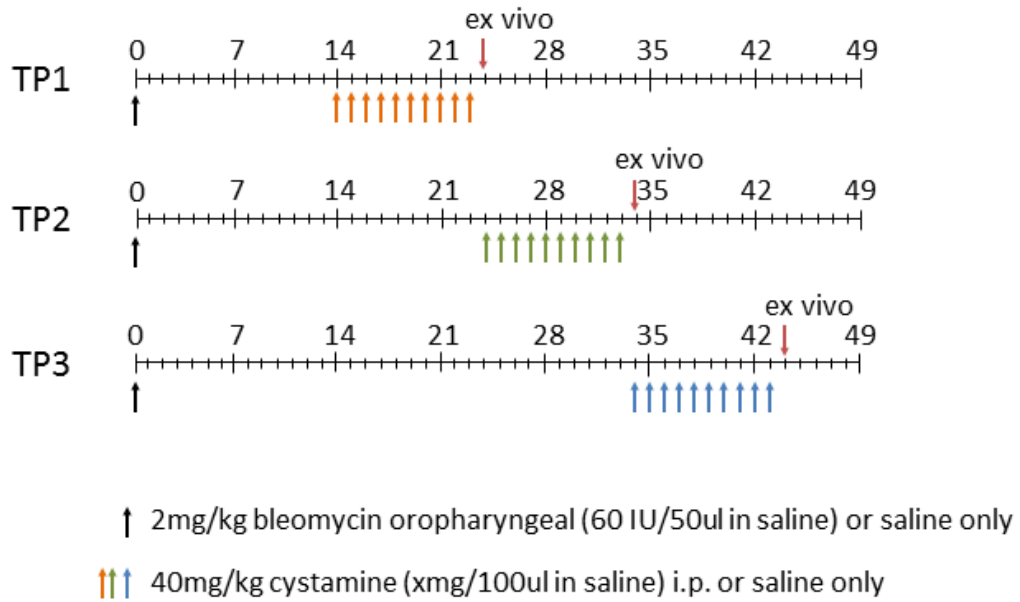


**Figure 2.1 Schematic diagram of treatment of mice in Time Course 1 (40mg/kg).** Day 0 shows Bleomycin administration. TP1 is shown in orange; TP2 is shown in green; TP3 is shown in blue. Each arrow represents a single IP injection of CyM to a total of 10.

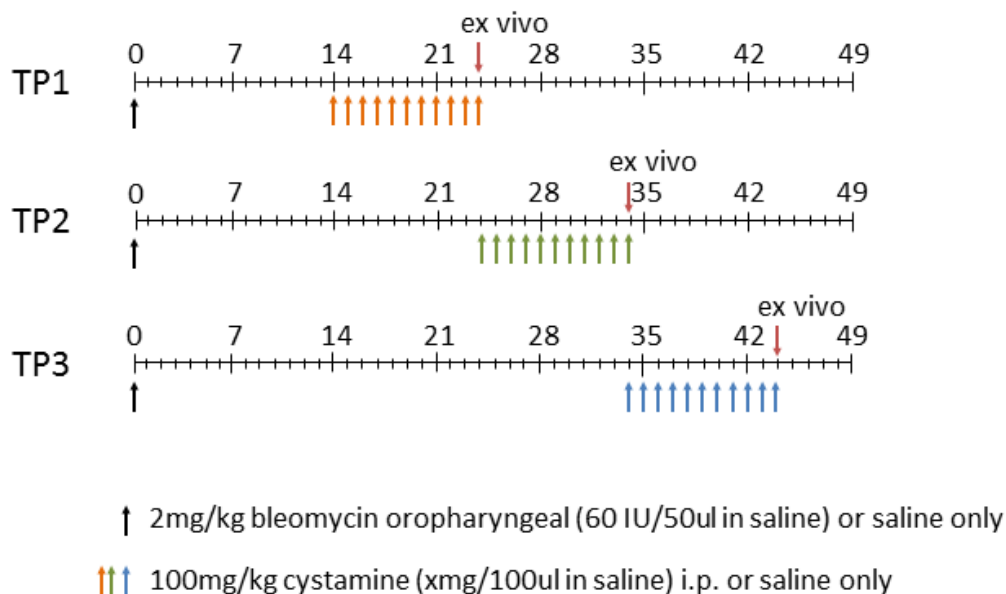


**Figure 2.2 Schematic diagram of treatment of mice in Time Course 2 (100mg/kg).** Day 0 shows Bleomycin administration. TP1 is shown in orange; TP2 is shown in green; TP3 is shown in blue. Each arrow represents a single IP injection of CyM to a total of 11.

## 2.46 Terminal Anaesthesia

Sacrifice was conducted in accordance with ASPA Schedule 1. Avertin, or tribromoethanol, is no longer sold commercially for anaesthesia, therefore a non-pharmaceutical alternative was made under guidance of the Named Veterinary Surgeon (NVS). This was done by dissolving 5g 2,2,2-tribromoethanol (Sigma-Aldrich) in 5ml 2-methyl-2-butanol (Sigma-Aldrich) under vigorous agitation in sterile conditions. This 100% Avertin solution was stored under light protection at 4°C. Just prior to use, a working solution was made by diluting the stock solution to 2.5% using warmed PBS. pH was assessed in every batch before use.

Terminal anaesthesia was carried out by administering 500µl of 2.5% Avertin by IP injection. This calculation is based on a 25g mouse and was adjusted accordingly per average cage weight. Induction required 1-2 minutes and mice were left for at least 5 minutes to enter deep anaesthesia and then checked by pinching the foot and for blink reflex. Blood was collected through cardiac puncture (AC) into plasma separation tubes containing lithium heparin (International Scientific Supplies Ltd. UK). Tissue was collected, weighed, and snap frozen on dry ice for protein analysis.

#### **2.47 Plasma Preparation from Whole Blood**

Whole blood was collected at Day 24, 34 and 44 post sacrifice as described previously in 2.43. Tubes were spun at 1500 x g for 15 minutes. The resulting supernatant above the separation gel was collected and aliquotted before storing at -20°C.

#### **2.48 Lung Processing**

Snap frozen tissue samples were powdered using pre-cooled pestle and mortars under cryogenic conditions using liquid nitrogen to ensure sample integrity and homogenisation. Powdered samples were stores at -80°C for further analysis.

## **2.49 Protein Extraction from Mouse Lung**

Homogenised lung powder was suspended at 30mg/ml in PBS containing Complete Mini Protease Inhibitor Cocktail with EDTA (Roche Diagnostics (UK) (1 tablet per 10ml extraction buffer). This was thoroughly mixed through drawing up and down with a pipette before vortex mixing. Samples were then spun at 14,000 x g for 2 minutes before collecting the supernatant, aliquotting and storing at -20°C for further analysis.

## **2.50 Hydroxyproline Assay**

Half of the homogenised powder from each mouse was weighed out and placed in pyrex test tubes (Fisher Scientific), covered with parafilm, and kept on wet ice during subsequent sample weighing. To these samples 1ml of sterile H<sub>2</sub>O was added, along with 125µl 50% Trichloroacetic acid (TCA) W/V. This was incubated on ice for 20 minutes until the solution clouded white. Samples were then centrifuged for 10 minutes at 1200 x g at 4°C. During centrifugation, a heat block was heated to 110°C in a fume hood. Samples were removed from the centrifuge and the supernatant carefully aspirated to leave only the protein pellet. In a fume hood, 1ml of 12M HCL was added and the tubes left uncovered and placed in the heat block at 110°C overnight.

The following morning, it was ensured that all liquid had evaporated. Tubes were removed from the heat block and cooled to room temperature before addition of 2ml of sterile H<sub>2</sub>O. Resuspended samples were covered with

parafilm and shaken aggressively on a shaker (with intermittent vortexing) for 2 hours. During this time, standards were diluted in H<sub>2</sub>O using trans-4-Hydroxy-L-proline (Sigma Aldrich, Dorset, UK) with the top standard at 750µg/ml. Following the 2 hours of mixing, samples were vortexed and a total of 200µl of each sample, diluted 1:5 with distilled water, were added to clean Eppendorf tubes. Dilution ensured the concentration range was within the standard curve. 500µl of chloramine-T (*Base ingredients; 70ml H<sub>2</sub>O, 1.4g chloramine-T, 6.083g Sodium Acetate, 10ml propan-2-ol*) was then added to each sample and standard. Samples were then incubated at room temperature for 20 minutes before addition of 500µl of Erlich's solution (Sigma Aldrich, Dorset, UK). This was then incubated in an oven at 65°C for 15 minutes. Following this samples were removed and incubated at room temperature for 2 hours. After 2 hours 100µl of each sample and standard were transferred to a 96 well plate in duplicate and read on a POLARstar Omega microplate reader (BMG Labtech, GmbH). Data was imported into MARS data analysis software (BMG Labtech, GmbH) and sample values interpolated from the standard curve. Sample values were then back calculated per mg of lung tissue and scaled up to whole lung, based on whole tissue weight obtained at harvest.

## **CHAPTER 3**

Characterisation of Primary Human Lung

Fibroblasts

## **3 CHAPTER 3: Characterisation of Primary Human Lung**

### **Fibroblasts**

#### **3.1 Introduction**

##### 3.1.1 Background

Fibroblasts are widely distributed in vertebrates and are the primary cell type, along with their differentiated successors, responsible for the deposition and turnover of the ECM. In IPF, the paradigm of a large increase in the net total collagen levels in the lung, along with the formation of FF and the body of supporting evidence from the literature, suggests that the accumulation of ECM is due, in part, to the increase in the number of fibroblasts present. There are a number of studies which show an increase in collagen transcription in IPF derived fibroblasts. This combined with the recruitment of fibrocytes, EMT and activation of resident fibroblasts could all contribute towards the pathogenesis of IPF.

In IPF it is hypothesised that the abundant fibroblasts can come from 3 main lineages. First is recruitment and activation of resident lung fibroblasts (Scotton and Chambers, 2007). Secondly, epithelial-mesenchymal transition in response to TGF- $\beta$  gives rise to myofibroblasts through detachment of epithelial cells from their basement membrane and reprogramming, after which the cells then express a mesenchyme phenotype (Willis et al., 2005). Finally, patients with IPF have shown to have an elevated level of circulating bone marrow derived fibrocytes

(Moeller et al., 2009) which share both mesenchymal and leukocyte markers which can be found in myofibroblasts in the fibrotic lung (Bellini and Mattoli, 2007). These mechanisms are hypothesised to give rise to myofibroblasts which are the main perpetrator within progressive lung fibrosis.

The exact differences *in vitro* between IPF and non-IPF fibroblasts have been described in the context of fibrosis progression, however the determination of which cells are fibroblasts was conducted by selecting markers of fibroblasts, myofibroblasts and airway smooth muscle cells (ASM). Immunofluorescence was chosen as a method for verification of cell type due to the ability of the technique to assess cell morphology as well as protein localisation. A number of antibodies were used in an attempt to distinguish fibroblasts in IPF and isolate them from potential smooth muscle cells that may be present in biopsy samples.

Fibroblast Activation Protein- $\alpha$  (FAP- $\alpha$ ) has been shown to be expressed in IPF with the first conclusive report in 2006 (Acharya et al., 2006). This antibody was selected to determine if there is a difference in expression of FAP- $\alpha$  between fibroblasts isolated from both patients with IPF and without. Furthermore, a comparison could be drawn from potential expression of FAP- $\alpha$  within ASM cells and both fibroblasts from IPF sufferers and non IPF donors.

Furthermore to discern the fibroblasts from the human airway smooth muscle cells,  $\alpha$ -smooth Muscle Actin was used to show the morphological differences in stress fibres within the cells. ASM cells show a tubular, filamentous distribution of  $\alpha$ -SMA whereas fibroblasts show a much more dispersed expression with less clear filamentous organisation (Panner and Honig, 1967). However it is noted that distinguishing ASM from myofibroblasts is known to be extremely difficult due to the lack of phenotype specific markers (Singh et al., 2010).

### 3.1.2 Aims & Objectives

- Determine the differences in cross linking enzyme expression between IPF and non-IPF pulmonary fibroblasts.
- Assess the ECM deposition rate and total ECM of IPF and non-IPF pulmonary fibroblasts deposited in culture
- Qualitatively assess the ECM structure of IPF and non-IPF pulmonary fibroblasts by SEM at high magnification
- Conduct immunohistochemical staining of primary IPF and control lung tissue to determine the presence of cross linking enzymes identified by PCR in culture.

## 3.2 Results

### 3.2.1 Senescence associated $\beta$ -Galactosidase staining

Upon receipt of previously derived cells,  $\beta$ -Galactosidase staining was conducted to determine the prevalence of senescence of cells stored long term in liquid nitrogen.

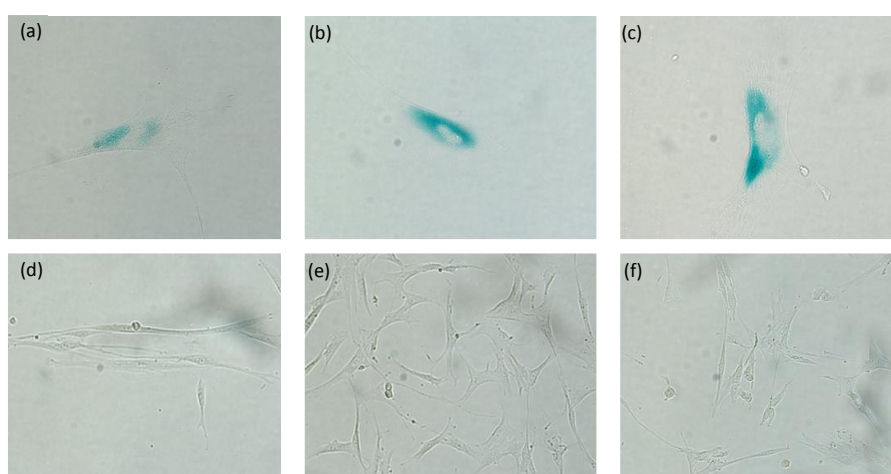


**Figure 3.1.  $\beta$ -Galactosidase staining of primary lung fibroblasts.** Images are representative of primary cultures. Panels A,B & C show senescent cells; D,E & F shows no staining, indicating proliferative cultures.

Figure 3.1 above shows 6 representative images of the senescence associated  $\beta$ -Galactosidase (SABG) staining. Images 3.1a,b and c show blue SABG staining whereas d, e and f show no SABG. Two donors out of 6 were found to have extensive SABG, therefore two other donors were obtained and further subjected to SABG staining to ensure responsiveness to divide in the presence of serum containing media. This resulted in a total of 3 IPF and 3 non-IPF donors for further analysis.

### 3.2.2 Immunocytochemical detection of fibroblast markers

Immunocytochemistry was conducted upon received donor fibroblasts from both control and IPF patients to assess the prevalence of fibroblast

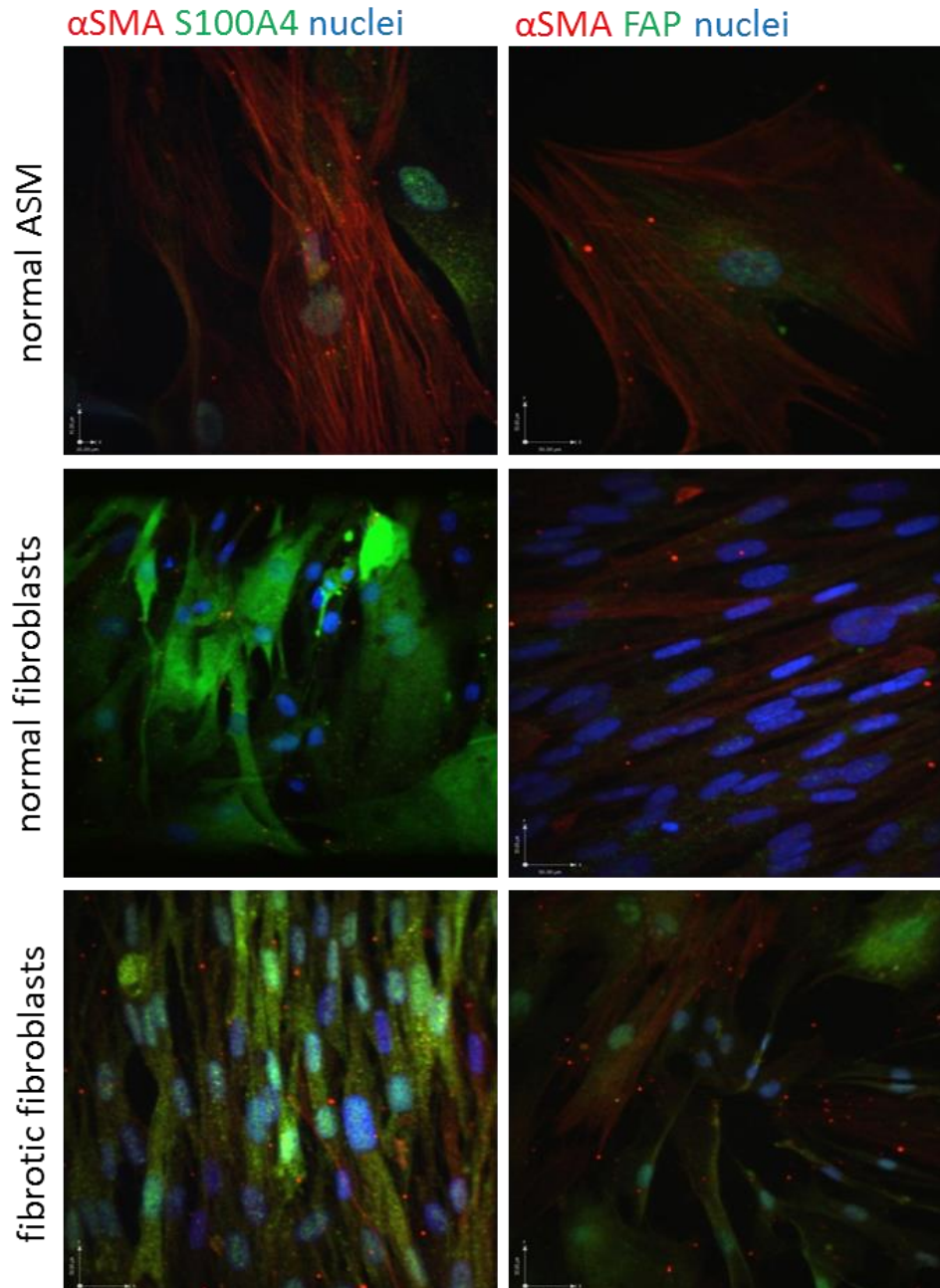


**Figure 3.2** Images of stained primary human airway smooth muscle (ASM) cells (used as controls), IPF and control patient derived fibroblasts. All cells are stained with anti  $\alpha$ -smooth muscle actin ( $\alpha$ -SMA, red) and DAPI (blue). Green staining is used for anti-S100A4 and fibroblast activation protein (FAP- $\alpha$ ) as indicated. Control and IPF derived fibroblasts have similar morphology and staining patterns. ASM cells express S100A4 and FAP at a lower level than fibroblasts and have more pronounced stress fibres.

markers and to examine  $\alpha$ -smooth muscle actin filament organisation. Human airway smooth muscle cells (HASMs) were also stained with these markers to determine the likeliness of the cells derived from patient biopsy were HASMs. IPF and control fibroblasts exhibit extensive staining for S100A4 whereas ASM cells show weak or none (Figure 3.2). All cells show a similar spindle like morphology with smooth muscle actin staining. ASM actin organisation is filamentous, along the polar axis of the cell similar to IPF fibroblasts. The difference in organisation of SMA between control and IPF fibroblasts is less pronounced than reported in the literature. There is some filamentous structure of the SMA fibres in the IPF fibroblasts however within control cells it was noted that some cells do have a similar SMA morphology to ASM. Isotype controls were clean. FAP- $\alpha$  expression is apparent in IPF derived fibroblasts with weak background staining in ASM and control fibroblasts. Using the markers selected, it can be concluded that the primary cells obtained from biopsy were most similar to that of the commercially bought control fibroblasts. Therefore, they are unlikely to be ASM cells or any other cell type found in abundance in the lung.

### 3.2.3 Real Time PCR analysis of ECM stabilising enzyme messenger RNA

Quantitative RT-PCR was conducted to assess the relative abundance of ECM cross linking transcripts produced by both control and IPF derived fibroblasts. Cells were cultured as previously described in section 2.9, RNA extraction as stated in section 2.10, cDNA synthesised as described in 2.11 and RT-PCR as stated in section 2.12 using Brilliant II SYBR® Green QPCR Master Mix (Agilent Technologies, CA, USA) to the manufacturers specification. The LOX and transglutaminase families of enzymes in normal and IPF derived fibroblasts cultured on tissue culture plastic by

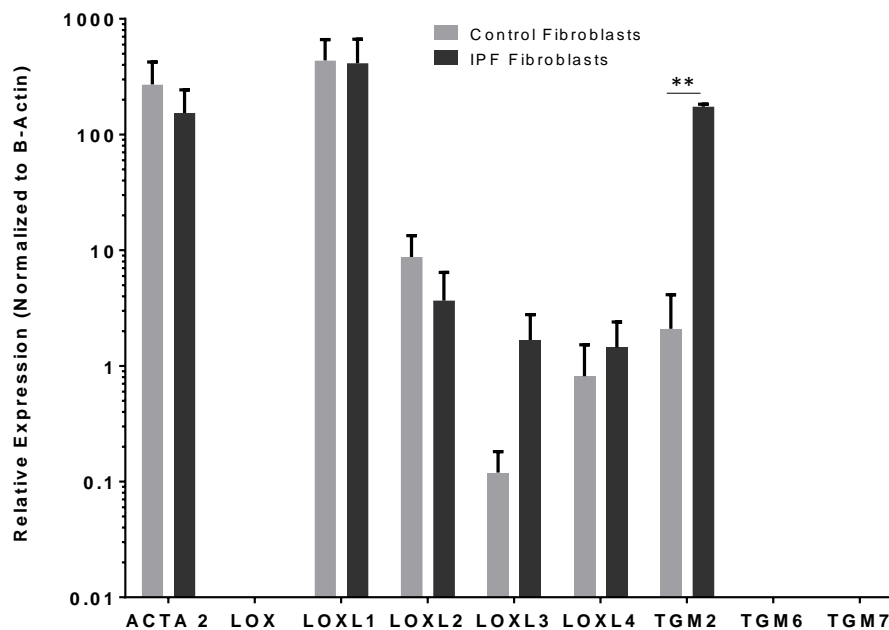


**Figure 3.3 Expression of cross-linking enzyme transcripts in control and IPF derived fibroblasts.** Quantitative gene expression of cross linking enzymes in three control and three IPF derived fibroblasts determined by real time PCR. Lysyl oxidase (LOX) was expressed at a very low level. Lysyl Oxidase like proteins (LOXL) 1-4 were robustly expressed in control and IPF derived fibroblasts. Transglutaminase 2 (TGM2) was expressed at a significantly higher level in the IPF derived fibroblasts. TGM6 and 7 were not detected.  $\alpha$ -smooth muscle actin (ACTA2) is used as positive control. \*\* $p < 0.005$  Data analysed with a two tailed student's *t*-test. Data presented  $\pm$ SD.

quantitative, real time PCR were assayed with  $\beta$ -Actin as the housekeeping gene.

Data was analysed using a two tailed student's t-test. *LOX* transcript was present at very low levels relative to *β-Actin* and *LOXL1-4* mRNAs were detected both cell types (Figure 3.3). *LOXL3* was expressed in both control and IPF derived fibroblasts however there is no significant difference (p value = 0.07). *TGM2* was expressed in normal fibroblasts and more strongly so in IPF derived fibroblasts (n=3) (p<0.05). Transglutaminases 6 & 7 were not present in either cell type. *ACTA2* was present at high levels in both cells types with no statistical difference between them.

#### 3.2.4 Extracellular matrix cross linking enzyme expression in the IPF lung

Immunohistochemistry was conducted in lung tissue of three control and three IPF donors from transplant tissue to determine the presence of LOXL2, LOXL3, TG2 and the TG2 mediated protein cross links.

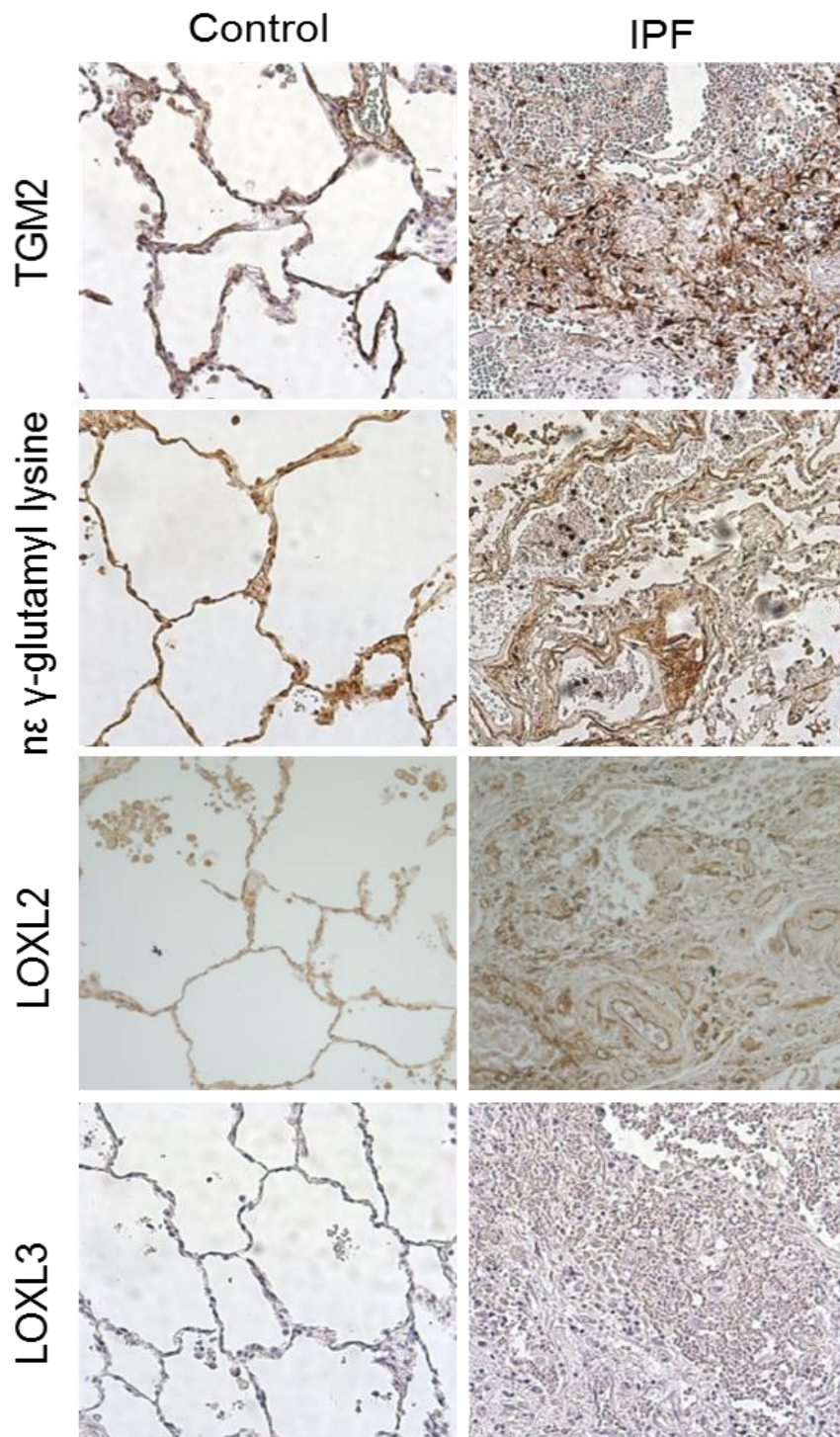


**Figure 3.4. ECM cross-linking enzymes and transglutaminase mediated cross-links are expressed in IPF tissue at x20 magnification.** Immunohistochemical staining showing representative images of three control lungs and three IPF lungs. Transglutaminase 2 (TGM2) is expressed in normal alveolar epithelium and widely expressed in IPF lung. TGM2 mediated n-ε γ-glutamyl lysine crosslinks are similarly distributed. Lysyl Oxidase like protein 2 (LOXL) is expressed in normal and IPF lung. LOXL3 is not present in normal alveoli but weakly positive in IPF lung. Brown indicates positive staining; Blue indicates haematoxylin counterstaining of nuclei.

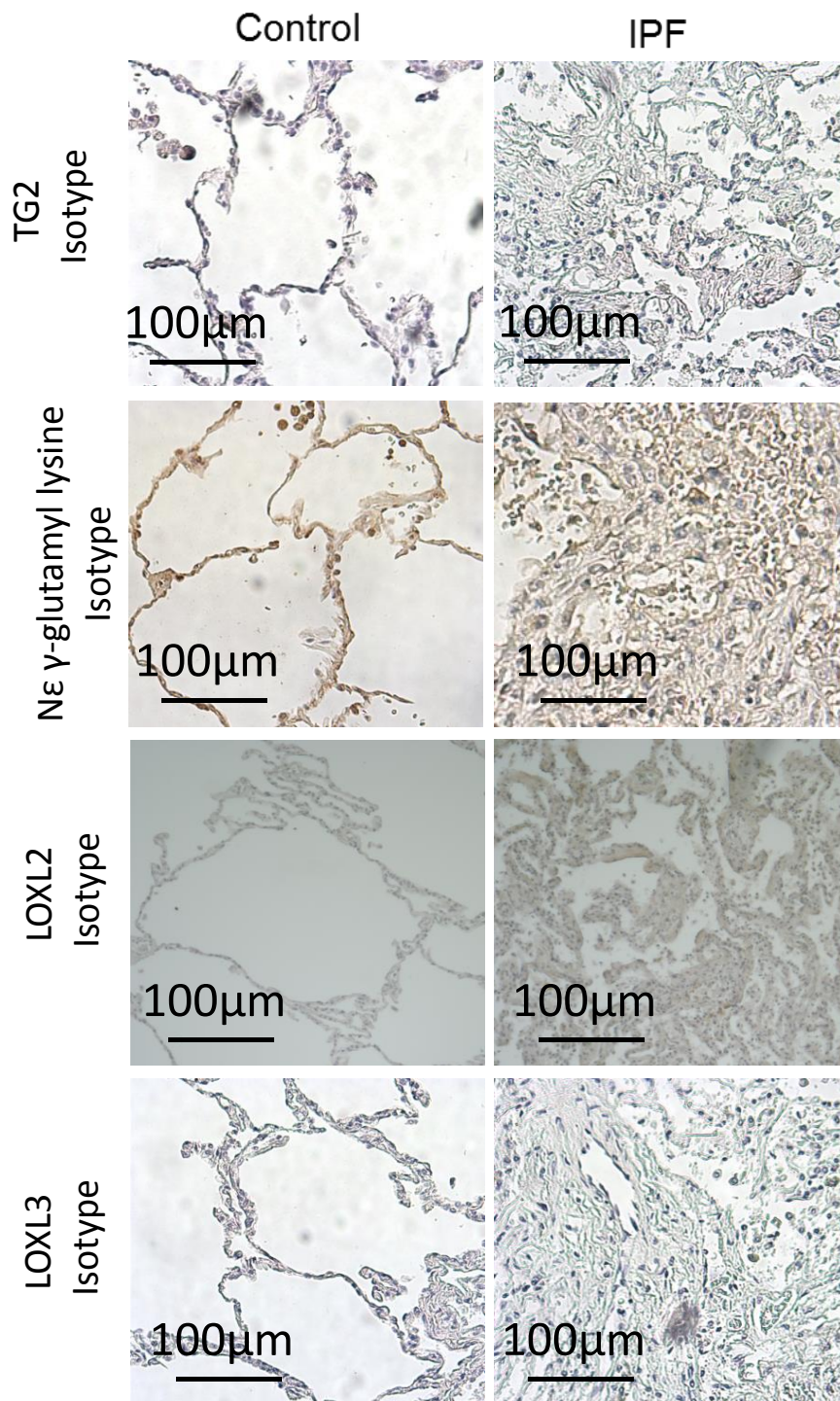


**Figure 3.5. Isotype control images of ECM cross-linking enzymes and transglutaminase mediated cross-links are expressed in IPF tissue at x20 magnification.** Immunohistochemical staining showing representative images of three control lungs and three IPF lungs. Brown indicates positive staining; Blue indicates haematoxylin counterstaining of nuclei. The IgM isotype for n-ε γ-glutamyl lysine crosslinks show mild staining but not as strongly as the anti n-ε γ-glutamyl lysine in both control and IPF tissue in figure 3.4.

The structure of the IPF tissue, when compared to control, is disorganised with very few discernible structures. There is an abundance of extracellular protein with no identifiable alveoli and a large increase in the number of cells within the given field of view. This destruction of the alveolar architecture is a hallmark of IPF. TG2 is expressed in both control and IPF tissue sections. In control, it is localised to the alveolar epithelium however in IPF the staining pattern is more widespread. IPF tissue show a more extensive staining throughout the tissue indicating possible diffusion of TG2 through the altered extracellular environment. The TG2 catalysed cross links, n-ε γ-glutamyl lysine, shows a similar pattern of expression to that of TG2.

LOXL2 is expressed at the protein level in both control and IPF tissue. Some localisation of LOXL2 to vascular endothelial cells is present in IPF tissue. There is more extensive LOXL2 staining however the intensity of the stain is very similar to control. Control lung was negative for LOXL3 staining and the IPF tissue was weakly positive in the areas of dense fibrosis indicating that in IPF LOXL3 is induced to be expressed.

### 3.2.5 ECM & conditioned media collagen content of IPF fibroblasts

To assess the ECM produced by both control and IPF fibroblasts, a series of experiments was designed to determine the total ECM, total collagen content and collagen synthesis rate. ECM was synthesised in culture from primary control and diseased fibroblasts. The method for decellularisation was shown to create a cell and debris free ECM coated culture surface (Figure 3.5a). Minor artefacts shown as white imperfections on the surface

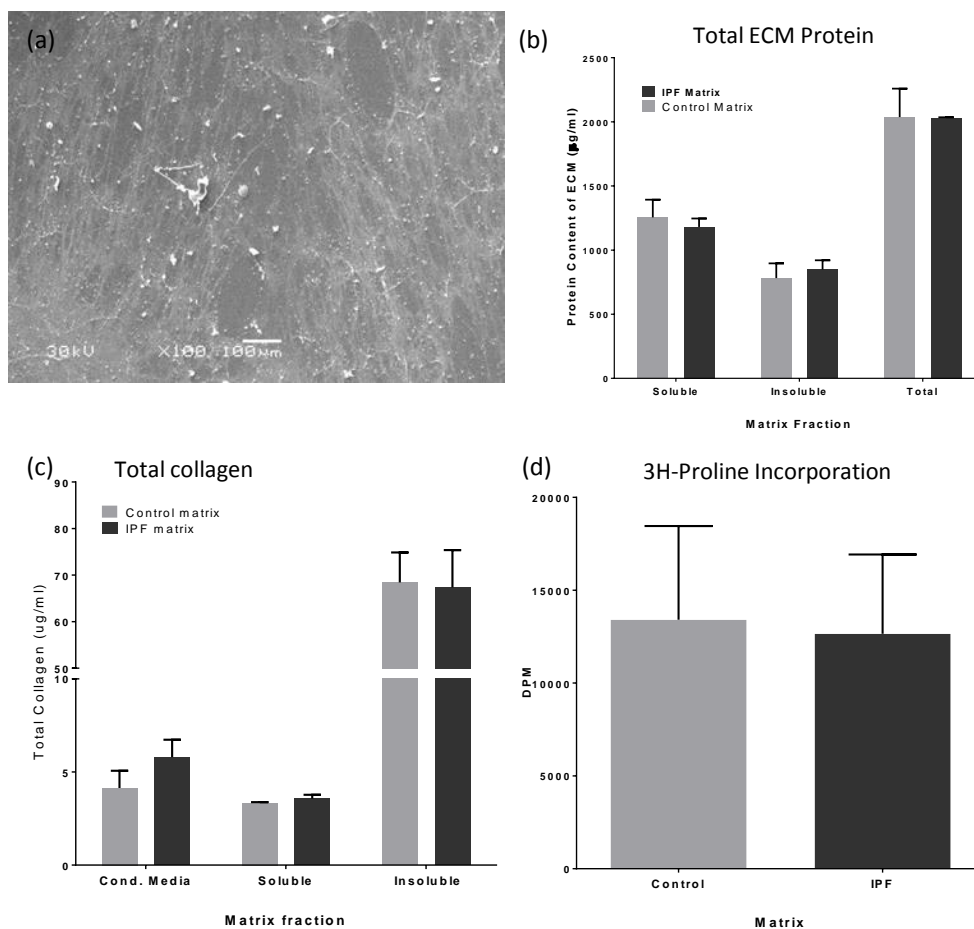


**Figure 3.6 Characterisation of fibroblast derived ECM.** (a) Fibroblast derived ECM preparation visualised by scanning electron microscopy showing a complex filamentous layer free from cells and debris. (b) Control and fibroblast ECM preparations analysed by bicinchroninic acid (BCA) assay contain similar levels of total protein in their soluble and insoluble fractions. (c) Measurement of total collagen in ECM preparations show this is similar in control and IPF derived fibroblasts and largely in the insoluble fraction. (d) Equal collagen synthesis between control and IPF derived fibroblasts is confirmed by tritiated proline incorporation assay. Data presented  $\pm$ SD.

of the ECM are hypothesised to be a result of the processing for SEM.

Total ECM protein was measured in two fractions. The soluble fraction which is readily dissolved in modified radio immunoprecipitation assay (RIPA) buffer and an insoluble fraction removed from the plate by physical scraping and solubilisation in a urea based buffer as described in 2.17. There was no significant difference in protein content of either ECM protein fraction between normal and IPF derived fibroblasts (n=3) ( $p>0.05$ ) (Figure 3.5b). Total collagen, measured using a hydroxyproline assay, was predominantly located in the insoluble fraction but does not differ between normal and IPF derived fibroblasts (n=3) ( $p>0.05$ ) (Figure 3.5c). Labelling ECM by incubating fibroblasts during ECM deposition with tritiated proline confirmed that deposition of proline labelled ECM (predominantly collagen) was also not significantly different between normal and IPF derived fibroblasts (n=3) ( $p>0.05$ ) (Figure 3.5d).

Due to the little difference observed between the quantity of IPF ECM in culture, quantitative RT-PCR was conducted to ascertain if the matrix varied in terms of relative collagen levels expressed by the cells rather than total quantity as shown by the hydroxyproline and tritiated proline incorporation assays. Cells were cultured as previously described in section 2.9 to passage 4, RNA extraction as stated in section 2.10, cDNA synthesised as described in 2.11 and RT-PCR as stated in section 2.12 using Brilliant II SYBR® Green QPCR Master Mix (Agilent Technologies, CA, USA) to the manufacturers specification with ribosomal 18S as the

housekeeping gene using KiCqStart SYBR Green Primers (Sigma Aldrich, Dorset, UK).

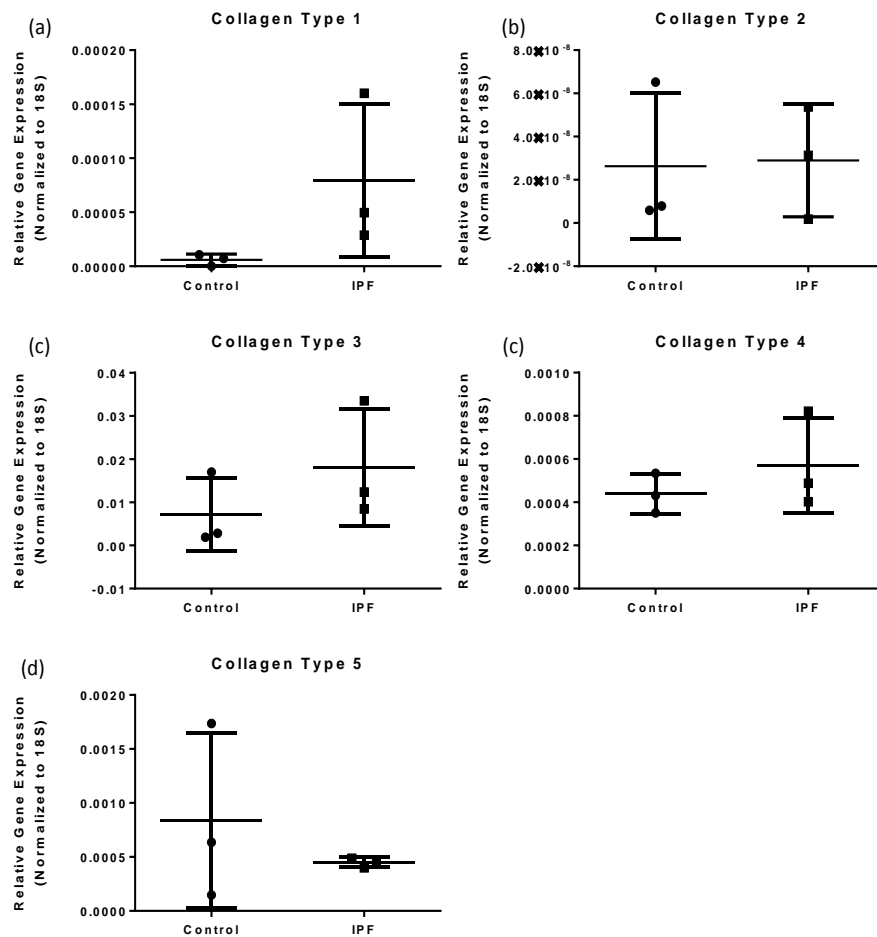


**Figure 3.7 Collagen Type I-V mRNA expression does not vary between IPF and control fibroblasts.** (a-e) Collagen types I-V mRNA does not vary between IPF and control fibroblasts assayed by real time PCR. Data presented  $\pm$ SD.

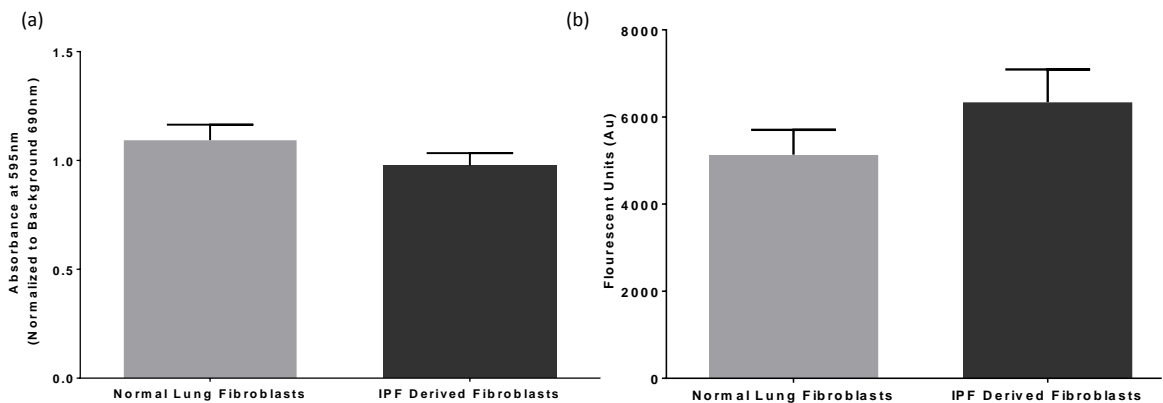
Due to the nature of primary cells, the observed variability between cells within the same group was high. Collagen type III was the most highly expressed at the transcript level, with Collagen II being the lowest expressed relative to 18s (Figure 3.7). Collagen I in control cells was

expressed at low levels relative to 18S and at similar levels between cells within the group. This is in contrast to the IPF group where the standard deviation is greater than that of control. No statistical difference was observed between the IPF and control fibroblasts (n=3) ( $p>0.05$ ).

### 3.2.6 Cell proliferation of normal and IPF derived fibroblasts

To analyse IPF fibroblast proliferation when compared to control fibroblasts, two separate methods of assessing cell proliferation were applied, with two different parameters of cell growth; cell number measured by MTT reduction and DNA synthesis by a thymidine analogue incorporation based assay. This was to determine if the rate of proliferation was increased in IPF fibroblasts.

Equal numbers of cells ( $0.2 \times 10^6$ ) were cultured as previously described in section 2.9 and growth arrested in serum free DMEM for 24 hours prior to the beginning of the assays. DMEM containing 10% FBS was added following growth arrest and cells cultured for 72 hours before assaying as described in 2.32



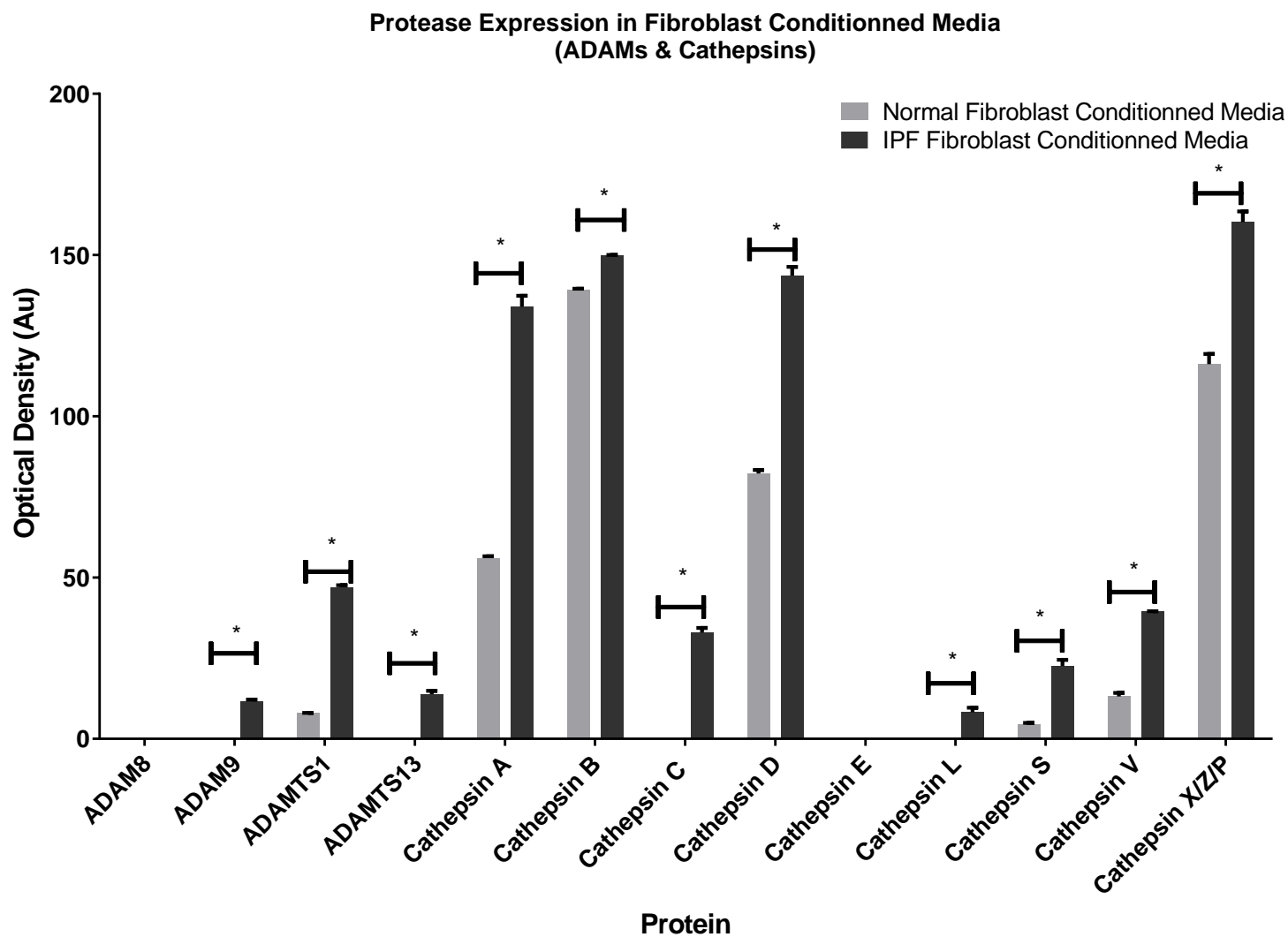
**Figure 3.8 Proliferation of primary lung fibroblasts in response to foetal bovine serum.** (a) MTT assay of control and IPF fibroblasts ( $n=3$ ) (b) EdU based assay of DNA synthesis on control and IPF fibroblasts ( $n=3$ ). a and b show no statistical difference in either cell number or DNA synthesis rate. Data was analysed using a two tailed student's t-test. Data presented  $\pm$ SD.

Figure 3.7b shows no statistically significant difference ( $p>0.05$ ) in an increase in cell number between control and IPF derived fibroblasts ( $n=3$ ).

Furthermore figure 3.7b show that there is no difference ( $p>0.05$ ) in DNA synthesis rate between control of IPF derived fibroblasts ( $n=3$ ), similar to that of the MTT assay. Both assays identify that there is no significant difference in growth rate between control and IPF derived fibroblasts in standard culture conditions.

### 3.2.7 Extracellular protease expression of primary fibroblasts

To assess the relative extracellular protease expression that could potentially degrade the ECM in culture, fibroblast conditioned serum free media was harvested from passage 4 cultures. Membrane bound antigen capture was utilised for the screening of multiple protease families as described in section 2.30. Densitometry was conducted on the membranes the same as described in 2.28 and normalised to the reference spot on the arrays. The proteases on the assay were chosen as the MMP family is known to be involved in IPF. MMP7 is the most consistently increased transcripts in IPF (Selman et al., 2006) and MMP1 is known to be increased, despite the increase in deposition of fibril forming collagens (Pardo and Selman, 2012). To allow for more rapid screening of relative protease levels, a Proteome Profiler antibody array was used to measure multiple proteases within the same sample without requiring multiple western blots.



**Figure 3.9 Optical density of ADAM family and Cathepsin proteases in IPF and control fibroblast conditioned media.** IPF fibroblasts express significantly more ADAM9, ADAMTS1, ADAMTS13, Cathepsins A, B, C, D, L, S, V and X when compared to control fibroblast conditioned media ( $n=3$ ) ( $*p=0.05$ ). Data analysed with *t*-tests in PRISM V6 (Graphpad Software, USA). Data presented  $\pm$ SD.

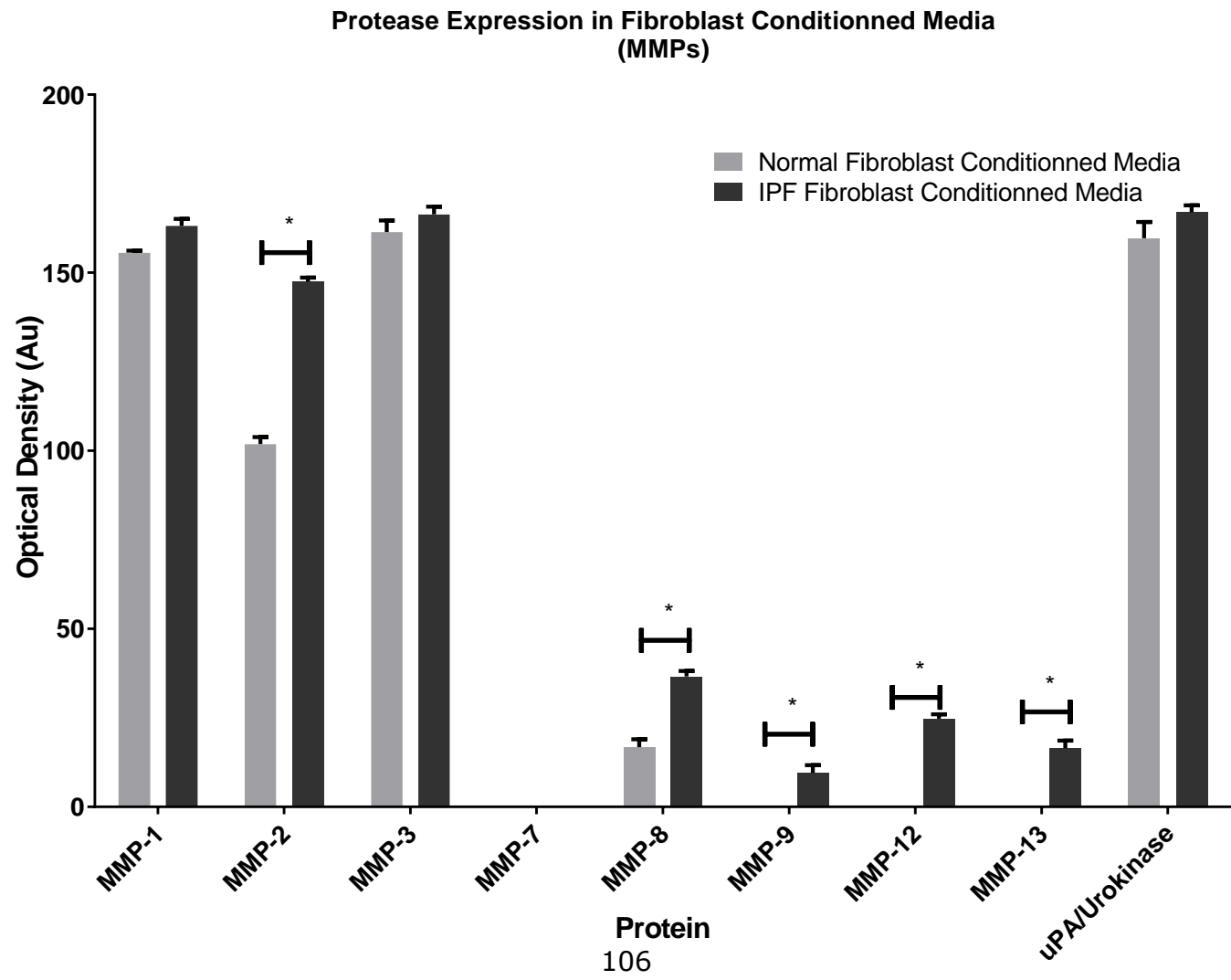


**Figure 3.10** Optical density of Matrix Metalloproteinases and Urokinase in IPF and control fibroblast conditioned media. IPF fibroblasts express significantly more MMP-2, 8, 9, 12 and 13 when compared to control fibroblast conditioned media (n=3) (\*p=0.05). Data analysed with t-tests in PRISM V6 (Graphpad Software, USA). Data presented ±SD.

IPF derived fibroblast conditioned media contained increased levels of a number of proteases. ADAM9, ADAMTS1 and ADAMTS13 show an increased expression compared to control (n=3)(p<0.05) as shown in Figure 3.9. Similarly Cathepsins A, B, C, D, L, S, V and X/Z/P also show an increased expression compared to controls (n=3)(p<0.05) as shown in Figure 3.8 also. The MMP family show an increased expression of MMP-2, 8, 9, 12 and 13 when compared to control fibroblast media (n=3)(p<0.05) as shown in Figure 3.10. MMP-1 and 3 show no difference in relative protein expression levels (p>0.05).

3.2.8 Scanning electron microscopy of primary IPF cultures & biosynthesised matrix

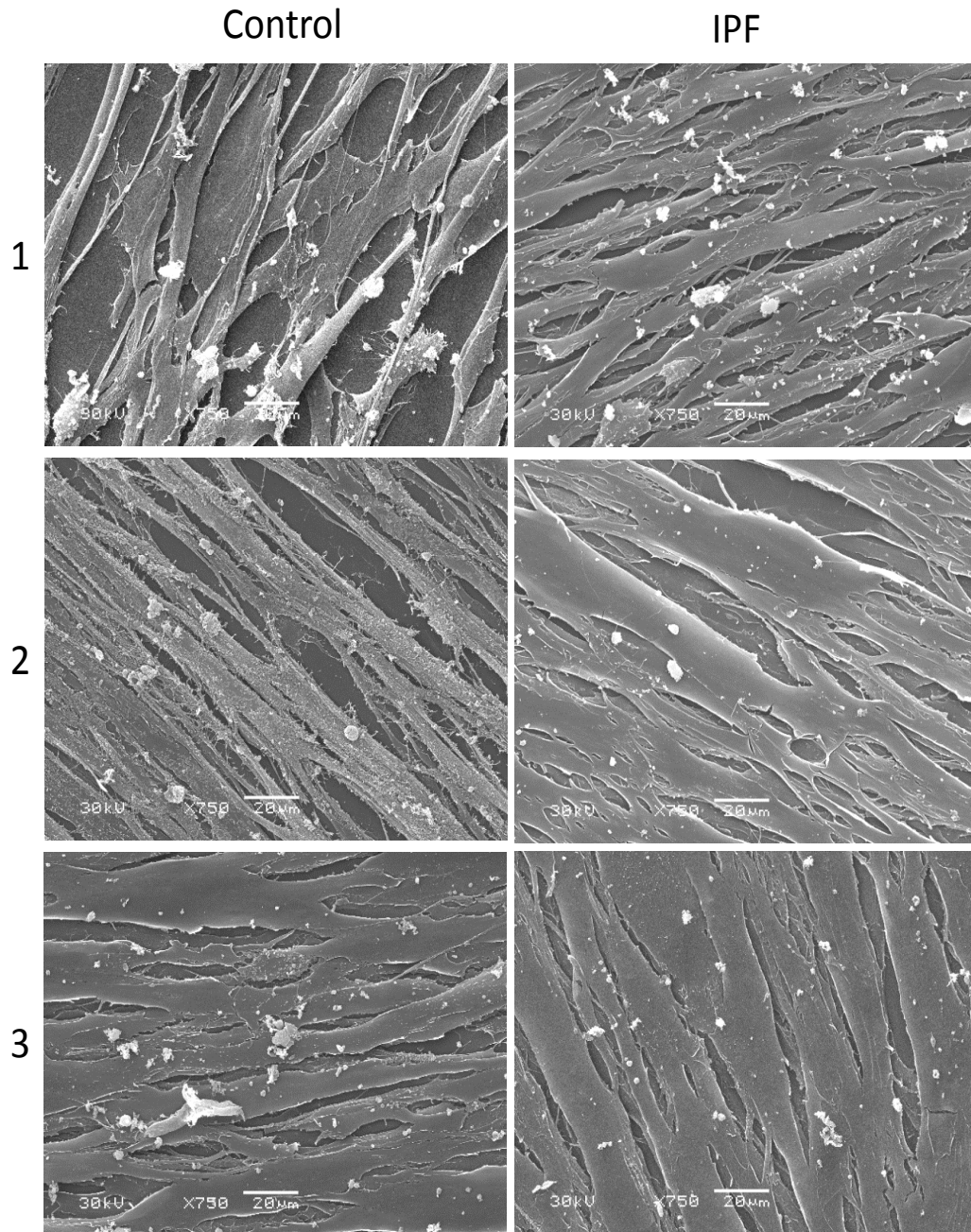


**Figure 3.11 Scanning electron microscopy of primary control and IPF derived fibroblasts at X750 magnification.** Low magnification images of fibroblast cultures show no visible differences.

Primary fibroblast cultures were examined by SEM to qualitatively assess the structure of the ECM to look for variation in structure as total protein assays determined the total matrix quantity to be equal between control and IPF ECM as shown in Figure 3.6. Samples were prepared and imaged as described in section 2.38. Images were taken in random fields across each sample by an independent person.

At low magnification no distinctive differences can be observed between IPF and control cultures. Some vacuum induced deformation can be seen on the larger cell bodies such as IPF 2 and 3 in Figure 3.11. The white artefacts throughout all samples are hypothesised to be extracellular glycoproteins which are dehydrated and deformed through the sample processing. Insoluble proteins such as mature collagen remain intact as can be seen as the small web like protrusions from the cell bodies.

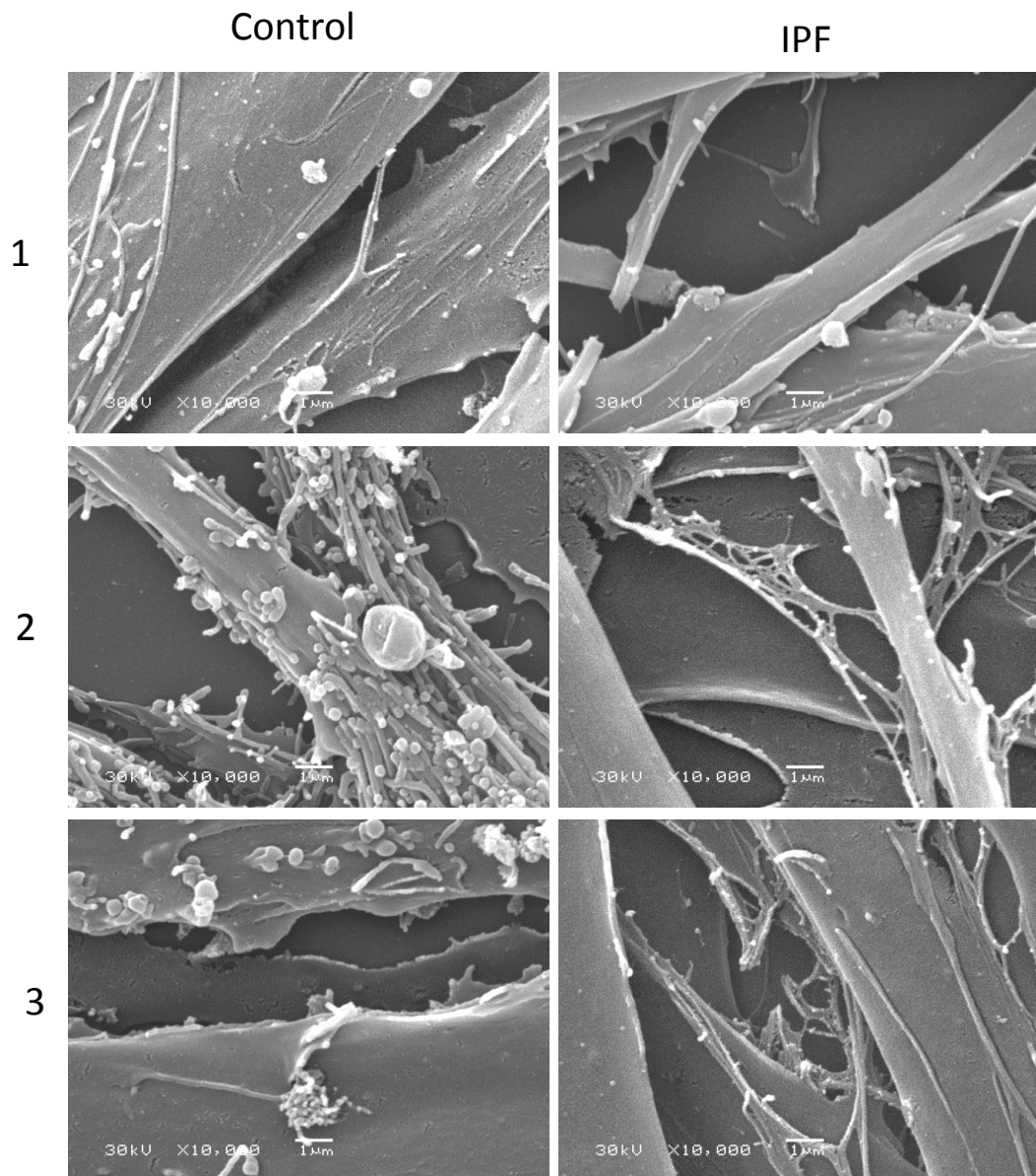


**Figure 3.12 Scanning electron microscopy of primary IPF derived and control fibroblast cultures at x10,000 magnification.** The cell-cell connections and extracellular structures form a web like appearance in the IPF derived cultures.

At higher resolution, extracellular structures are more easily visualised. Images were taken at x10,000, in random fields of view, on the same samples as presented in Figure 3.11. Artefacts seen previously in higher resolution can still be seen, however the resolution allowed us to determine that these are most likely artefacts formed by critical point drying with liquid CO<sub>2</sub>. Delicate extracellular structures formed in cell culture which have not been fully fixed with glutaraldehyde may be dehydrated in the

alcohol gradients and critical point drying of the sample processing. Furthermore there is significant vacuum induced deformation in IPF 1 showing fractures in the sample.

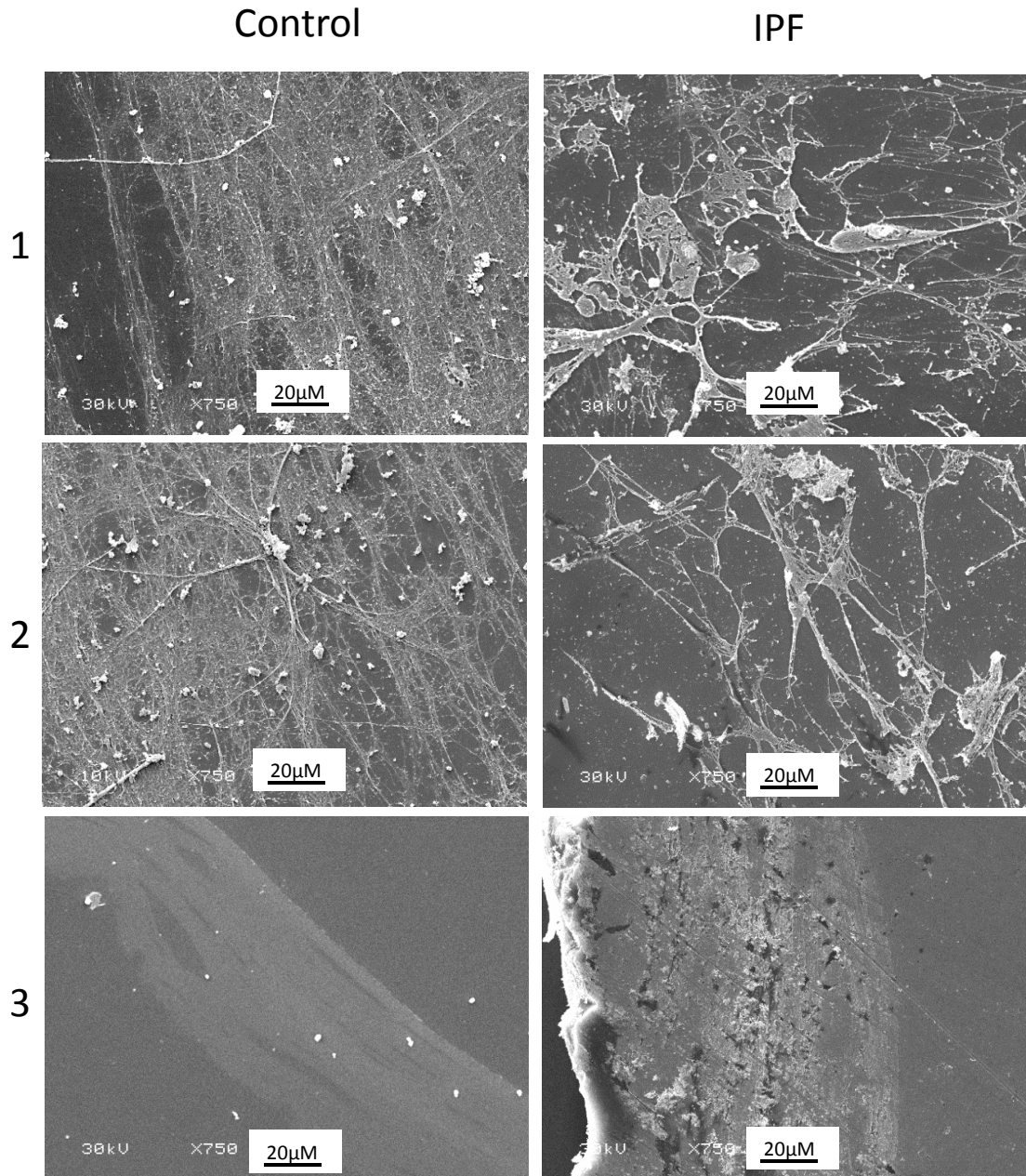


**Figure 3.13 Scanning electron microscopy of primary control and IPF derived fibroblast ECMs at X750 magnification.** Low magnification images of fibroblast cultures show a more organised structure within the control cultures when compared to the IPF, which has a more web like appearance compared to fine filamentous arrangement of controls.

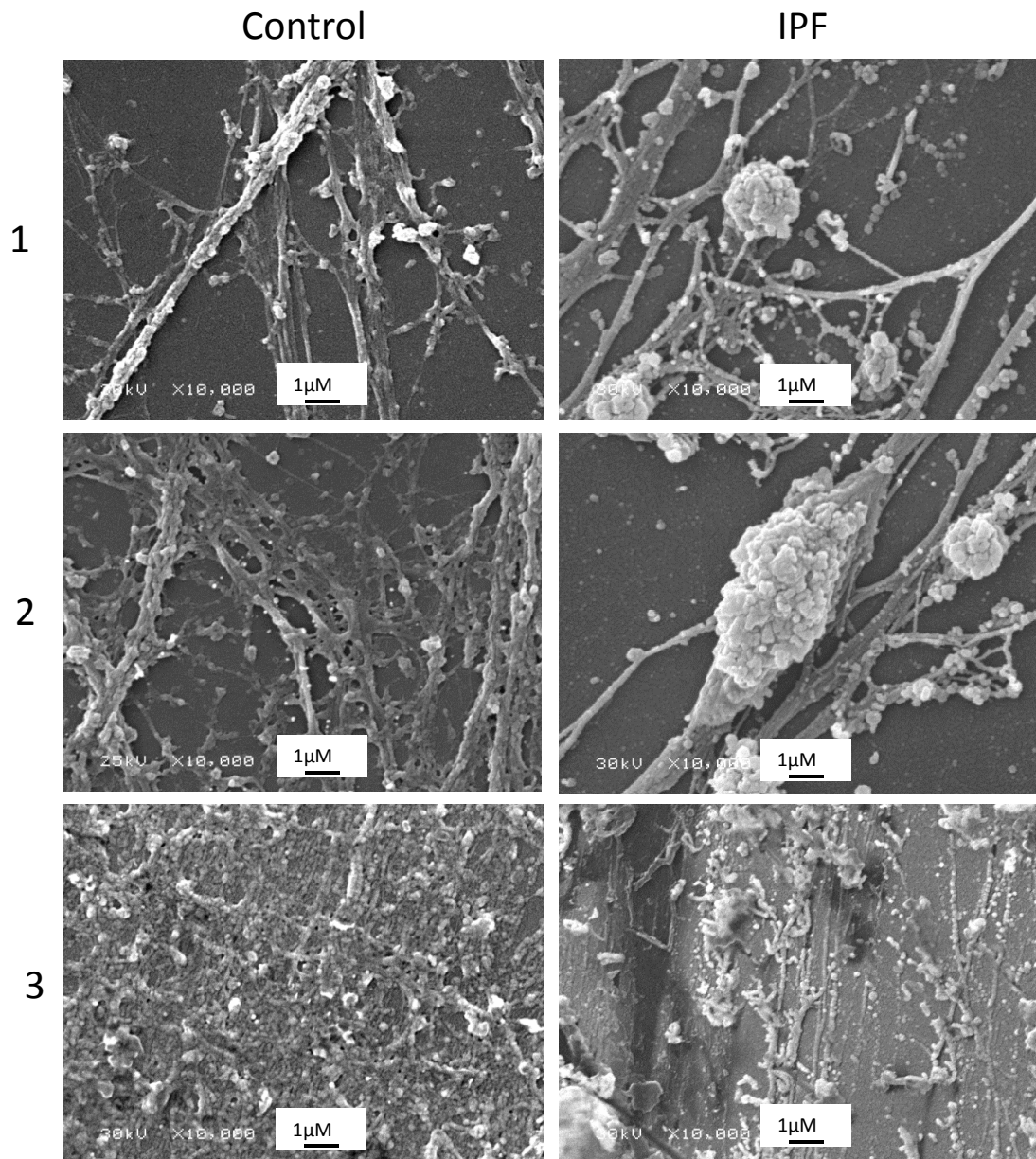


**Figure 3.14 Scanning electron microscopy of primary IPF derived and control fibroblast ECMs at x10,000 magnification.** At higher resolution, the web like structures seen in the IPF cultures have a similar micro-structure to that of controls. There is an abundance of clusters of white artefacts from processing in the IPF cultures suggesting relatively higher level of proteoglycans.

As no reliable method of scoring these SEM images exists, drawing definitive conclusions from the images is subjective. Therefore these images can only be used to state that the decellularisation process used leaves an in-tact ECM, free of cellular debris. The extracellular structures and cell-cell connections within the IPF cell cultures exhibit a more 'web'

like appearance when compared to control cultures (Figure 3.12). This can be seen most prominently in IPF 2 and 3. These structures do not appear in control cultures. Also, control cultures have fewer cell-cell connections compared to IPF and where these connections are in place, they are less complex in structure than those seen in the IPF cultures. The connections themselves are single fibres of protein compared to the web like structures observed in the IPF cultures. Control ECM does not show as much defined structure as that of IPF ECM. However this could be due to a change in the composition of the ECM, leading to a higher production of soluble ECM proteins such as glycoproteins, which are denatured during the SEM sample processing.

### **3.3 Discussion**

We hypothesised that IPF fibroblasts produced increased levels of ECM cross linking enzymes, and produced greater quantities of ECM as described in the literature. These results suggest that there is a potential role for TG2 in ECM maturation and stabilisation in IPF. IPF fibroblast cultures produce a higher level of TG2 mRNA. This is supported by immunohistochemistry in IPF tissue which shows extensive expression of TG2 as well as the TG2 catalysed cross link. The LOX family mRNA in culture show no statistical difference between control and IPF, however LOXL3 shows a strong trend towards an increased mRNA levels in the IPF cultures.

Senescence is having been described recently in IPF (Dmitri et al., 2012, Yanai et al., 2015), is an important concept which may impact potential cell biology experiments being carried out. Within these series of experiments contained in the thesis, generation of large quantities of fibroblasts from primary patient samples was necessary. Therefore, if senescent populations were found in culture as shown in 3.2.1, the donor could not be used as it was not possible to generate enough cells to carry out the required experiments. This decision was a logistical one, in selecting out the populations which could not provide enough cells. In IPF it can be noted that populations of senescent myofibroblasts exist within the lung. These cells secrete increased amounts of cytokines which promotes a pro-inflammatory environment which would support a progressive fibrosis. Senescent cells are mostly considered to

downregulate ECM production (Krizhanovsky et al., 2008) and increase ECM proteolytic mechanisms (Sarrazy et al., 2011). In IPF it is proposed that the myofibroblasts populations that undergo senescence are resistant to pro-apoptotic stimuli and promote further fibroblasts recruitment through secretion of increased levels of cytokines. Therefore, indirectly we may have selected out an important sub-population of cells with regard to ECM turnover. However, the generation of a large number of ECM's required the ability to proliferate in the presence of serum containing media, meaning that with extensive SABG staining this would not have been possible. For future work, it could be considered that seeding donors with extensive SABG staining onto ECM's generated from control and non-senescent IPF donors would possibly provide an insight into how senescence directly impacts ECM structure and subsequent function. Furthermore, we could explore the differences of ECM function between those generated from both senescent and non-senescent IPF cells to indicate as to the biological function of local ECM within the IPF lung as it is known that both populations of cells exist. Two of the procured cryopreserved IPF cell samples stained for extensive SABG. This allowed for the procurement of additional donors and ensuring the collection of three control and three IPF donors. Donor number, due to primary cell and tissue variation is one limitation of this study. Statistical analysis with variation of primary samples may prove challenging in further work.

LOXL2 has previously been implicated in the pathogenesis of IPF (Woodcock and Maher, 2014, Chien et al., 2014) and it has been shown

that attenuation of LOXL2 activity in murine models of IPF reduces the extent of fibrosis (Barry-Hamilton et al., 2010). However, in the samples analysed, LOXL2 expression does not differ between control and IPF fibroblasts at the mRNA level, or the tissue sections as shown by IHC. This may be due to the heterogeneity of the disease itself and the location from where the tissue and cells were isolated. Furthermore, data from the protease profiler suggests that IPF fibroblasts do not produce MMP7. This is supported by data from Zuo *et al.* (2002) who showed that MMP7 is primarily associated with abnormal alveolar epithelium as seen in IPF and not primarily expressed within the fibroblast foci.

Extracellular matrix production was assessed using multiple techniques including total protein assay, radio-labelled amino acid incorporation and PCR for major collagen components. Interestingly the *in vitro* findings indicate that there is no difference in total ECM protein, collagen I-V mRNA expression or collagen deposition rate between control and IPF fibroblasts. It has been noted in the literature that there is a disparity between in results of ECM synthesis in IPF fibroblasts (Ramos et al., 2001b). This also extends to other aspects of cell functions such as proliferation and apoptosis (Raghu et al., 1989, Raghu et al., 1988, Jordana et al., 1988). The heterogeneity of the fibroblast populations within the IPF lung and the location of the biopsy taken may have resulted in the derivation of different fibroblast subpopulations.

Interestingly the data presented here shows that IPF fibroblast proliferation is no different to that of control fibroblasts. Fibroblasts isolated from IPF patient biopsy and cultured to passage 5-8 showed that IPF fibroblasts proliferate at a slower rate than control fibroblasts from the fourth day post seeding for up to 14 days (Ramos et al., 2001a). The experiments presented here assessed growth over 3 days. Therefore the observed effect here is backed up by the findings of Ramos *et al.* (2001).

Multiple proteases were analysed in the conditioned media from both IPF and control fibroblast populations. MMP-2, 8, 9, 12 and 13 are shown to be increased in the IPF conditioned media. Interestingly this is not always reported. Nkyimbeng *et al.* (2013) reports increases in MMPs 1,2,7,9 and 13 but no change in MMP-8 (Nkyimbeng et al., 2013). Furthermore, Craig *et al.* (2015) in a review states that MMP's 1, 7, 8 and 9 in blood and lung are increased (Craig et al., 2015). The findings here corroborate the increases in MMP-8, 9 and 13 however there is no increase shown in MMP-1. The current hypothesis in IPF is that ECM accumulation may be due to an imbalance in the Tissue Inhibitors of Matrix Metalloproteinases (TIMPS) (Ramos et al., 2001a). Therefore, even overexpression of TIMPS may inhibit normal proteolytic mechanisms and result in a net ECM accumulation (Fukuda et al., 1998, Hayashi et al., 1996, Selman et al., 2000). . Also observed within our data is an increase in Cathepsins A, B, C, D, L, S, V and X/Z/P. These cysteine proteases are known to have strong collagenolytic and elastinolytic activity (Chapman et al., 1997). Little is currently known about the exact role of the Cathepsin family in IPF,

however recently it has been shown that there is an increase in total cysteine cathepsin activity in the Bleomycin model detected by PET scanning of a cysteine cathepsin specific probe (Withana et al., 2016). The data suggests that macrophage accumulation and high cathepsin activity both during the onset of fibrogenesis and when fibrosis is extensively established. Further work could consider the various proteases identified by this screen, and assess the ability of these proteases to digest IPF ECM.

Future work will assess the impact of control and IPF derived biosynthesised ECM on cellular function to determine if there is a qualitative difference between the ECM types. Furthermore expression of TG2 and the LOX family will be investigated during culture on both IPF and control ECM, to look for possible regulation of cell-ECM signalling, leading to the profibrotic environment that is characteristic of IPF.

### **3.4 Conclusions**

IPF derived fibroblasts produce more TG2 than non-IPF fibroblasts. This is supported by immunohistochemistry of IPF lung sections *in vivo*. Furthermore, the enzyme product of TG2 cross linking (n-epsilon-gamma glutamyl lysine) is also increased in IPF tissue. No statistical difference between collagen synthesis, total ECM protein or proliferation was found between IPF and non-IPF fibroblasts.

## **CHAPTER 4**

Impact of IPF ECM on fibroblast function

## 4 CHAPTER 4 - Impact of IPF ECM on fibroblast function

### 4.1 Introduction

#### 4.1.1 Background

ECM remodelling and deposition in IPF ultimately leads to respiratory failure. It has been shown in the chapter 3 that expression of the transcript for TG2 is increased in IPF fibroblasts. Therefore, the potential downstream effects of this enzyme, is to create proteolytically resistant protein cross links rendering the ECM resistant to normal proteolysis

It is known that ECM stiffness can affect seeded cell proliferation (Chaudhuri et al., 2014). Stiffer matrices have been shown to increase proliferation of hepatocellular carcinoma cells (Schrader et al., 2011). This influence of the ECM on cell proliferation may be a key factor in the pathogenesis of IPF. A recent paper published by Parker *et al.* (2014) describes a profibrotic microenvironment of the ECM in IPF, which also confers a positive feedback loop, driving fibroblast populations to a myofibroblasts phenotype (Parker et al., 2014). Furthermore, the gene expression profiling conducted in this publication highlights ECM regulated genes which are also of interest in this study.

LOXL1 and LOXL3 expression are co-regulated by both the ECM and the cell, increasing expression in response to IPF ECM (Parker et al., 2014).

Both feedback from the ECM can regulate these genes, and the cell genotype itself. This could be through expressing an abundance of one type of integrin or signalling molecule receptor such as TGF $\beta$ R which primes the cell to respond more or less strongly to a varying ECM. However MMP's 2, 3 and 10 are regulated predominantly by the disease state of the ECM, increasing in response to IPF ECM. The major finding of Parker *et al*'s study indicated that IPF ECM drives the expression of ECM components associated with IPF ECM. This includes a multitude of transcripts such as, but not limited to, *COL1A1*, *COL1A2*, *LAMB2*, *LAMA2*, *AGRN* and *VCAN*. In respect to IPF pathogenesis, this described method of ECM dysregulation and increase in collagen synthesis in response to a collagen rich matrix, seems to offer an insight into the disease progression and expansion of lung fibroblast populations.

In the normal lung, collagen I and III binding to the  $\alpha$ 2 $\beta$ 1 integrin inhibits proliferation through the dephosphorylation of AKT by protein phosphatase 2A(Ivaska *et al.*, 2002, Xia *et al.*, 2012). However in IPF fibroblasts this response seems to be diminished as  $\alpha$ 2 $\beta$ 1 expression within the FF in IPF lungs is reduced and inhibition of proliferation through this pathway is reduced. An increase in cell surface PDGF $\beta$ R through the cell adhesion regulated receptor degradation (Baron and Schwartz, 2000), may form another important factor in the fibroblast population expansion within the IPF lung. PDGF is a potent mitogen to fibroblasts (Bonner *et al.*, 1990). It has been shown that cultured macrophages from patients with interstitial lung fibrosis produce high levels of PDGF (Martinet *et al.*, 1986, Pantazis

et al., 1986). Therefore this may provide an insight into the propagation of a profibrotic microenvironment for fibroblasts in the IPF lung.

We hypothesised that the ECM confers a pro-fibrotic phenotype to resident and recruited cells within the IPF lung. To test this hypothesis, a series of experiments were designed to assess the impact of the ECM on gene expression, proliferation, apoptosis and other cellular functions.

#### 4.1.2 Aims & Objectives

- To assess the impact of IPF ECM on fibroblast cross-linking enzyme expression
- To analyse the bioactivity of IPF ECM with respect to proliferation, adhesion and apoptosis of control and IPF fibroblasts
- To manipulate ECM cross-linking and assess the impact on proteolysis *in vitro*.
- To determine the effect of cross-linking inhibition on proliferation, apoptosis and adhesion of IPF and control fibroblasts.

## **4.2 Results**

### 4.2.1 Real Time PCR analysis of ECM stabilising enzyme messenger RNA during matrix interchange

To assess the impact of IPF ECM on fibroblast cross linking gene expression, we designed an experiment in which both IPF and control fibroblasts were seeded on cell secreted biosynthesised ECM from both control and IPF fibroblasts. ECM was generated from 3 IPF and 3 control cell types. All 6 cell lines were subsequently seeded onto all matrices resulting in 36 experimental conditions. All experiments were conducted in 3 technical replicates and the whole experiment conducted 3 times.

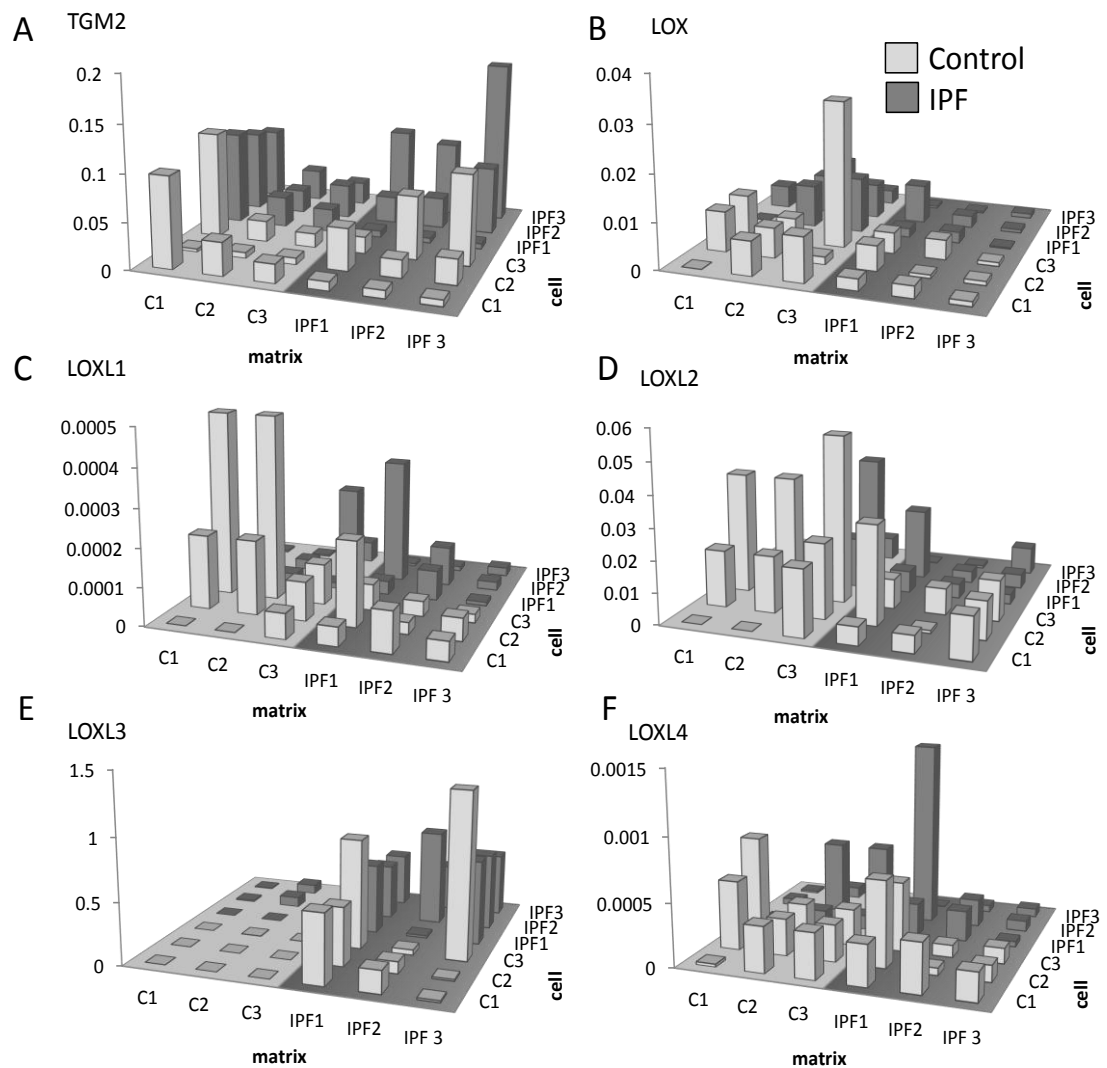


**Figure 4.1 Cross-linking enzyme mRNA expression of control and IPF fibroblasts on control and IPF matrices showing donor effect.** IPF ECM type shows no significant effect upon expression of TGM2 (a), LOXL1 (c), LOXL2 (d), LOXL3 (e) or LOXL4 (f). LOXL3 expression is significantly increased on IPF derived ECM ( $p < 0.001$ ). Control ECM induces increased expression of LOX ( $p < 0.05$ ). Data was compiled and analysed using a two way ANOVA. Data was normalised to  $\beta$ -Actin as a housekeeping gene. \* =  $p < 0.05$ , \*\*\* =  $p < 0.001$ .

TGM2 and the LOX family transcripts were assayed using Sybr Green real time PCR to examine the expression levels when seeded onto both control and IPF ECM. Control and IPF ECM was synthesised as described in 2.15. Control and IPF cells were seeded onto all matrices as depicted in figure 4.1 and left for 24 hours. Following this RNA was harvested as described

in 2.10, cDNA synthesised as described in 2.11 and real time PCR conducted as described in 2.12 using Brilliant III Sybr Master Mix (Agilent Technologies). *TGM2* mRNA expression levels appears to be driven by cell type more than the ECM the cells are seeded on to however no statistical difference was observed. IPF matrix not did increase expression of *TGM2*, *LOXL1*, *LOXL2* or *LOXL4*. Control matrix induced increased expression of LOX ( $p < 0.05$ ) (Figure 4.1b). IPF matrix strongly induced *LOXL3* mRNA expression ( $p < 0.001$ ) (Figure 4.1e) compared to control matrix. Expression levels of *LOXL3* on control ECM is very low or not present in two control cell types. *LOXL2* mRNA is not significantly increased by control ECM ( $p > 0.05$ ) however the trend shown (Figure 4.1D) tends towards control ECM increasing *LOXL2* expression.

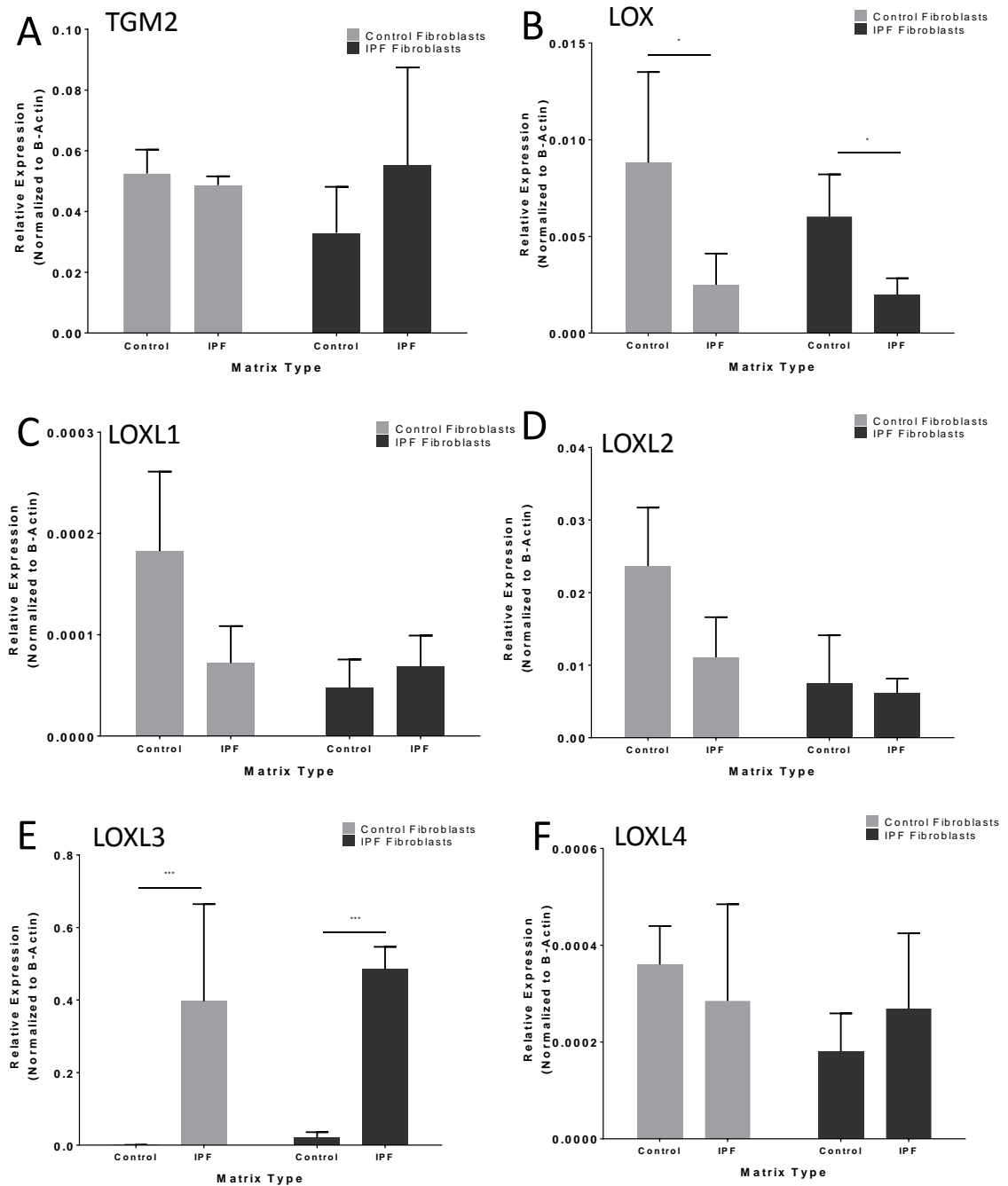


**Figure 4.2 Cross-linking enzyme mRNA expression of control and IPF fibroblasts on control and IPF matrices showing donor effect.** IPF ECM type shows no significant effect upon expression of TGM2 (a), LOXL1 (c), LOXL2 (d), LOXL3 (e) or LOXL4 (f). LOXL3 expression is significantly increased on IPF derived ECM ( $p < 0.001$ ). Control ECM induces increased expression of LOX ( $p < 0.05$ ). Data was compiled and analysed using a two way ANOVA. Data was normalised to  $\beta$ -Actin as a housekeeping gene. \* =  $p < 0.05$ , \*\*\* =  $p < 0.001$ .

#### 4.2.2 Analysis of conditioned media LOXL3 during matrix interchange

Conditioned media harvested from the experiment described in 4.2.1 was assayed with a LOXL3 protein ELISA as described in 2.31. The total LOXL3 protein in conditioned media from fibroblasts seeded onto IPF ECM is increased ( $p < 0.05$ ). This is in line with the mRNA expression as shown in Figure 4.1e. IPF matrix induces LOXL3 protein expression, regardless of the disease status of the fibroblasts seeded onto them.

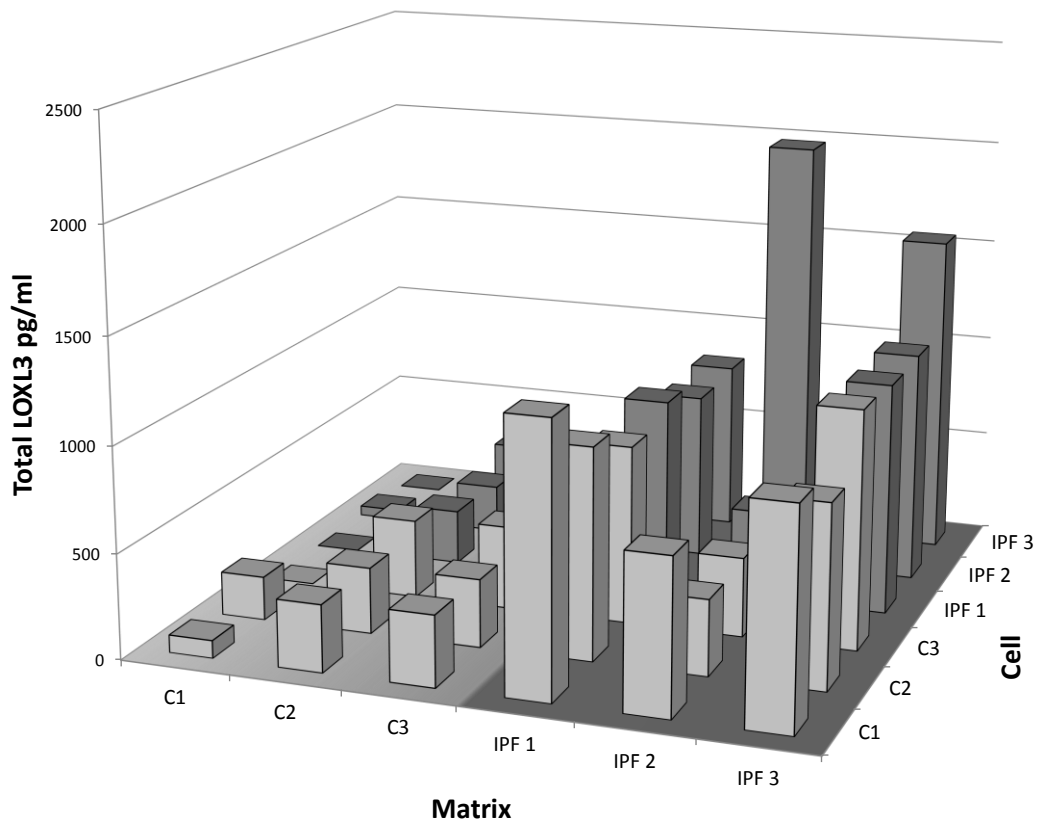


**Figure 4.3 LOXL3 content of fibroblast conditioned media during matrix interchange.** LOXL3 protein levels are increased in conditioned media from fibroblasts seeded onto IPF derived ECM ( $p < 0.05$ ). Data was compiled and analysed using a two tailed student's t-test.

#### 4.2.3 Analysis of TG2 activity during matrix interchange

Conditioned media harvested from the experiment described in 4.2.1 was assayed with the TGase activity kit as described in 2.39.

IPF matrix induces an increase in extracellular TGase activity when control

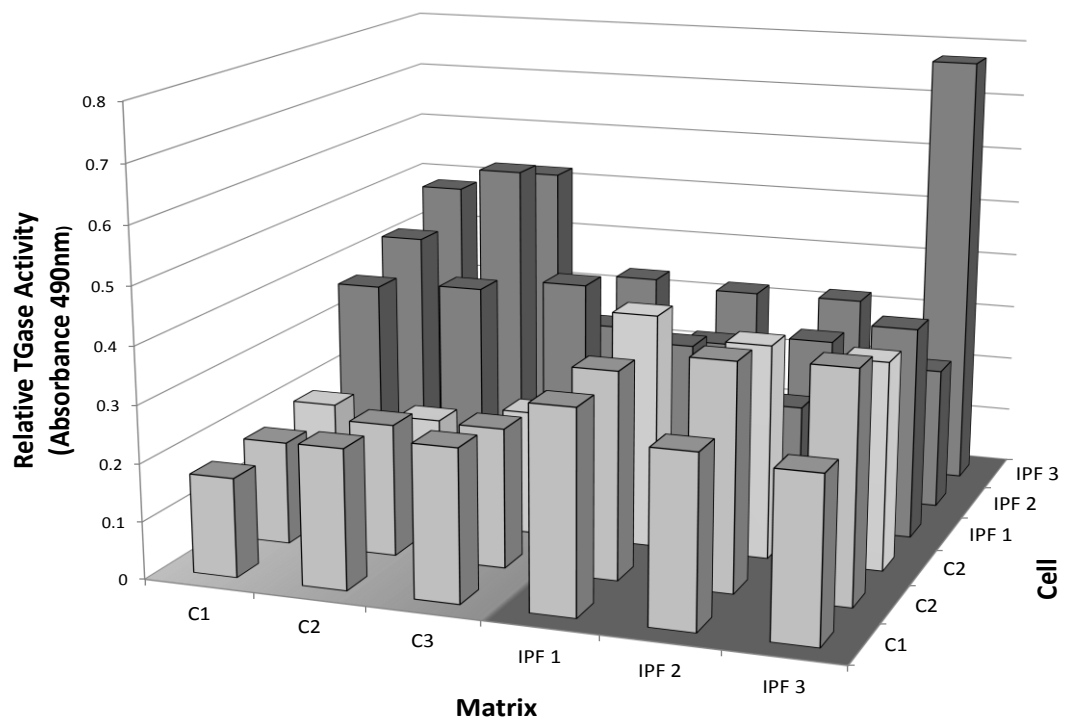


**Figure 4.4 Total TGase activity of fibroblast conditioned media during matrix interchange.** Total TGase activity is increased in control fibroblast conditioned media by IPF derived ECM ( $p < 0.01$ ). IPF fibroblasts express a higher baseline of TGase activity on IPF matrix compared to control fibroblasts on control matrix ( $p < 0.05$ ). Data was compiled and analysed using a two tailed student's t-test.

fibroblasts are seeded onto it compared to control ECM ( $p < 0.01$ ). IPF fibroblasts also have a higher baseline TGase activity when seeded on their respective matrices when compared to control fibroblasts on control ECM ( $p < 0.05$ ). When IPF fibroblasts are seeded onto control ECM, TGase activity is increased in the conditioned media compared to IPF fibroblasts on IPF ECM ( $p < 0.05$ ).

#### 4.2.4 Cell proliferation of normal and IPF derived fibroblasts during matrix interchange

To assess the effect of IPF ECM on proliferation, an experiment was designed to seed control fibroblasts onto three IPF and three control matrices, and expose them to 5% FBS and PDGF-bb. Commercially available Human Pulmonary Fibroblasts (HPF) at passage 4 were seeded onto both control and IPF derived ECM and exposed to DMEM either serum

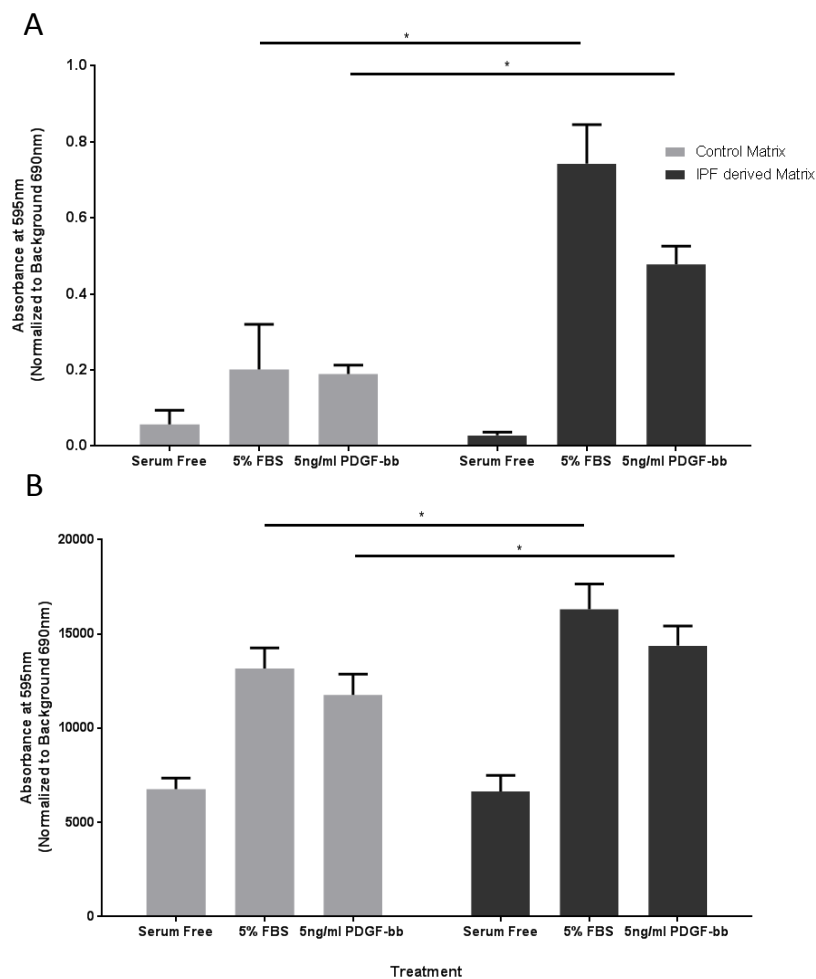


**Figure 4.5 Proliferation of control fibroblasts seeded onto control and IPF matrices and exposed to FBS and PDGF-bb** (A) MTT reduction of control fibroblasts seeded onto control and IPF matrices. IPF matrix supports increased proliferation in response to 5% FBS ( $p < 0.05$ ) and 5ng/ml PDGF-bb ( $p < 0.05$ ). (B) EdU incorporation of control fibroblasts seeded onto control and IPF matrices. IPF matrix supports increased proliferation in response to 5% FBS ( $p < 0.05$ ) and 5ng/ml PDGF-bb ( $p < 0.05$ ). Data analysed with two tailed student's t-test. Data presented  $\pm$ SD.

free, with 5% FBS or 5ng/ml PDGF-bb. Proliferation was assessed by two independent techniques; MTT reduction as an indication of cell number as described in 2.32 or EdU incorporation as a marker of DNA synthesis as described in 2.33. Cells were exposed to mitogens for 72 hours, and proliferation measured.

Both MTT and EdU assays show the same trend. Control and IPF matrices show no difference in seeded cell proliferation when no mitogen is present in the media. Control fibroblasts show increased proliferation when seeded onto IPF matrices in the presence of FBS in both MTT assay; Control 0.202AU (SD=0.119) vs. IPF 0.743AU (SD=0.103)  $p < 0.05$  (Figure 4.4A) and EdU assays; Control 13168.02AU (SD=1085.38) vs. IPF 16314.08AU (SD=1346.46)  $p < 0.05$  (Figure 4. 4B). Furthermore this effect is conserved when seeded fibroblasts are exposed to 5ng/ml PDGF-bb in both MTT assay; Control 0.190AU (SD=0.023) vs IPF 0.478AU (SD=0.048)  $p < 0.05$  (Figure 4.4A) and EdU assays; Control 11769.74AU (SD=1097.27) vs. IPF 14377.94AU (SD=1044.84)  $p < 0.05$  (Figure 4.4B). These data suggest that IPF ECM supports an increased proliferative capacity of seeded control fibroblast populations in response to 5% FBS and PDGF-bb.

#### 4.2.5 Manipulating adhesion and proliferation during matrix interchange

We next examined whether IPF ECM was more adhesive to fibroblasts than normal ECM. To validate our cell adhesion method and ensure accurate measurements of cellular adhesion, a trial was conducted using known cell numbers of control fibroblasts seeded onto a collagen substrate, as described in section 2.38. Wells of a 96 well plate were coated with Type I human placental collagen as described in section 2.37 for the optimisation. Known numbers of control fibroblasts were seeded into collagen coated wells and left to adhere for two hours and assayed as described in 2.1.38

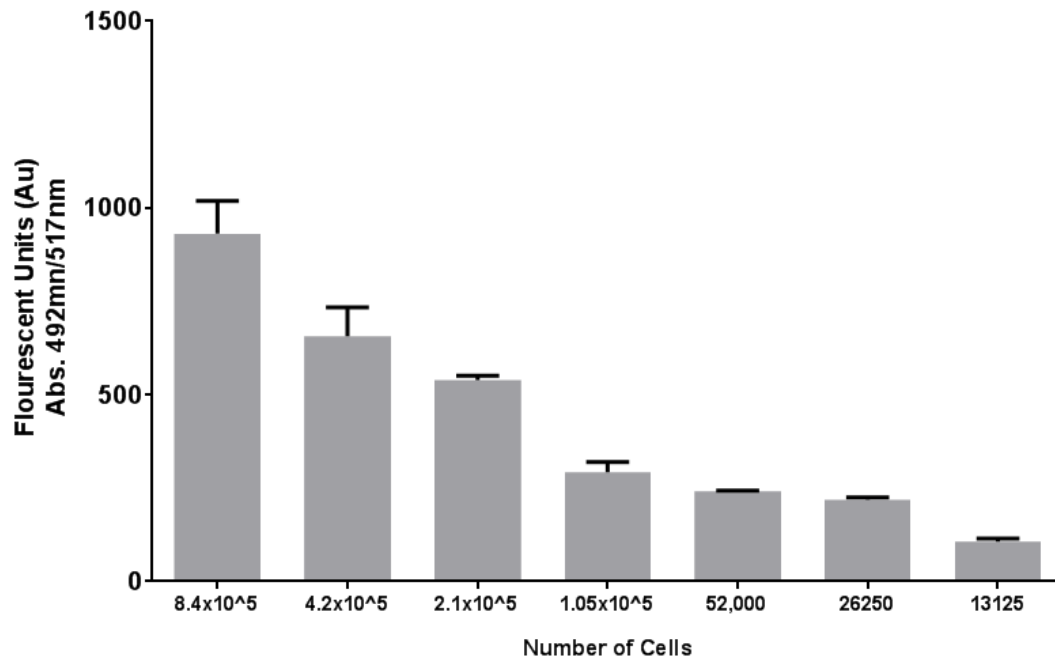


**Figure 4.6 Average well fluorescence of Cell-Tracker dye labelled fibroblasts seeded into Type I collagen coated wells.** Cell numbers ranging from  $8.4 \times 10^5$  to 13125 seeded into collagen coated wells and the average well fluorescence read. As cell numbers decreased, the average well fluorescence decreased. Analysed using Spearmans Rank correlation ( $p < 0.01$ ,  $r = 1$ ).

Cell numbers show a statistically significant relationship to fluorescence ( $p < 0.01$ ,  $r = 1$ ) using spearmans rank correlation as shown in Figure 4.8.

This shows that cell numbers are directly proportional to total fluorescence. The same technique was then applied to seeding control fibroblasts on both control and IPF ECM as described in 2.38 with cross-linking enzyme inhibitors of TG2 and the LOX family.

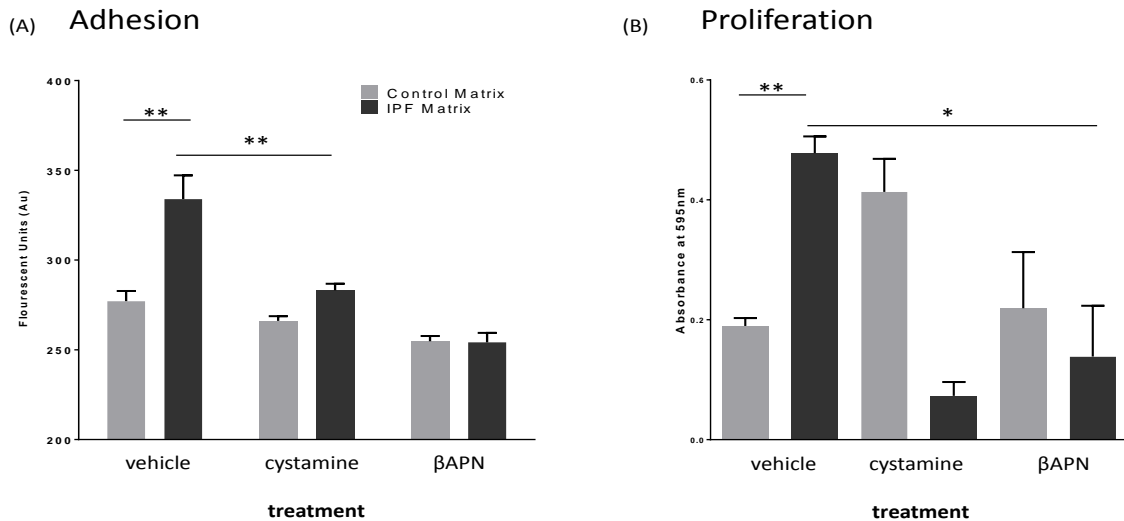


**Figure 4.7 Control fibroblast adhesion and proliferation on control and IPF ECM treated with cross-linking inhibitors.** (A) Fluorescence of adhered cells on IPF and control ECM, untreated or with CyM or betaAPN. IPF ECM shows greater cell adhesion compared to control ECM ( $p < 0.01$ ). CyM treatment during ECM synthesis reduces subsequent seeded cell adhesion ( $p < 0.01$ ), as does betaAPN treatment ( $p < 0.01$ ). (B) IPF ECM supports increased proliferation compared to control ECM ( $p < 0.01$ ). Cystamine and betaAPN treatment during ECM synthesis reduces the increased subsequent seeded cell proliferation compared to the vehicle only ( $p < 0.01$  and  $p < 0.05$  respectively). Data presented  $\pm$ SD. \* =  $p < 0.05$ , \*\* =  $p < 0.01$ .

ECM preparations were produced by three control and three IPF fibroblast cell lines treated with inhibitors of TG2 (CyM) and the LOX family (betaAPN) following which ECM was prepared as described in 2.1.15 with control fibroblasts seeded onto them. Data were analysed using a two way ANOVA with Tukeys's multiple comparison test. IPF ECM shows an increased cell adhesion compared to control; 277.10AU (SD=17.08) vs. 333.97AU (SD=39.77) ( $p < 0.01$ ) as shown in Figure 4.7A.

IPF ECM synthesised with CyM show a reduction in the increased adhesion seen on IPF ECM; IPF 333.97AU (SD=39.77) vs. IPF+CyM 283.15AU (SD=11.04)  $p<0.01$ . Furthermore,  $\beta$ APN inhibition of the LOX family also showed a reduction. Generation of control ECM in the presence of the transglutaminase 2 inhibitor (CyM) had no effect on fibroblast adhesion. IPF ECM supports increased proliferation compared to control ECM ( $p<0.01$ ). Cystamine and  $\beta$ APN treatment during ECM synthesis reduces the increased subsequent seeded cell proliferation compared to the vehicle only ( $p<0.01$  and  $p<0.05$  respectively). This indicates an importance of ECM cross-linking in seeded cell proliferation.

#### 4.2.6 IPF ECM does not enhance protection against induced apoptosis

To investigate the effect of IPF ECM on induced apoptosis, control and IPF ECM were generated, and new cell populations seeded onto them. ECM was prepared as described in 2.15 with  $2 \times 10^4$  control or IPF fibroblasts seeded onto them. After 24 hours, media was changed to media containing either (A) staurosporine ( $1 \mu\text{M}$ ) or (B) fas ligand ( $100 \text{ng/ml}$ ) for 6 hours before harvest for western blot for Cleaved PARP and Caspase 3 activation and TUNEL assay.

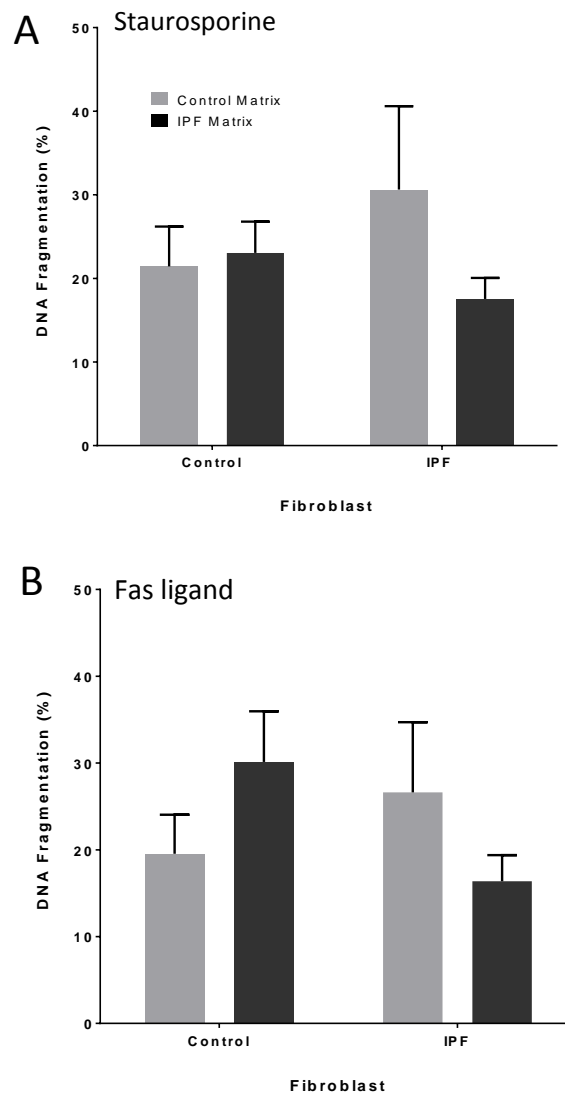


**Figure 4.8** Three control and three IPF derived fibroblasts were cultured on three control and three IPF derived ECM preparations and apoptosis induced by (A) staurosporine (1 $\mu$ M) or (B) fas ligand (100ng/ml). IPF matrix did not affect the percentage of TUNEL positive cells induced by either agent when compared with control ECM. Data was analysed using a two way ANOVA. Data presented  $\pm$ SD.

Staurosporine induction shows no difference in the number of TUNEL positive cells between IPF and control matrices or cell disease status (4.8A)( $p > 0.05$ ) indicating no difference in the number of apoptotic cells between control and IPF ECM. Fas ligand at 100ng/ml also showed no statistical difference between IPF and control matrices (4.8B) ( $p > 0.05$ ).

This was confirmed by western blot as described in sections 2.1.27-29 for PARP cleavage and Caspase 3 activation (4.7C). No difference in PARP cleavage, Caspase 3 activation was determined by densitometry.

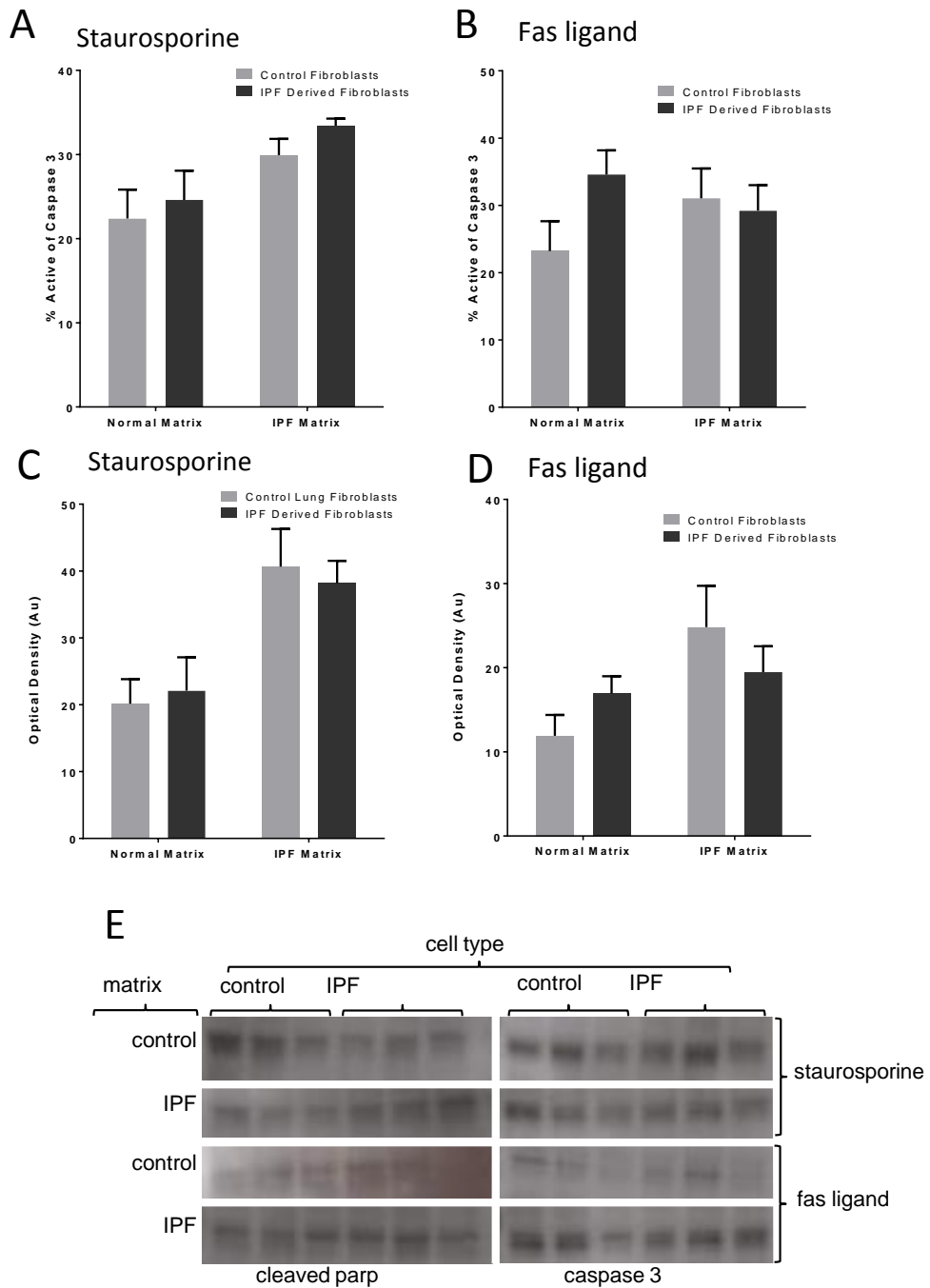


**Figure 4.9** Western blotting of three control and IPF derived fibroblasts cultured on control and IPF derived ECM and treated with staurosporine (1 $\mu$ M) or fas ligand (100ng/ml), shows no difference in cleaved PARP or caspase 3 between ECM types. Data was analysed using a two way ANOVA. Data presented  $\pm$ SD.

#### 4.2.7 Immunohistochemistry of myofibroblast markers in IPF tissue

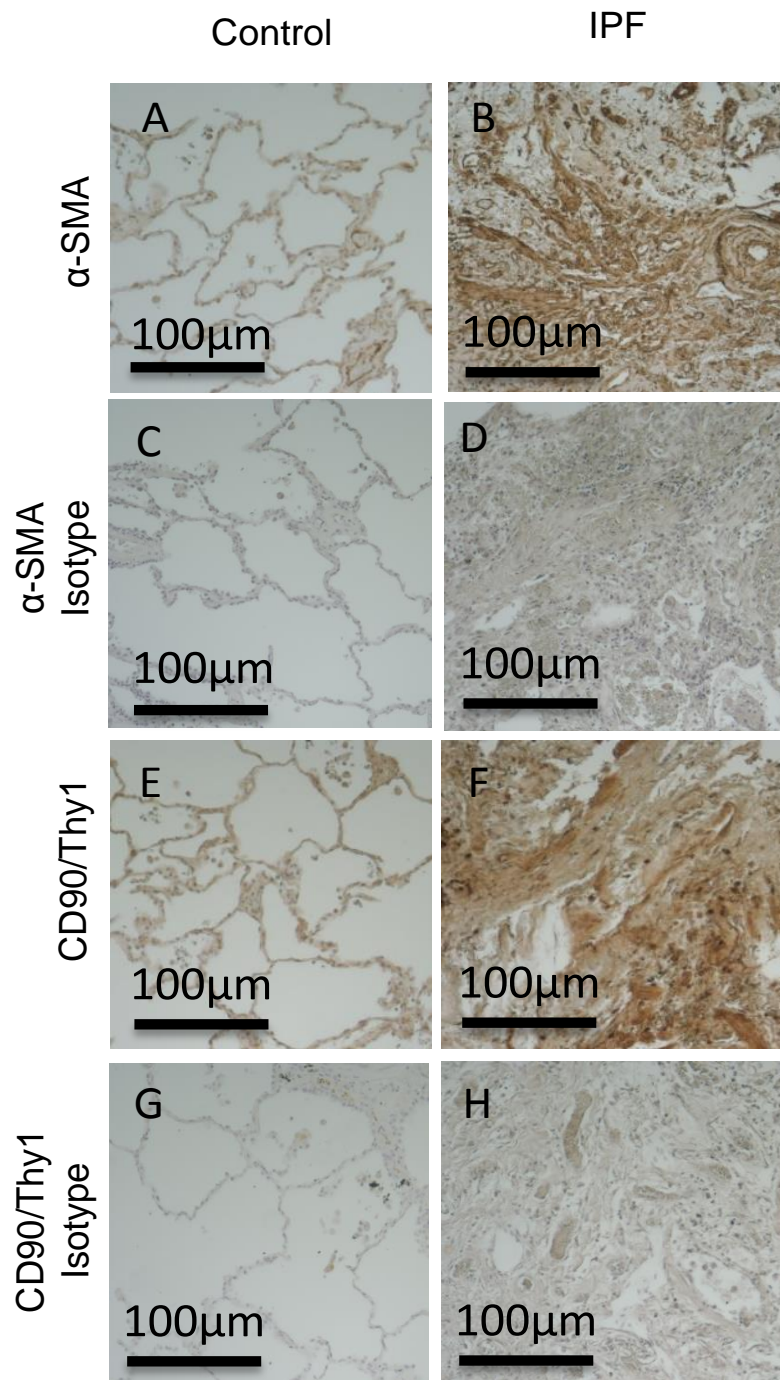


**Figure 4.10 Immunohistochemistry of primary IPF and non-IPF lung tissue stained for smooth muscle actin and Thy1 (CD90) as markers of fibroblast populations.**  $\alpha$ -SMA expression in control tissue (A) is diffuse in the alveolar wall with relatively low expression compared to IPF (B) which shows extensive staining across the sections. CD90 staining exhibits a similar pattern to that of  $\alpha$ -SMA in both control and IPF tissue. Representative images shown. (n=3).

Immunohistochemistry was conducted to determine the presence of fibroblast markers  $\alpha$ SMA and CD90/Thy1 in primary human IPF and non-IPF control tissues. The IHC technique used is described in 2.39. Antibody dilutions were  $\alpha$ SMA at 1:200 and CD90/Thy1 at 1:200.  $\alpha$ -SMA expression in control tissue (Figure 4.10A) compared to IPF which shows extensive staining across the sections (Figure 4.10B), indicating a high myofibroblast population. CD90 staining exhibits a similar pattern to that of  $\alpha$ -SMA in both control (Figure 4.10E) and IPF tissue (Figure 4.10F). The slightly more diffuse staining in the CD90 stained IPF tissue may indicate this marker is a little less specific than  $\alpha$ -SMA. However the IPF tissue does stain significantly more strongly for  $\alpha$ -SMA and CD90.

#### 4.2.8 Optimisation of ECM proteolysis assays

It was hypothesised that IPF ECM is resistant to natural proteolytic turnover by virtue of excessive ECM cross-linking. Therefore an assay was designed to investigate the resistance of IPF ECM to proteolysis by MMP mediated digestion. Fibroblasts were incubated in medium containing tritiated proline, which is then converted by prolyl hydroxylase in the fibroblasts to hydroxyproline in the fibroblast secreted collagen in the cell deposited ECM. MMP mediated digestion was then measured by tritium liberation from ECM preparations.

Prior to large scale experiments, the method was optimised for MMP concentration and time scale of digestion. Radio labelled ECM was synthesised as described in 2.16 and decellularised as in 2.15. Radio labelled, cell free ECM was then digested over 15 minutes to 4 hours with recombinant activated MMP1, MMP1 reconstitution buffer containing APMA and DMEM/f12 only control. DMEM/f12 culture media was then collected and the liberated radioactivity counted as described in 2.19 as a measure of ECM proteolysis.

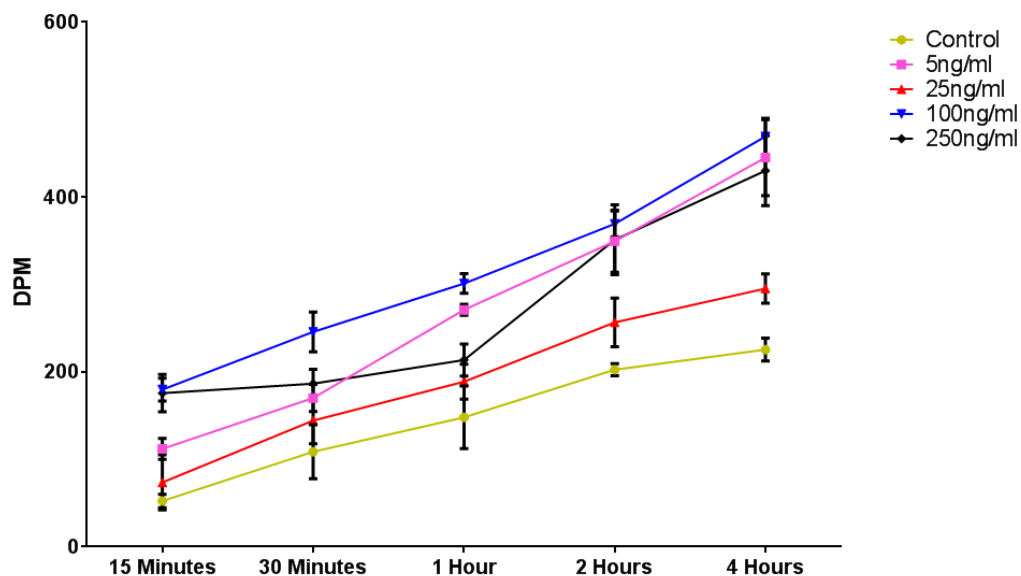


**Figure 4.11. Tritiated hydroxyproline release from normal human lung fibroblast synthesised ECM** Liberation of radio labelled collagen fragments as a product of MMP1 mediated proteolysis, normalised to scintillant only background. Control digest media containing APMA shows a progressive release of 3H-hydroxyproline indicating endogenous protease activation by APMA. Concentrations of 5ng/ml MMP1 (Pink), 25ng/ml (Red), 100ng/ml (Blue) and 250ng/ml (Black) all show significant increase in DPM over control at 4 hours MMP1 exposure. Saturation of MMP1 concentration occurred at 100ng/ml where addition of 250ng/ml showed no additional 3H-hydroxyproline release. Interaction  $p < 0.0001$ , 4.72% of total variation; Time  $p < 0.0001$ , 64.32% of total variation; MMP1  $p < 0.0001$ , 27.86% of total variation;  $n=3$ . Data presented  $\pm$ SD. DPM= disintegrations per minute.

Data were analysed using a two way ANOVA with Tukey's multiple comparison test. All MMP1 concentrations at 4 hours show a significantly increased disintegrations per minute (DPM), compared to control; 5ng/ml  $p < 0.0001$ ; 25ng/ml  $p < 0.01$ ; 100ng/ml  $p < 0.0001$  and 250ng/ml  $p < 0.0001$  respectively as shown in Figure 4.11.

DPM increases are saturated above 100ng/ml in regard to addition of 250ng/ml MMP1 showed no additional effect on 3H-Hydroxyproline liberation ( $p > 0.05$ ). Therefore MMP1 at 100ng/ml was chosen as the protease concentration for digests. Furthermore, 4 hours was determined to be the most suitable time point to reduce any background effect on samples while maximising tritium release from the ECM.

#### 4.2.9 Manipulation of proteolysis through cross link enzyme inhibitors

To determine the effect on ECM degradation of LOX family or TG2 cross links, an experiment was designed in which enzyme specific cross links could be inhibited during ECM synthesis to assess the subsequent effect on proteolysis. Using the method optimised in 4.2.8 radio labelled ECM was synthesised as described in 2.16 and decellularised as in 2.15. MMP1, 2 and 7 were used at 100ng/ml with APMA vehicle control in to digest control and IPF ECM's, during synthesis, were treated with either CyM,  $\beta$ APN or an experimental LOXL3 inhibitor compound, PXS-5120A (Pharmaxis, Australia) as described in 2.9.

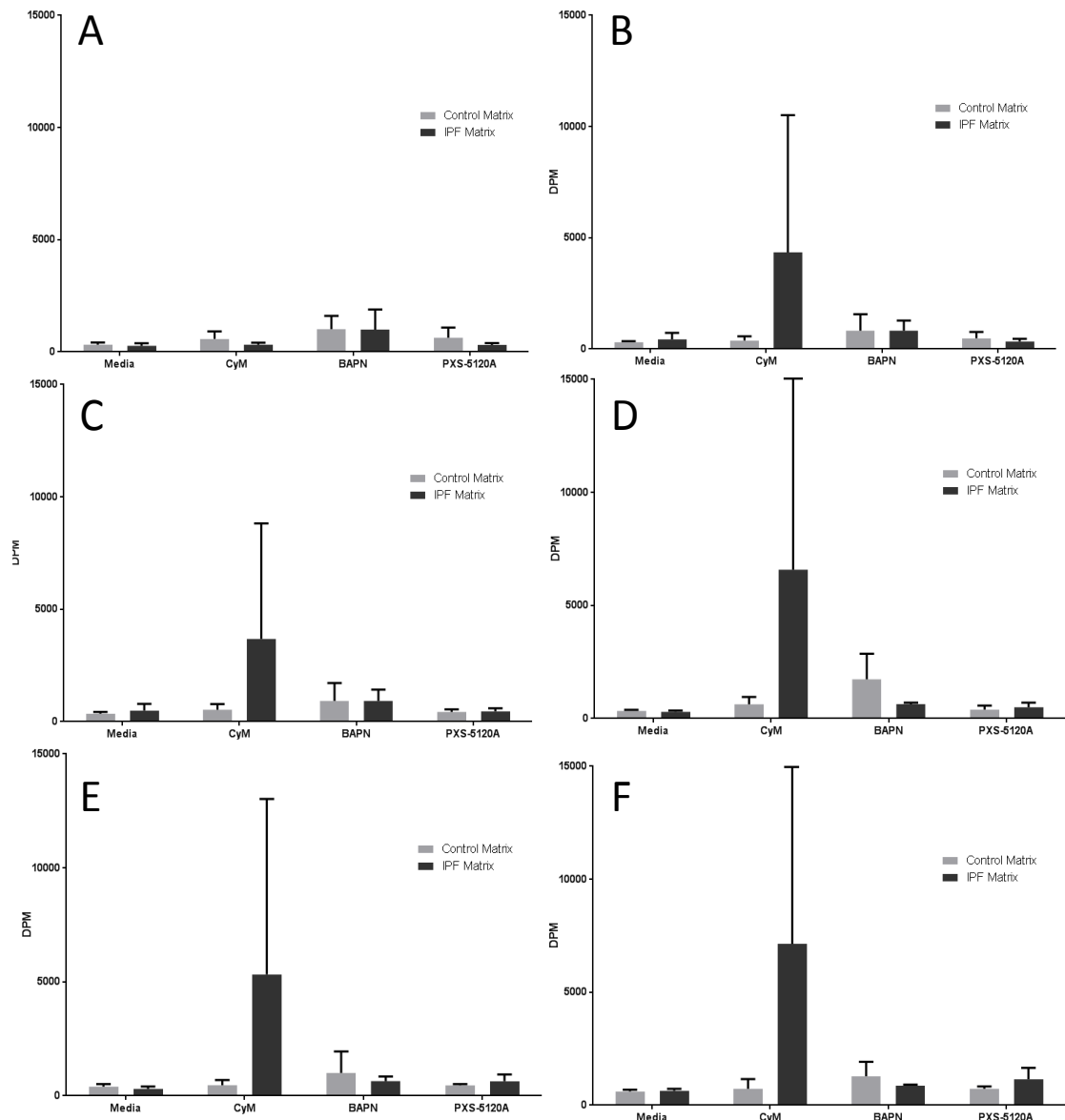


**Figure 4.12 Tritiated hydroxyproline release from control and IPF synthesised ECM.** Liberation of radio labelled collagen fragments as a product of proteolysis, normalised to scintillant only background. DMEM only control (A) shows a low level of baseline turnover with no significant effect of TG2, LOX family or LOXL3 inhibition during synthesis. APMA vehicle control (B) shows no significant increase in proteolysis of cross linking inhibitor treated ECMs ( $p>0.05$ ), however TG2 inhibition during IPF ECM synthesis shows a trend towards an increase in proteolysis. Addition of MMP1 (C), MMP2 (D), MMP1 and 2 (E) and MMP7 (F) show the same trend as the APMA control, however this trend is not significant ( $p>0.05$ ).  $n=3$ . Data presented  $\pm$ SD. DPM= disintegrations per minute.

Inhibition of TG2 mediated cross linking during IPF ECM synthesis shows a trend towards an increase in degradation following decellularisation, however this was found to not be statistically significant due to the large variation between the primary IPF fibroblasts ( $p>0.05$ ). Addition of DMEM

containing AMPA to the ECM's showed a trend towards an increase in proteolysis of CyM treated ECMs. Addition of recombinant MMP1, 2 and 7 showed no additive effect over the vehicle control. Control ECM showed no significant effect of CyM on resistance to proteolysis. LOX family or specific LOXL3 inhibition showed no effect on proteolysis of either control or IPF ECM.

Due to the large effect of the AMPA control on the samples, another set of experiments was conducted using the catalytic domain of active MMP1, therefore removing the requirement for MMP activation using APMA.

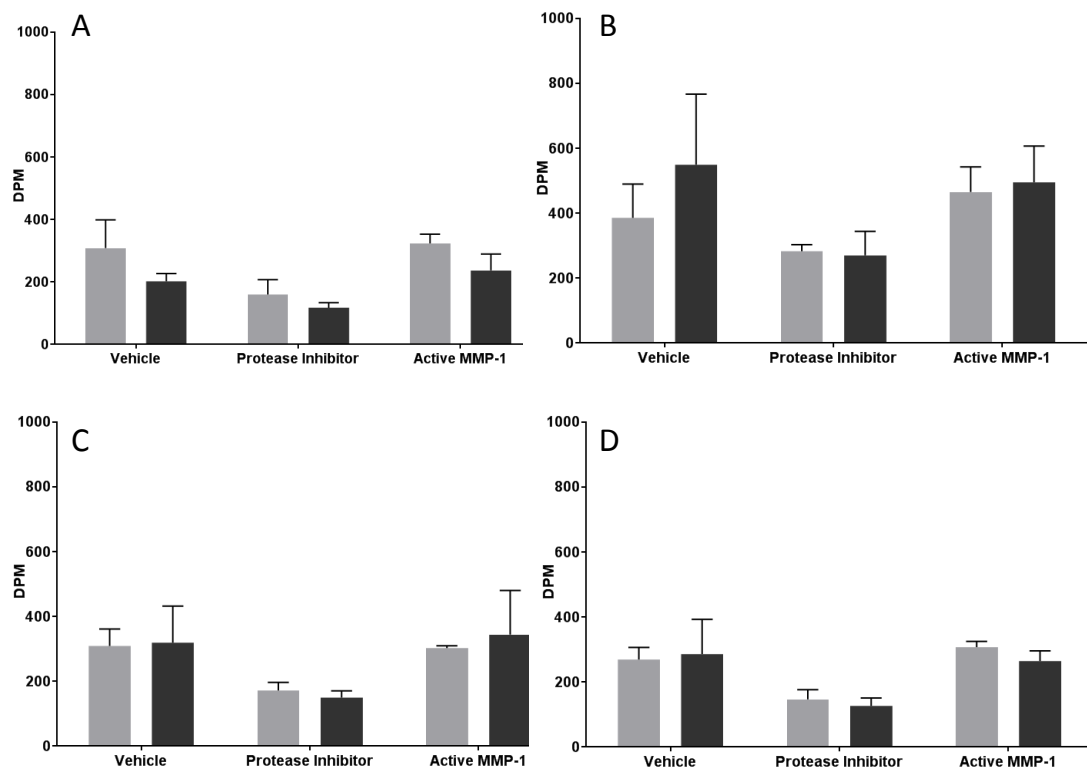


**Figure 4.13 Tritiated hydroxyproline release from control and IPF synthesised ECM and digested with recombinant catalytic domain of MMP1** Liberation of radio labelled collagen fragments as a product of proteolysis, normalised to scintillant only background. Control (light grey) and IPF (dark grey) ECMs were digested with DMEM only as control, DMEM with complete protease inhibitor cocktail or DMEM with 100ng/ml active MMP1. (A) Untreated ECM's show no significant difference between control and IPF ECM proteolysis. (B) CyM treated, (C) βAPN treated and (D) PXS-5120A treated ECMs show a similar trend to that of untreated. n=3. Data presented ±SD. DPM= disintegrations per minute.

Samples were analysed with a two way ANOVA using Tukey's multiple comparisons test without assuming consistent standard deviation. When samples were compared control to IPF, no statistical difference was observed ( $p>0.05$ ). Protease inhibitor on all matrices showed a trend towards a reduced 3H-hydroxyproline release; however this is not statistically significant. Active MMP1 digestion of all matrices showed no additional effect over vehicle control.

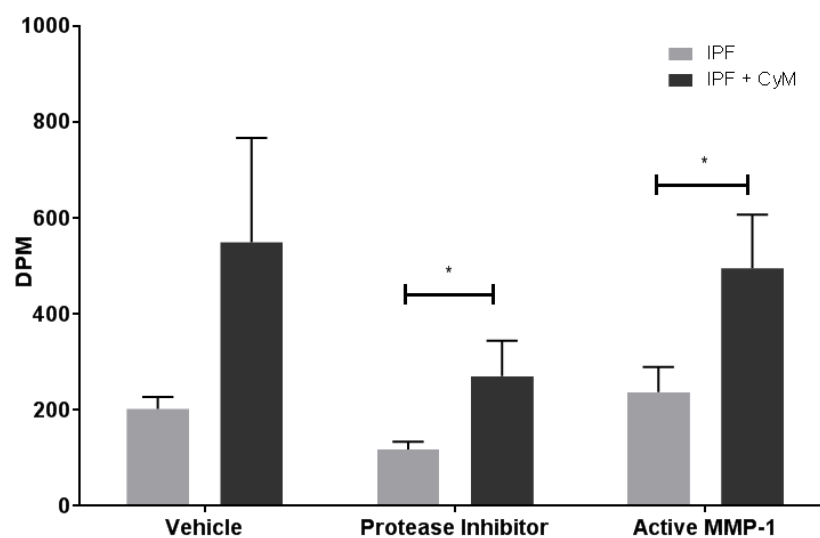


**Figure 4.14 Tritiated hydroxyproline release from IPF synthesised ECM or IPF ECM synthesised with TG2 inhibitor; and digested with recombinant catalytic domain of MMP1.** Vehicle control shows no significant difference between untreated IPF and CyM treated IPF matrices ( $p>0.05$ ). Digest media containing complete protease inhibitor shows that CyM treated ECM releases increased amounts of 3H-hydroxyproline compared to untreated IPF ECM ( $p<0.05$ ). Active MMP1 digest media shows a significant increase in 3H-Hydroxyproline release from CyM treated IPF ECM compared to untreated IPF ECM ( $p<0.05$ ).

IPF ECM treated with CyM during synthesis shows a significant increase in 3H-Hydroxyproline release from the ECM when in the presence of complete protease inhibitor as shown in Figure 4.14 Tritiated **hydroxyproline release from IPF synthesised ECM or IPF ECM synthesised with TG2 inhibitor; and digested with recombinant catalytic domain of MMP1**. Vehicle control shows no significant difference between untreated IPF and CyM treated IPF matrices ( $p>0.05$ ). Digest media containing complete protease inhibitor shows that CyM treated ECM releases increased amounts of 3H-hydroxyproline compared to untreated IPF ECM ( $p<0.05$ ). Active MMP1 digest media shows a significant increase in 3H-Hydroxyproline release from CyM treated IPF ECM compared to untreated IPF ECM ( $p<0.05$ ).

(IPF=117.75 DPM (SD=17.26) vs. IPF + CyM =270.45 DPM (SD=73.55))( $p<0.05$ ). When digested with media containing complete protease inhibitor, IPF fibroblast matrix treated with CyM, showed a trend towards a decrease in tritium liberation, however this is not significant. Furthermore, digestion of both untreated IPF ECMs and IPF ECMs treated with CyM shows that CyM treated IPF ECM released more 3H-Hydroxyproline into the digest media than untreated IPF (IPF=237.56 DPM (SD=51.84) vs. IPF + CyM=495.10 DPM (SD=111.51))( $p<0.05$ ). This effect was also seen in the vehicle control containing only DMEM/f12, however, this effect appeared to be a conserved effect of the TG2 inhibitor during ECM synthesis.

### 4.3 Discussion

The dynamic and crucial role in ECM-cell interaction is well described with little doubt that many complex signalling mechanisms regulate many cell behaviours. It has been previously described that LOXL3 expression can be partially regulated by the ECM (Parker et al., 2014). Here we have demonstrated that IPF ECM can induce LOXL3 mRNA and protein expression in both IPF and control fibroblasts. LOXL3 is a relatively newly described protein (Jourdan-Le Saux et al., 2001) with a highly conserved catalytic domain. The induction of this enzyme by IPF ECM may contribute to the positive pro-fibrotic feedback loop as described by Parker and colleagues (2014). This may be due to the increase in ECM stiffness conferred by collagen cross linking, which is known to increase cell proliferation (Hadjipanayi et al., 2009), adhesion (Wells, 2008, Leight et al., 2012) and reduce apoptosis (Leight et al., 2012). However, in these experiments, protection from apoptosis was not observed on IPF ECM when induced by either 1 $\mu$ M staurosporine or 100ng/ml fas-ligand.

Another consideration of these results is the culture method itself. When growing cells on plastic, or on ECM deposited onto plastic, the mechanical forces experienced by the cell populations will be very different to that of in vivo tissue. All cells have mechanisms to sense the mechanical stiffness of their environment (Discher et al., 2005) and plastic itself is extremely rigid in terms of an extracellular substrate. This may impact the response of the control fibroblasts more so than the IPF fibroblasts when considered in terms of our hypothesis that IPF ECM is stiffer than control. Cells are

known to proliferate quicker on stiffer, more rigid ECMs, therefore even culture on plastic may impact the cellular function. Furthermore, observations within stem cell biology have shown that the rigidity of ECM's can influence stem cell differentiation (Chen and Simmons, 2011, Lee et al., 2011). This influence on cell fate is known to drive the differentiation of fibroblasts to the myofibroblast phenotype which is abundant in IPF. This propagation of a pro-fibrotic environment through dysregulated ECM stiffness may be a key player in governing many mechanisms of cell behaviour in IPF.

As previously described in 3.2.7, many MMP's are increased in the assayed IPF fibroblast conditioned media. The addition of 4-Aminophenylmercuric acetate (APMA) to ECM containing inactive proteases would induce activation by the same method of activation as described by the manufacturer (R&D Systems, MN, USA) resulting in redundancy of the additional MMP's. This activation of resident ECM proteases may account for the proteolysis observed in the vehicle control, and the subsequent increase in 3H-Hydroxyproline liberation seen from IPF ECM treated with CyM; which may be due in part to the inhibition of epsilon gamma glutamyl Lysine formation by TG2. This reduction in the peptide cross link formation, which confers high proteolytic resistance (Chau et al., 2005), would attenuate the effect of endogenous proteases in the digest cultures. This can be seen as IPF ECM synthesised without TG2 inhibitor does not show a spike in DPM, whereas the ECM's with reduced epsilon gamma glutamyl Lysine showed a trend towards an increase in DPM. This may be in part be

the mechanism underlying the effect observed. This can be further elucidated by the effect of CyM on IPF ECM digested with the catalytic domain of MMP1. The additional MMP1 added to the digest media shows no additive effect over the baseline level of proteolysis when compared to vehicle control. However, the effect of inhibition of stabilisation can be observed between IPF ECM and IPF ECM synthesised with CyM in that it releases 3H-Hydroxyproline at a quicker rate than that of TG2 stabilised ECM. It is well documented that TG2 catalysed cross linking *in vivo* results in increased tissue stiffness (Allen et al., 2012, Jung et al., 2013, Steppan et al., 2014) and therefore it is plausible that increased TG2 activity within the IPF lung would result in the same profibrotic ECM production. Therefore inhibiting the cross linking process may not only increase the rate of ECM degradation and turnover, but reduce the increased proliferative effect of stiff ECM as I have demonstrated *in vitro*.

The relatively small sample size used in these experiments, limited the statistical power of the experiments carried out. Three possible problems could be observed within the data presented here. The difficulty in finding a true effect is considerably more difficult, especially with the known large variation in primary patient derived cells. This leads to a high standard deviation, and a reduced robustness of the statistical testing. However, immortalisation or transformation of primary cells into cell lines may yield cellular behaviours that differ from their non-immortalised counterparts (Hopfer et al., 1996). Therefore primary, low passage cells were chosen as the biological response for these samples used would be closer to that

of an *in vivo* situation. Furthermore, no commercial IPF fibroblast line is currently available.

Another consideration was that of the Positive Predictive Value (PPV). The PPV is the chance that the finding of a positive result is a true effect and not a false positive. Therefore with the samples available, it was determined that multiple, independent techniques be used to assess cellular function, such as those used during the PDGF-bb induced proliferation experiments. As well as the PPV, the consideration that any true positive effect observed would be subject to the 'winners curse,' where the result is exaggerated through the degree to which the measurable parameter differs to achieve significance (Ioannidis, 2008).

#### **4.4 Conclusions**

IPF ECM induces increased expression of *LOXL3* mRNA and LOXL3 protein. TG2 activity is predominantly determined by the disease state of the fibroblasts rather than the ECM it is seeded upon. IPF ECM supports and increased proliferation in seeded control fibroblasts in the presence of FBS and PDGF-bb. This can be attenuated by inhibition of TG2 and the LOX family during ECM synthesis. IPF ECM does not protect against staurosporine or FAS ligand induced apoptosis.

IPF lung tissue contains extensive staining for TG2,  $\epsilon$ - $\gamma$ -glutamyl lysine cross links. Furthermore, LOXL3 staining is weakly present in the fibrotic areas of the IPF lung, whereas it is not present in control lung tissue.

IPF ECM treated with CyM during synthesis shows a trend towards increasing ECM degradation; however the effect is not statistically significant. Digestion of IPF ECM treated with CyM, when compared to untreated IPF ECM shows an increase in ECM turnover. Addition of APMA to CyM treated IPF ECM shows a trend towards an increased turnover however this is not statistically significant.

## **CHAPTER 5**

Facilitation of excess ECM removal by cross linking  
enzyme inhibition in the murine bleomycin fibrosis  
model

## **5 CHAPTER 5 - Facilitation of excess ECM removal by cross linking enzyme inhibition in the murine Bleomycin fibrosis model**

### **5.1 Introduction**

#### 5.1.1 Background

As reviewed in chapter 1, the Bleomycin model is the most accessible and well documented model for studying pulmonary fibrosis. The molecular changes at the transcript level have been shown to be a suitable model for patients with an active fibrosis, compared to a slow progressive disease (Peng et al., 2013). Bleomycin instillation via a number of routes including intravenous (IV), intratracheal (IT) (Lindenschmidt et al., 1986) and subcutaneous injection (SC) (Li et al., 2012b) all induce pulmonary fibrosis through DNA damage however IT administration produces the most acute lung injury due to the direct contact of Bleomycin with the alveolar epithelium. However, it has been noted that a more suitable timescale to study human disease with the Bleomycin model, may be a longer timescale to exhibit a chronic phenotype (Limjunyawong et al., 2014). The complexity of IPF as a disease means that a true isomorph model is practically implausible with no known cause of the disease. In essence, what the Bleomycin model represents is an acute lung injury, followed by scar formation and lung remodelling which progressively resolves around 6 weeks post administration (Lawson et al., 2005, Moore and Hogaboam, 2008, Chung et al., 2003).

Previous work presented in chapter 4 has shown that TG2 inhibition during ECM synthesis reduces seeded cell proliferation and adhesion on IPF ECM. As also shown, fibroblasts from IPF patients produce equal quantities of ECM; in particular collagen. This could mean that the excess ECM synthesis seen *In Vivo* is a result of the increased number of fibroblasts resident within the fibrotic lung. Bleomycin also induces extensive EMT (Limjunyawong et al., 2014) which also contributes to the abundant pulmonary myofibroblast population. The increased proliferative support by IPF ECM may contribute to the expansion of these populations of fibroblasts and provide a positive feedback loop to sustain and expand the fibrotic extracellular environment (Parker et al., 2014, Bonnans et al., 2014). We have demonstrated that inhibition of TG2 during ECM synthesis reduces the increased proliferation seen on IPF matrices in the presence of foetal bovine serum and PDGF-bb. This inhibition of ECM cross linking may provide a possible mechanism, *in vivo*, of reducing ECM accumulation through reducing cell proliferation within the lung on newly synthesised ECM; and also through increased ECM degradation by endogenous proteolytic enzymes. Furthermore CyM has no effect on the transcription of *COL1A1*, *COL3A1*, *TGM2* or *LOX3* (as shown in section 3.2.5) meaning that any effect observed regarding the total levels of these proteins is not affected by CyM treatment through increases or decreases in transcription but an indirect effect potentially regarding enzymatic modification, degradation or signalling molecule release.

In a pilot study, utilising the murine Bleomycin model we tested the hypothesis that TG2 inhibition during Bleomycin induced fibrosis resolution reduces total lung collagen at 24, 34 and 44 days post Bleomycin administration. All animal work was conducted as comprehensively detailed in 2.41 to 2.49.

### 5.1.2 Aims & Objectives

- To assess the ability of CyM to inhibit TG2 during bleomycin induced injury in *ex vivo* lung tissue.
- To determine the effect of CyM on bodyweight of mice during a pilot study of the Bleomycin model at three independent timepoints of fibrosis resolution at two different doses; 40mg/kg and 100mg/kg.
- To examine the efficacy of CyM administration via intraperitoneal injection to reduce total lung hydroxyproline at three independent timepoints, during a pilot study of the Bleomycin model of fibrosis resolution during the course of the bleomycin model at 40mg/kg and 100mg/kg.

## 5.2 Results

### 5.2.1 *Ex Vivo* analysis of TG2 activity in Bleomycin treated mouse tissue

Before attempting to utilise live animals, an experiment was designed to determine if the effect of TG2 inhibition by CyM is conserved in *ex vivo* mouse lung tissue. To create a model of *ex vivo* Bleomycin induced tissue injury, lung and liver was harvested from 3 male C57BL/6 aged 6-8 weeks old was treated with Bleomycin to assess the relative TG2 activity levels following Bleomycin induced injury and to assess the efficacy of CyM to inhibit TG2 activity *ex vivo*. The full experimental protocol can be found in 2.43. Treatment with Bleomycin *in vitro* was chosen that was equivalent to the administration *in vivo* at 60UI (5µg/ml) for the lung tissue, which is the same as a single intratracheal dose in a C57BL/6 mouse to induce fibrosis used in the *in vivo* model used in this thesis. CyM was added to the explants at t0 along with Bleomycin and 23 hours post Bleomycin treatment, 1 hour before harvest to assess the bioavailability of CyM after either 1 or 24 hours in culture.

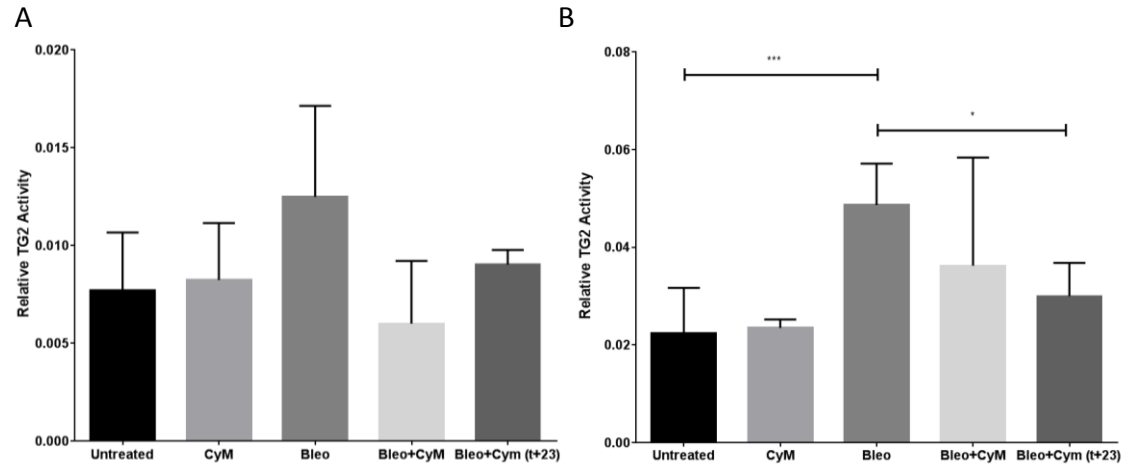


**Figure 5.1 Bleomycin and CyM treatment of ex vivo (A) liver and (B) lung samples from 8 week C57BL/6 mice. (A)** Bleomycin treatment of liver samples at 15ug/ml showed no statistically significant effect upon total TG activity however there is a trend towards Bleomycin increasing TG activity. CyM treatment also showed no reduction from baseline but a trend towards decreasing total TG2 activity when administered at the same time as Bleomycin treated **(B)** Lung samples showed a significant increase in total TG2 activity following Bleomycin treatment; Untreated 0.022AU (SD=0.009) vs. Bleomycin 0.028AU (SD=0.008)  $p < 0.001$ ,  $n = 3$ . CyM addition at t+23 hours showed a significant decrease of total TG activity; Bleomycin 0.028AU (SD=0.008) vs. Bleo+CyM (t+23) 0.030AU (SD= 0.006)  $p < 0.05$ ,  $n = 3$ . AU= arbitrary unit of relative TG2 activity. Data analysed using two tailed paired t-tests. Data presented  $\pm$ SD. Bleo=Bleomycin. \*\*\* =  $p < 0.001$ , \* =  $p < 0.05$

Bleomycin treatment at 15ug/ml did not induce a significant increase in total TG activity in the ex vivo liver samples (Figure 5.1A). CyM showed no effect on control samples, but the trend suggests a potential reduction in the Bleomycin treated samples when administered with Bleomycin ( $p > 0.05$ ). Variability is quite high due to the variation between the 3 mice used and the SD is high due to the relatively low power of the experiment but as this was a small pilot ex vivo study prior to in vivo work, this is acceptable due to the effect observed in the lung tissue samples.

Bleomycin treatment of lung tissue (Figure 5.1B) at 5ug/ml shows an increase in conditioned media TG activity; Untreated 0.022AU (SD=0.009) vs. Bleomycin 0.028AU (SD=0.008)  $p < 0.001$ ,  $n = 3$ . This increase is reduced with CyM addition at 23 hours post Bleomycin to almost basal

levels; Bleomycin 0.028AU (SD=0.008) vs. Bleo+CyM (t+23) 0.030AU (SD= 0.006)  $p < 0.05$ ,  $n = 3$ . Addition of CyM with Bleomycin at t0 shows no significant effect due to the high variability between the samples ( $p > 0.05$ ). Therefore this data demonstrated that CyM addition to Bleomycin treated *ex vivo* Lung tissue attenuated conditioned media total TG activity levels when administered 23 hours post Bleomycin.

### 5.2.2 Bodyweight of mice post Bleomycin administration

A well-documented indicator of bleomycin induced lung damage is body weight of the mice in the following 10 days during the inflammatory period as described in chapter 1. Therefore, all mice were weighed daily and clinical symptom monitored. Previous work from the Jenkins group in

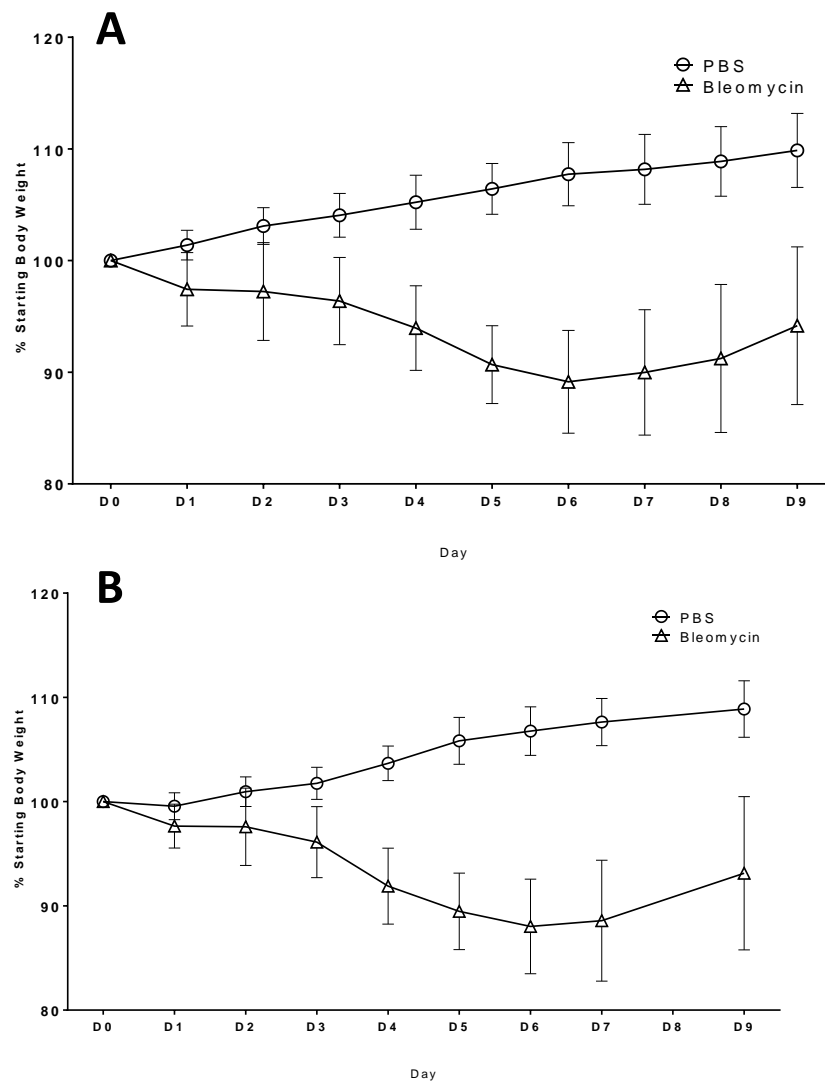


**Figure 5.2 Body weight of PBS control and Bleomycin treated mice.** All mice administered 60IU OP Bleomycin lost on average ~10% bodyweight over 6 days post dosing. Day 7 onwards all mice gained weight consistently. **(A)** Day 0-9 mouse bodyweights of 40mg/kg timecourse; Saline n=12, Bleomycin n=28. **(B)** Day 0-9 bodyweights of 100mg/kg timecourse; Saline n=12, Bleomycin n=25. Numbers of mice represent surviving mice that did not exceed stated severity limits. Data sets analysed with two way ANOVA with repeated measures. Data presented  $\pm$ SD. D=day

Respiratory Medicine at the University of Nottingham suggests that OP administration of Bleomycin at this dose will result in approximately 20% of animals exceeding the moderate severity limit for clinical symptoms of the study. No animals had any notable adverse side effects of the anaesthetic during ear marking and oropharyngeal (OP) dosing.

All animals receiving PBS only showed no significant weight loss or decline in health such as increased respiration, piloerection or hunching. Over 9 days post dosing, these mice all gained approximately 10% of initial starting weight. Animals that received 60UI Bleomycin in 50 $\mu$ l PBS by OP dosing showed a consistent weight loss, lasting up to 6 days post administration. Data was assessed for normality of distribution using D'Agostino-Pearson omnibus test before further analysis. Both experiments tested positive for normal distribution when normalised to their starting weight, therefore a two-way ANOVA with repeated measures was conducted to assess the effect of Bleomycin on body weight over time. The 40mg/kg study (5.2A) shows that Bleomycin significantly decreases bodyweight over time (Bleomycin  $p < 0.0001$ ; Time  $p = 0.0007$ ; Interaction  $p < 0.0001$ ). The 100mg/kg (5.2B) study shows the same effect as an independent experiment with the same initial conditions (before CyM administration) (Bleomycin  $p < 0.0001$ ; Time  $p = < 0.0001$ ; Interaction  $p < 0.0001$ ).

During the first 9 days of the 40mg/kg study, only 1 mouse in the Bleomycin treated group exceeded the severity limit, and in the 100mg/kg study 4 animals exceeded the severity limit by weight loss (moderate; as set out by the Home Office, UK in Guidance on the Operation of the Animals (Scientific Procedures) ACT 1986) set within the project licence, therefore this mouse was immediately sacrificed in accordance with Schedule 1 of ASPA by anaesthetic overdose.

### 5.2.3 Bodyweight of 40mg/kg treated mice

Bodyweights of all mice were recorded throughout the study. This is due to the side effects of CyM administration being poorly documented in the Bleomycin model, and the first indication of adverse effects is a decline in body condition and weight loss. Initially, mice were weighed and health checked every day following Bleomycin or PBS OP dosing until weight loss ceased and all animals in each cage gained weight for three consecutive days as an indication of recovery from the toxic effects of the Bleomycin. Following this, mice were weighed and health checked twice a week minimum to ensure the highest quality of care. During each period of IP injections, all mice were weighed once daily to assess the effect of CyM on bodyweight and clinical symptoms for side effects of the CyM. A total of 3 mice from the Bleomycin groups exceeded the severity limits during the duration of the study and were sacrificed in accordance with Schedule 1. Two of the mice exceeded the maximum 25% original body weight loss and 1 exhibited laboured breathing due to the acute lung injury following Bleomycin administration.

All mice steadily gained bodyweight over the experimental period. No adverse effects of the 40mg/kg dose were noted during the ten consecutive days of administration in TP1 (Figure 5.3A), TP2 (Figure 5.3B) or TP3 (Figure 5.3C). No significant effect on bodyweight of CyM treated mice was observed over the ten-day treatment period, either in the PBS control or Bleomycin treated. Final numbers of animals can be found in 5.2.5 (Figures 5.5 A, B and C)

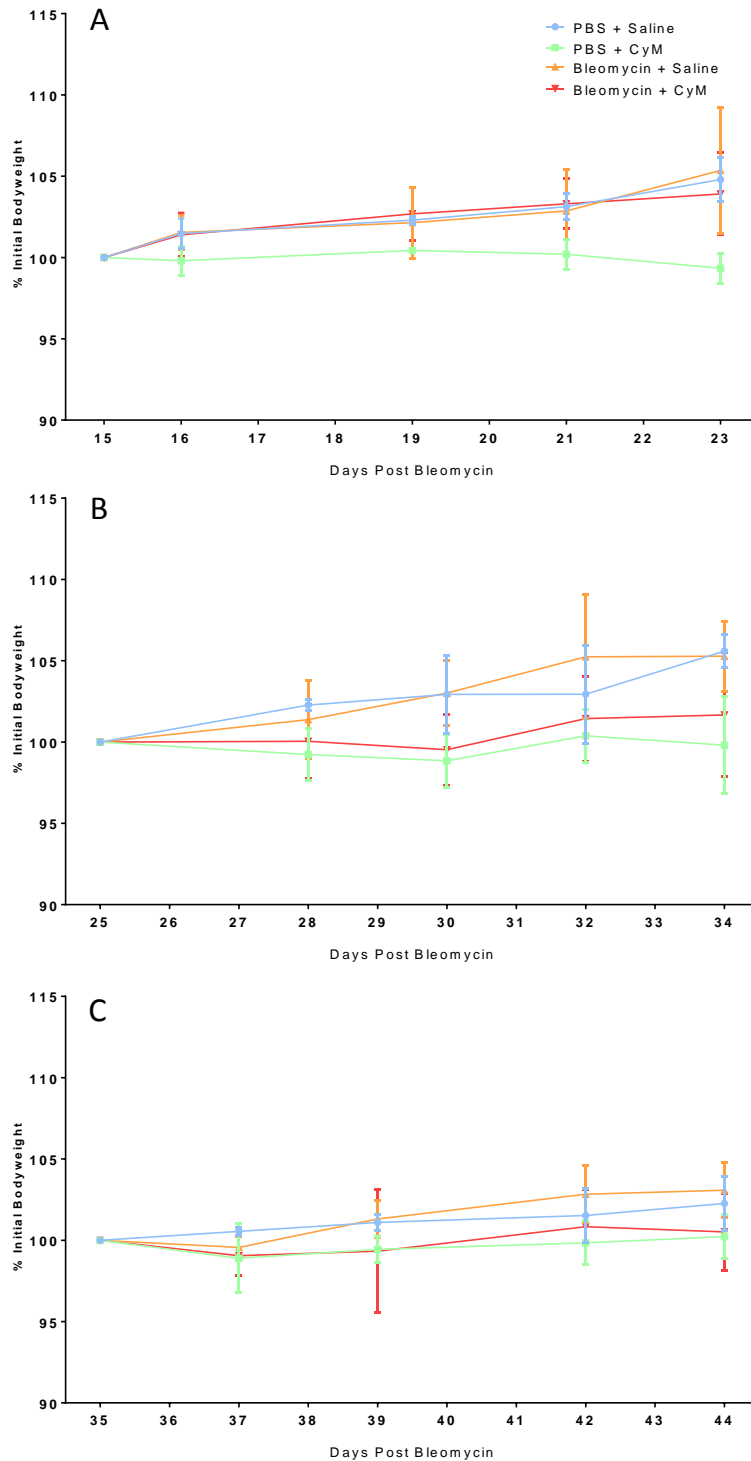


**Figure 5.3 Percentage of initial bodyweights of mice treated with 40mg/kg CyM during Bleomycin induced fibrosis at day 24, 34 and 44.** (Early fibrosis (A), active fibrosis (B) and late fibrosis (C) respectively). CyM administration shows no adverse effect on bodyweight of either PBS or Bleomycin treated mice at three different dosing intervals. Data was normalised to the starting bodyweight at the beginning of each dosing period. Data presented  $\pm$ SD.

#### 5.2.4 Bodyweight of 100mg/kg treated mice

The same method of health checking and body weight analysis was employed during the experimental period when investigating 100mg/kg dosing. Animals who received saline injections showed no significant effect on bodyweight or reactions to daily IP dosing. Animals receiving CyM showed transient periods of lethargy following IP administration of CyM at 100mg/kg. This was brought to the attention of the NVS who advised the study be continued as these observed side effects did not breach licence compliance and were considered within the boundaries of moderate severity classification. Animals with acute lung injury from Bleomycin had an increased period of subdual compared to PBS controls, however the effect was transient and mice returned to normal behavioural patterns within 15 minutes. Further involvement of the NVS and the NTCO was sought during the subsequent dosing to ensure compliance. However, no other side effects were noted and the observed effects did not increase in severity. Administration at TP1 (Figure 5.4A) shows a trend towards a plateau in weight of Bleomycin mice treated with CyM when compared to Bleomycin mice treated with saline. This effect was not observed in the PBS treated groups, either with CyM or saline. Therefore it can be inferred that any effect on bodyweight may be combination of acute lung injury and the drug. Furthermore, there is a large variation in bodyweight among the Bleomycin+CyM mice. Final numbers of animals can be found in 5.2.6 (Figures 5.6 A, B and C).

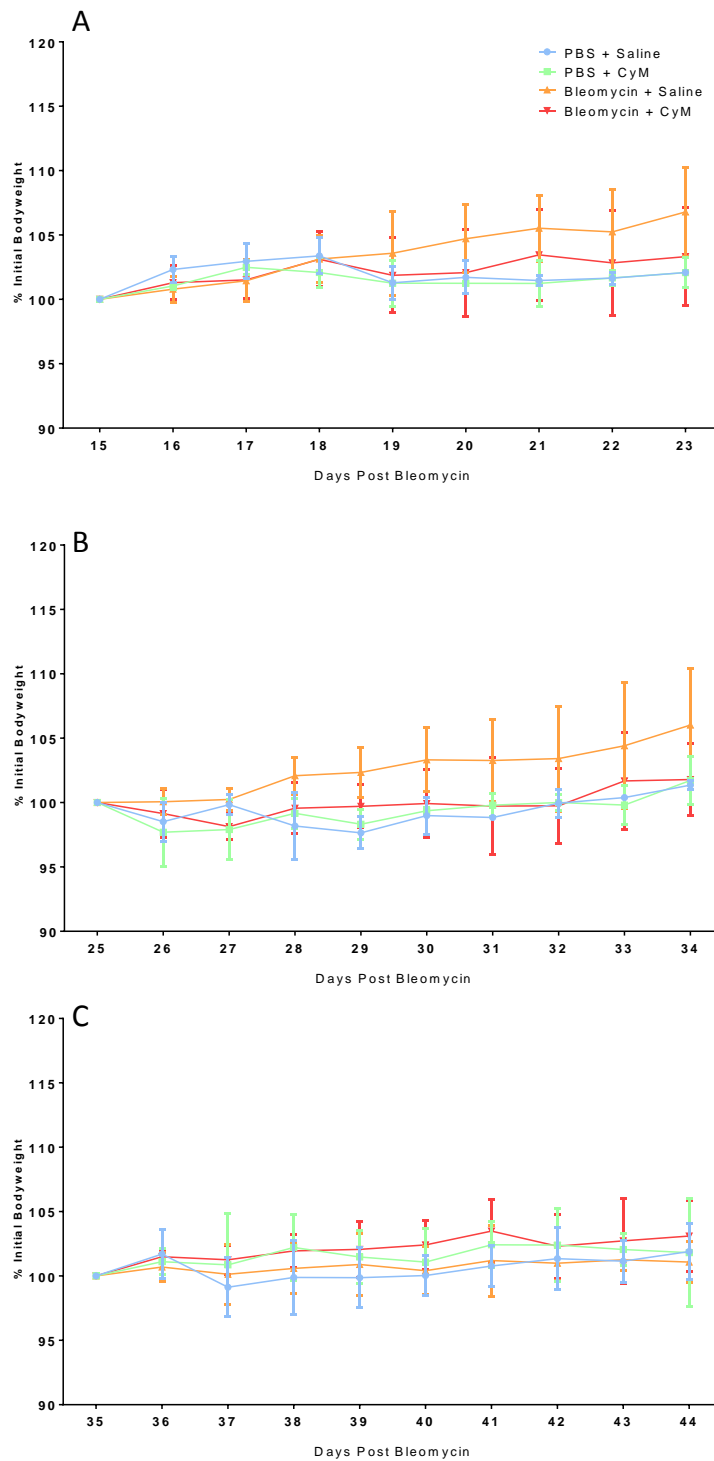


**Figure 5.4 Bodyweights of mice treated with 100mg/kg CyM during Bleomycin induced fibrosis at day 24, 34 and 4. (Early fibrosis (A), active fibrosis (B) and late fibrosis (C) respectively). CyM administration shows no adverse effect on bodyweight of either PBS or Bleomycin treated mice at three different dosing intervals. Data was normalised to the starting bodyweight at the beginning of each dosing period. Data presented  $\pm$ SD.**

### 5.2.5 Total lung hydroxyproline of 40mg/kg treated mice

To examine the level of fibrosis, a hydroxyproline (HYP) assay was carried out as described in 2.50. This allowed for quantification of total lung HYP as a marker of total lung collagen and the extent of fibrosis. During tissue collection, it was ensured that all connective tissue was carefully removed from the lungs so that extraneous, collagen rich tissue was not included in samples for the HYP assay. Figure 5.5 shows the progressive timecourse of Bleomycin induced lung injury on days 24 (A), day 34 (B) and day 44 (C). This pilot study was aimed at determining the most effective time of administration of CyM to reduce total lung HYP.

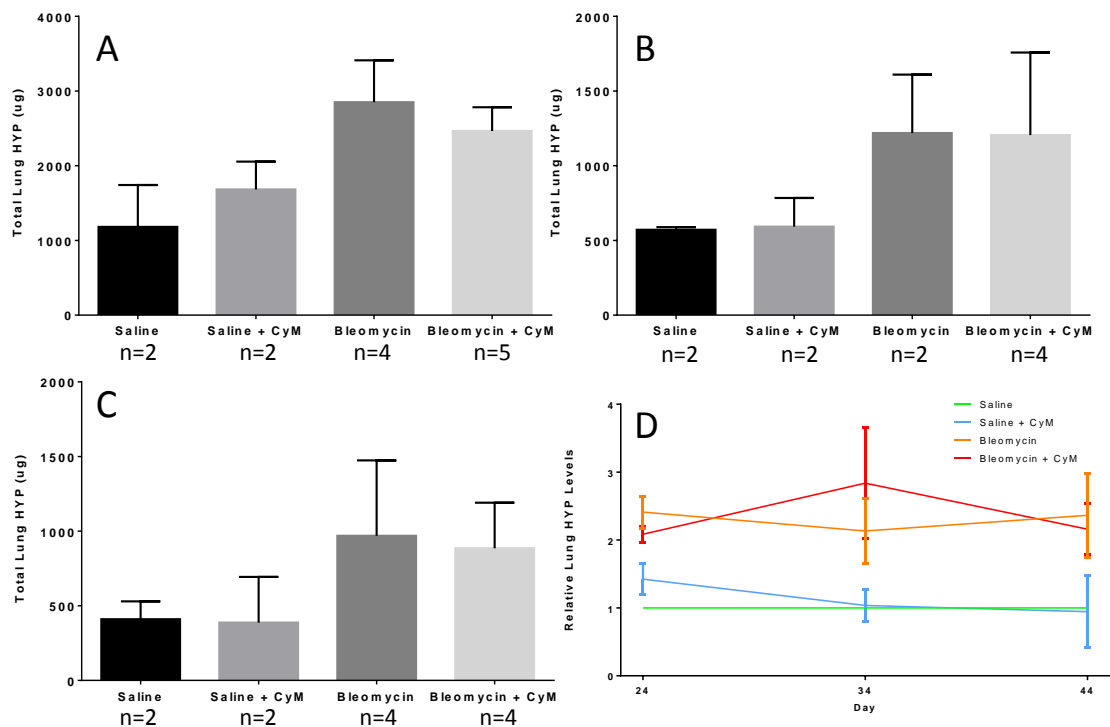


**Figure 5.5 Total lung hydroxyproline levels during bleomycin induced fibrosis, treated with CyM;** (A) Early fibrosis, (B) active fibrosis and (C) resolving fibrosis. (D) compiled timeline of lung HYP levels relative to saline controls. Data was analysed with Mann-Whitney tests In all phases of the model, Bleomycin shows a trend towards an increase in total lung HYP. However, CyM at 40mg/kg shows little or no effect on total lung HYP levels. Data presented  $\pm$ SD.

At day 24 post Bleomycin, total lung HYP levels show a trend toward increasing, however due to low sample numbers and non-Gaussian distribution of data, this is not significant as shown in Figure 5.5 ( $p < 0.05$ ). Sample numbers will be comprehensively discussed in section 5.3. This trend is continued across day 34 and 44 (Figure 5.5B and C respectively). CyM dosing once daily via IP shows no significant effect on total lung HYP levels. CyM administration to mice without lung injury from Bleomycin showed no significant effect on total lung HYP levels.

## 5.2.6 Total lung hydroxyproline of 100mg/kg treated mice

A total lung HYP assay was carried out as detailed in 2.50 and analysed as the previous section 5.2.5 to assess the effect of a higher dose of CyM on fibrosis over the timecourse from days 24 up to 44 post Bleomycin administration.

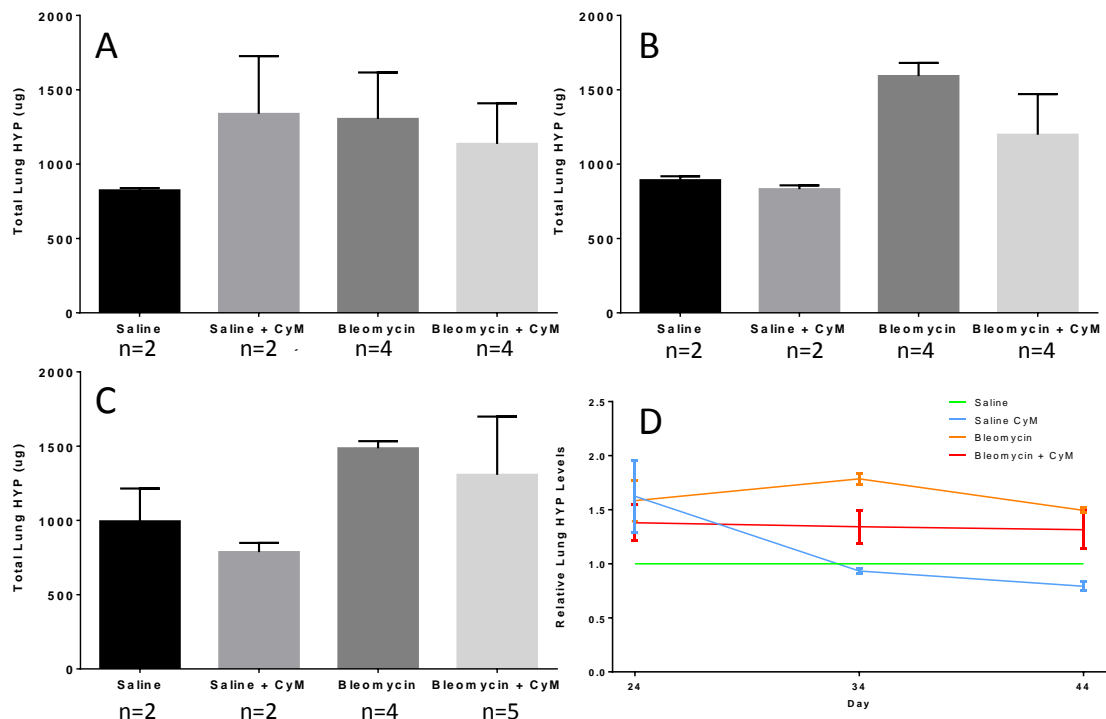


**Figure 5.6 Total lung hydroxyproline levels during bleomycin induced fibrosis, treated with CyM;** (A) Early fibrosis, (B) active fibrosis and (C) resolving fibrosis. (D) compiled timeline of lung HYP levels relative to saline control. Data was analysed with Mann-Whitney tests. In all phases of the model, Bleomycin shows a trend towards an increase in total lung HYP. However, CyM at 100mg/kg shows a trend towards decreasing total lung HYP at day 34 or when administered during active fibrosis (B). Data presented  $\pm$ SD.

Bleomycin shows a trend towards increasing total lung HYP at day 24, 34 and 44 (TP1, TP2 and TP3 respectively) as shown in Figure 5.6A, B and C. However due to low n numbers, normality testing is not feasible and statistical analysis of an n of two is not acceptable. Interestingly, there is

a trend toward CyM increasing total lung HYP during early fibrosis which would need further investigation.

At day 34 (Figure 5.6B), CyM administration shows a trend towards decreasing total lung HYP. This can be more easily seen in 5.6D utilising relative lung HYP levels. At day 34 (Figure 5.6B) and day 44 (Figure 5.6C), CyM shows little or no effect on total lung HYP when administered to mice without acute lung injury from Bleomycin.

### 5.3 Discussion

The pilot study presented in Chapter 5 was originally designed utilising two independent repeats of one dose of 40mg/kg, replicating the findings of Oh and colleagues (Oh et al., 2011) while obtaining outcomes that were not analysed in this publication, such as total lung HYP and histology for TG2 and TG2 mediated cross links. Power calculations based on results from previous work within the Bleomycin model in our group (Jenkins, R.G., Tatler, A., Habgood, A., John, A., Division of Respiratory Medicine, School of Medicine, University of Nottingham) suggested that a sample size of 4 for controls and 9 for Bleomycin groups would allow for robust statistical analysis. A number of papers were reviewed in designing this study (Dedeoglu et al., 2002, Oh et al., 2011, Suh et al., 2014, Tremblay et al., 2006), which aimed to reduce the extent of lung fibrosis in the Bleomycin model. Primary concern was that of animal welfare and reducing the impact of the experimental procedures upon the mice. Careful consideration of the correct dosage of CyM was of utmost concern as there are relatively few studies conducted using this compound in models of respiratory disease. 40mg/kg was determined to be the optimal dose to minimise side effects (Waynforth, 1980) while maintaining bioactivity as described by Oh (2011).

The potential mechanism of action *In Vivo* we propose is that CYM inhibition of TG2 activity during the deposition of profibrotic ECM reduces the abundance of n-ε-γ-glutamyl lysine peptide cross links between collagen and fibronectin. The reduction in this proteolytically resistant

peptide link may aid in normal, endogenous ECM proteolysis and decrease ECM volume in the Bleomycin model of fibrosis. As seen at day 34 post Bleomycin administration, there is a trend towards a reduced level of total lung HYP when mice are administered 100mg/kg/day CyM. The *ex vivo* lung tissue experiments showed that CyM is capable of inhibiting TG activity in the mouse tissue which can therefore be translated into the *in vivo* experiments.

Following the initial experiment, the total lung HYP assay was run to assess the impact of the dose upon lung fibrosis and to determine if the dose required changing, as no side effects were noted, indicating a higher dose could be tolerated. As shown in figure 5.5, no effect was observed. Therefore a decision was made to increase the dose to 100mg/kg for the second time course. This was initially planned to be a repeat of 40mg/kg to increase the sample numbers for robust statistical analysis, however it was concluded that increasing the dose, and assessing the outcomes of that would be more beneficial to this project. Therefore if a potential effect was observed at 100mg/kg, another independent repeat could be conducted at a later date. Furthermore, this would reduce the number of animals used in the longer term, in obtaining a result relevant to the mechanism of TG2 in the Bleomycin model. Furthermore, it is planned to repeat the 100mg/kg study and obtain additional samples for immunohistochemistry, differential cell counts and mRNA profiling.

As discussed in chapter 4, data analysis on low n numbers is extremely difficult to interpret, if at all. Oh *et al.* (2011) in their statistical analysis, used t-tests to assess significance. However, the results for the presented project were tested using non-parametric Mann-Whitney tests. This is due to the inability to make assumptions of distribution on data in animal studies with relatively low sample number. Furthermore, normality testing was not viable with sample numbers that were available. Much literature was consulted on this subject of analysing this data (Altman and Bland, 2009, Festing, 2002, Motulsky, 2010, Sheskin, 2011) and it was concluded that non-parametric analysis offered the most robust method of analysis, removing any assumptions about the data. Increasing sample numbers to eight or above would allow for normality testing using the D'agostino-Pearson method in future work based on these preliminary results, allowing for more robust statistical analysis, however presented here is the most robust method, given the available sample numbers.

Oh *et al.* (2011) report a reduced fibrosis in TG2 null mice with epithelial TG2 amplifying the inflammatory response through increased production of IL-6. This effect could underlie the propagation of fibrosis in IPF patients through generating the consistent low level of inflammation that is observed in patients (Barnes, 2008). The alveolar epithelial damage could initiate fibrogenesis but increased TG2 production from both fibroblasts and epithelial cells may continue to support a profibrotic environment. This may be through increasing IL-6 production along with increasing ECM cross linking, meaning that the constant low level of inflammation is self-

sustaining. We hypothesise that this may be due to increased TG2 catalysed cross linking of the ECM which supports increased cell proliferation, and the maintaining of increased IL-6 production by the increased cell number, and by the increased levels of TG2 present in the tissue. This potential mechanism could be halted by TG2 inhibition. Added to this data, Oh *et al.* (2011) also describes that TGF- $\beta$  stimulates increases in TG2 activity, fibronectin expression, and cross-linking and  $\alpha$ -SMA expression. This effect was ablated with CyM treatment of human fibroblasts in cell culture. Furthermore, epithelial cell production of TG2 in their mouse model induced an inflammatory response, resulting in TGF- $\beta$  activation. Therefore, TGF- $\beta$  stimulated TG2 activity can be shown to be reciprocal paradigm where epithelial TG2 can activate TGF- $\beta$  which then in turn causes an increase in TG2 activity in the underlying fibroblasts. Therefore, our intervention with CyM may not only target fibroblast derived TG2 in the bleomycin model, but the epithelial TG2 activation of TGF- $\beta$ . This would require further investigation in future work.

The chosen route of administration of the drug was IP injection in normal saline once daily. This was chosen as an initial method of administration as the solvent for CyM is normal saline, and it is known that normal saline, injected at body temperature has little effect on solubilised drug action (Hedrich and Bullock, 2004). To reduce possible irritation of the drug at higher doses, the compound was administered in 200 $\mu$ l volume in the 100mg/kg study, whereas at 40mg/kg, 100 $\mu$ l was used. Furthermore, prior to dosing each day, the pH of the solution was taken and found to be

around 7.4, which is acceptable for injection. To optimise the dosing methods further if this study were to be repeated, an osmotic mini pump may be an alternative to deliver CyM continuously at a slower rate than that of a single IP. This would be supported by our observations that at higher doses, animals became subdued for up to 15 minutes post administration. The bioavailability of CyM is not completely understood. However, one could hypothesise that free CyM is rapidly reduced *In Vivo* by protein thiols, yielding 2-mercaptoethylamine (Iwata et al., 1998, Gibrat and Cicchetti, 2011), leading to the inability to inhibit TG2 by the same mechanism as CyM through competitive amine inhibition (Siegel and Khosla, 2007, Jeitner et al., 2005). Future work should take into account the availability of the drug further through sustained administration by osmotic pump. Alternatively other known TG2 inhibitor compounds could be considered such as putrescine, spermidine or monodansyl cadaverine.

## 5.4 Conclusions

CyM is suitable for IP injection in the Bleomycin model of fibrosis in the mouse at 40mg/kg and 100mg/kg daily. CyM inhibits Bleomycin induced TG2 activity in *ex vivo* lung tissue when added 23 hours post Bleomycin induced injury. CyM shows no significant effect on bodyweight of mice with healthy lungs or mice with acute lung injury at 40mg/kg or 100mg/kg when administered for 10 consecutive days. No significant effect of CYM was observed on total lung HYP levels during three time points following Bleomycin administration at either 40mg/kg or 100mg/kg daily. There is a trend towards a reduction in total lung HYP levels when CYM is administered between days 24 up to 34, however no significance was found.

## **CHAPTER 6**

### General Discussion

## 6 General Discussion

### 6.1 General Discussion

The aim of this thesis was to examine the potential role of ECM cross linking and stabilisation in IPF. Studies were initially carried out using primary IPF derived fibroblasts, non-IPF fibroblasts and commercially available normal human lung fibroblasts. The findings *in vitro* were then transferred to the murine Bleomycin model of fibrosis.

The most significant finding in this thesis is that IPF ECM supports increased proliferation of subsequent seeded cell populations. It was hypothesised that this may be due to increased ECM stiffness conferred by TG2 catalysed ECM cross links. Therefore, experiments were conducted to disseminate the potential effect of both TG2 and LOX family stabilisation of the ECM on fibroblast proliferation. IPF matrix supports increased proliferation, which is subsequently reduced when TG2 is inhibited during ECM synthesis.

Noted is the study by Chaudhuri *et al.* (2014) which showed that ECM stiffness alone may induce malignant phenotypes in mammary epithelium. This switching of phenotype is jointly regulated by ECM stiffness and its composition (Chaudhuri *et al.*, 2014). These findings, along with the observations in our experiments may provide a potential explanation for the size of the observed effect. As no difference in total collagen, collagen I-V mRNA levels or collagen synthesis was observed, it can be

hypothesised that there is no compositional differences in the ECM's with regard to collagen. Therefore, the additive proliferative effect of IPF ECM being reduced to that of control ECM indicates that in 2D culture conditions, the cross-linking activity of TG2 and the LOX family can have an impact upon proliferation, even though there was no observed difference in collagen composition. This however does not rule out variation in other ECM proteins such as fibronectin, vimentin and laminin. This could be further investigated to assess whether the ECM components vary between control and IPF ECMs and subsequently their impact upon TG2 & LOX family inhibition during ECM synthesis.

The impact of the ECM on gene expression of seeded fibroblast populations was assessed by PCR. IPF ECM strongly induces *LOXL3* expression compared to control ECM. This correlates with a study conducted by Parker *et al.* (2014) where both *LOXL1* and *LOXL3* were shown to be co-regulated by both ECM and cell type. Taken with the data presented in this thesis, it suggests that IPF fibroblasts are predisposed to greater increases in *LOXL3* expression in response to IPF ECM. *TGM2* on the other hand appears to be regulated predominantly by the disease status of the cells with IPF derived fibroblasts contributing more to the increase in expression than the ECM type. The expression profiles observed in *TGM2* and *LOXL3* were further analysed using a total TG activity assay and a total *LOXL3* ELISA. Data shows a similar pattern to that of the mRNA expression, therefore indicating that increases in transcription are supported by subsequent

increases in total TG activity and total LOXL3 levels in the fibroblast conditioned media.

During the initial characterisation of the IPF fibroblasts in this thesis, it was noted that IPF fibroblasts produce a greater amount of *TGM2* relative to  $\beta$ -Actin compared to control fibroblasts as shown in chapter 3. It is known that TG2 expression is increased in IPF (Meyer and Nathan, 2014). This was further analysed in IPF tissue sections which showed more extensive staining for TG2, and the similar distribution of the TG2 catalysed ECM cross links. In the IPF lung, I have shown that TG2 is present and that it is active in creating ECM cross links. Therefore, this mechanism of ECM stabilisation is present and active within the IPF lung when compared to control lung tissue. In the Bleomycin model of fibrosis it has been reported that *TG2*<sup>-/-</sup> mice present a reduced fibrosis in response to injury, suggesting that ECM cross linking plays an important role in fibrogenesis (Olsen et al., 2011). Therefore the creation of calcium dependent  $\alpha$ - $\epsilon$ - $\gamma$  glutamyl lysine cross links, may be a valuable potential target in IPF therapy to increase lung compliance and improve patient lung function.

Experimental data in chapter 3 interestingly shows no difference in total ECM synthesis, collagen transcription or deposition between control and IPF fibroblasts. It is widely reported that ECM is found in greater abundance in IPF (Craig et al., 2015, Dancer et al., 2011, Kuhn and McDonald, 1991), however this is not observed in culture of these primary IPF derived cells. It has been described that the collagen/dry weight ratio

with advanced fibrosis is reduced (Fulmer et al., 1980). This is hypothesised to be due to the relative increase in other interstitial components such as inflammatory cells and serum proteins. Therefore the relative abundance of total protein within the IPF lung is increased, yet the increase is inclusive of an increase in collagen synthesis. Noted in this study is the implication that IPF is a disease of collagen localisation, form and quality, suggesting that the macroscopic structure of the ECM may play an important role in IPF pathogenesis. However, the data generated in this thesis does not support the *in vivo* findings of Fulmer *et al.* (1980) as total protein deposited from IPF fibroblasts is not increased over control. It is hypothesised that a reduced level of ascorbic acid in the DMEM formulation may have contributed to a reduced collagen level *in vitro* as ascorbic acid is essential for normal collagen formation (Murad et al., 1981, Qiao et al., 2009, Russell et al., 1981). Therefore supplementing culture media with ascorbic acid in a physiologically relevant concentration may improve upon the findings presented in chapter 3.

Due to the limitations on the number of donors contained in this thesis, as described in chapter 4.3, robust statistical analysis has been challenging due to the variation in the primary cell cultures. The relative sample size used in this project is low due to the availability of primary fibroblast lines from IPF patients. Furthermore, the proliferative capacity of all cells was assessed prior to any experimental protocols to ensure a minimum of 3 controls and 3 IPF. It was noted that two out of the 5 IPF donor cell samples had extensive  $\beta$ -galactosidase staining associated with senescence

(Debacq-Chainiaux et al., 2009). To furthermore ensure uniformity among experiments, yet generate enough cells to perform sequential experiments, cells were grown no higher than passage 4. A lower passage number limited the genetic drift in the cell populations, reducing the effect of culture on gene expression patterns (Hughes, 2008).

Removal of cells from their microenvironment *in vivo* reduces the impact of local mechanical, chemical and physical stimuli. The human lung is a highly complex system containing multiple cell types and highly organised architecture (Crapo et al., 1982). Studying IPF using cell monoculture methods may result in potential loss of important mediators being overlooked as their input is not present. This is not a critique of this study in particular, but of cell monoculture as a method for translational research in medicine. Therefore, utilisation of more physiologically appropriate systems, such as animal models, have been shown to be more of a physiologically relevant model than cell culture. However care must still be taken when interpreting results from animal models of IPF as induction of fibrosis usually requires instillation of a noxious agent to achieve initiation and progression of fibrosis, which will in turn affect biological data obtained (Moeller et al., 2008). No true isomorph model exists to date of IPF, however data obtained from current models such as silica, Bleomycin and irradiation, may lead to improved models for human IPF and elucidate mechanisms of disease initiation or progression that are shared between methods of induction.

A notable finding in this thesis is that addition of APMA to IPF ECM synthesised in the presence of CyM shows a strong trend towards an increased  $^3\text{H}$ -hydroxyproline liberation. We hypothesise that this is due to the activation of resident proteases within the ECM that are not active during normal cell culture. This is supported by the data from the proteome profiler indicating increased levels of MMP-2, 8, 9, 12 and 13. As MMP activation is achieved by incubation with APMA during reconstitution of recombinant MMP's, this hypothesis pertains to the activation of an increased level of proteases on a less stabilised ECM due to the inactivity of TG2.

Transglutaminase 2 is the most constitutively expressed enzyme of the transglutaminase family (Iismaa et al., 2009). Bleomycin treatment of *ex vivo* mouse lung increases relative TG2 activity compared to control. This activity was observed to be reduced following addition of CyM, 23 hours following injury. Therefore it was hypothesised that this mechanism was conserved into *in vivo*. We hypothesised that administration of CyM via IP injection at 40mg/kg would reduce the extent of fibrosis. This work was based on a study looking at epithelial TG2 contribution to fibrosis (Oh et al., 2011). As discussed in 5.3, time constraints on an altered protocol meant that including a repeat of 100mg/kg CyM dosing regime at D44 was not plausible. Therefore the major limitations of this animal work are that samples numbers are low, leading to high variation in the data sets.

CyM, also known as 2,2'-Diaminodiethyl disulfide dihydrochloride, has been shown to be an effective inhibitor of TG2 activity *in vitro*, however assessment of TG2 activity in lung homogenates from treated animals was not obtained in a single timecourse experiment due to the amount of tissue required for the HYP assay to determine total lung collagen. The drug did not manifest any severe side effects that were not covered under licence. However the moderate sedative observed is hypothesised to be an off target effect, similar to that of a very low dose of ketamine or propofol. However this would need further investigation in a pharmacokinetic study. The drug was well tolerated, with adjustments to total volume being made to ensure a low possibility of irritation and discomfort at the 100mg/kg dose, which resulted in no abnormalities relating to the injection procedure. There is evidence for both TG2 mediated TGF- $\beta$  activation (Huang et al., 2010) and TGF- $\beta$  induction of TG2 (Jung et al., 2007, Shin et al., 2008). Therefore it would be sensible to hypothesise that this could be interpreted as a mechanism of a profibrotic feedback loop. Shin *et al.* (2008) note that N-acetylcysteine inhibits TGF- $\beta$  mediated activation of TG2. Therefore in our model using Bleomycin, a trial of N-acetylcysteine treatment during fibrosis resolution may enable us to assess the effect of a new alternative to CyM. Along with alternative drugs, alternative endpoints may be considered such as lung function of mice subject to fibrosis and therapeutic intervention. This would allow direct measurement in real time of the effect of the compound on reducing the decline in lung function associated with lung fibrosis or improving the lung function which

may be associated with fibrosis resolution in the Bleomycin model, however currently this has never been assessed.

Isotope labelling of ECM components and subsequent analysis of ECM dynamics in the Bleomycin model has previously been assessed by Decaris *et al.* (2014). Through quantification of fractional synthesis rates of a number of ECM proteins and LOX mediated pyridinilone cross-links, it was shown that the majority of LOX mediated collagen cross links are present in the insoluble matrix fraction (Decaris *et al.*, 2014). This supports the paradigm of cross linking and collagen maturation being associated with relative protein stability. Data presented in chapter 4 shows that inhibition of LOX family mediated collagen stabilisation during ECM synthesis reduces subsequent seeded fibroblast proliferation in response to both FBS and PDGF-bb.

The PDGF receptors (PDGFR) are a family of membrane tyrosine kinases that transduce the effects of PDGF on fibroblast and smooth muscle growth, motility and chemotaxis (Claesson-Welsh, 1996, Heldin and Westermark, 1999). Cellular adhesion to the ECM mainly induces signalling mediated by the integrin family which coordinate a multitude of cellular behaviours, however Baron *et al.* (2000) presented data suggesting a regulation of PDGFR degradation through mediating the number of responsive PDGF receptors on the membrane surface (Baron and Schwartz, 2000). This proposed mechanism is supported by our data in that cross link inhibited ECM shows a lower rate of proliferation in response

to PDGF. Our data suggests that ECM stabilisation may play a role in aberrant fibroblast proliferation in IPF.

With the increasing rate of IPF diagnosis in the UK (**Figure 1.2**) there is an increasing necessity to pursue new lines of enquiry regarding the treatment of IPF. Of primary concern is improving patient quality of life through reducing the decline in lung function, associated with increased pulmonary compliance and impaired gas exchange. The major findings in this thesis that inhibition of TG2 mediated cross link formation reduces seeded fibroblast proliferation and adhesion may be a targetable mechanism in the treatment of IPF. Reducing native or recruited fibroblast population expansion may reduce the total ECM synthesised as the disease progresses. Furthermore, as described previously interruption of the proposed TGF- $\beta$ /TG2 profibrotic feedback loop may enable the reduction to the extent to which the disease develops. Due to the complexity of the disease itself, and the heterogeneity in the fibroblast populations within the IPF lung (Habiels and Hogaboam, 2014), it is unlikely that a single enzyme inhibition will revert the pathogenesis of the disease. However, a better understanding of the mechanisms associated with ECM-cell interaction may provide a stepping stone to development of multiple targetable processes within the IPF that will eventually lead to a reduction in mortality associated with IPF.

Very recently on 5<sup>th</sup> of January 2016, the company Gilead Sciences, Inc. announced that the phase two trial of a monoclonal anti-LOXL2 antibody, Simtuzumab, for the treatment of IPF was to be terminated early due to

lack of efficacy (ClinicalTrials.gov number NCT01769196). Interestingly, this supports the data presented in this thesis.  $\beta$ APN, the LOX family inhibitor, showed less of an effect on ECM degradation than the TG2 inhibitor CyM. Therefore, by extrapolation we suggest that inhibition of LOXL3 would have similar results to the now ceased Simtuzumab trial. However, inhibition of the LOX family with a broader style of small molecule inhibitor may prove to be more effective in reducing the amine oxidase activity of the LOX enzymes as there are 5 members of the family with highly conserved C terminal domains which all exhibit the same amine oxidase activity. This approach would however be potentially risky due to the potential for severe side effects observed since compounds such as  $\beta$ APN have been shown to cause osteolathyrism and angiolythyrism in experimental animals (Spencer and Schaumburg, 1983). These conditions are a result of dysregulation of normal collagen synthesis in which the structural integrity is compromised due to lack of LOX family activity. If such a drug was given systemically to IPF patients, there is a potential for side effects such as hernia, aortic dissection and exostoses. Improper collagen stabilisation in critical structures such as the aorta may prove to be a barrier to LOX family inhibition, however, if an inhaled or more direct route of administration of such a compound could be conceived, it may prove to be a useful tool in reducing collagen accumulation in IPF.

The potential for TG2 as a therapeutic target in IPF is a yet unexplored path when taken in the context of ECM cross linking and proteolytic resistance. Therefore, further investigation into this enzyme's protein cross

linking function in IPF may lead to a therapy that may slow the progressive decline in lung function, or even halt it altogether.

## 6.2 Future Work

Further work following this thesis would require quantitative analysis of both cell derived ECM cross link and *in vivo* ECM from both animal and human tissue. This has been conducted to detect TG2 catalysed cross link by HPLC (Skill et al., 2001), which would enable sensitive quantification of TG2 activity in IPF tissue. Furthermore, utilising this in our animal model, would allow determination of the efficacy of CyM on inhibiting TG2 mediated cross link formation.

### 6.2.1 Investigation into the *in vivo* effects of CyM administration on total lung hydroxyproline in the Bleomycin model of fibrosis

Initial work would consist of increasing sample numbers of the animal work presented in chapter 5 to assess the efficacy of CyM mediated TG2 inhibition of total lung HYP levels. The trend shown in this thesis that there is a trend towards a reduced total lung collagen level, however a sample number of 8 would provide more robust analysis. A current field that is of great interest, especially in regenerative medicine, is that of scaffolding in tissue engineering. Further utilisation of the Bleomycin model and TG2 inhibition would allow decellularisation of the lung tissue and subsequent seeding of the ECM scaffold with both control and IPF fibroblasts from human patients to assess the effect of a 3D lung architecture on proliferation, adhesion and apoptosis. Other subsequent endpoint measures could be assessed such as ECM component synthesis & ECM

degradation epitopes as commercially provided by Nordic Biosciences. This would allow accurate quantification of both ECM component specific and protease specific fragments of ECM turnover. Analysis of this kind would enable us to directly quantify which components of ECM degradation are affected by IPF and whether cross linking inhibition has a significant effect on ECM turnover at the protein level. This could be expanded into patient tissue samples, providing availability, to correlate the murine findings with the human data to ensure a translational approach to new therapy development.

#### 6.2.2 Investigation of alternative compounds for TG2 inhibition

Other possible TG2 inhibitors could be assessed both *in vitro* and the transferred to *in vivo* mouse models to investigate the possible reduction of side effects which were noted with CyM. The data presented underlying the inhibition of TG2 is intriguing in that the evidence suggests a potential therapeutic target for IPF, however consideration must be taken for the negative consequences of CyM, whereas alternative compounds such as spermidine or a glutamine based isosteres may exhibit a reduced side effect profile. The best studied of which are the 3-halo-4,5-dihydroisoxazoles (Siegel and Khosla, 2007). Increasing sample numbers in the animal study conducted in this project would be the most important next step, along with obtaining tissue for IHC, would ensure robust statistical analysis with protein localisation data along with investigation of alternative TG2 inhibitor compounds. Usage of TG2<sup>-/-</sup> mice would not be

useful in our study due to the requirement of the development of fibrosis, and it has been previously shown that these mice develop a lesser degree of lung fibrosis under experimental conditions (Olsen et al., 2011). However, the possibility of using an inducible TG2 knock out mouse would provide an extremely powerful tool for studying the timecourse of importance of TG2 during the time course of fibrogenesis. This would allow us to induce fibrosis in the normal manner with Bleomycin and then at specific time points, knock out TG2 transcription to study its effect. However, the limiting factor in such experiments would be the cost of producing such an animal. Nevertheless, this would be one of the most powerful tools for studying TG2 function in experimentally induced murine fibrosis.

### 6.2.3 *In vitro* phenotyping of genetically engineered TG2 overexpressing cell lines and their matrices

*In vitro* generation of fibroblasts that overexpress TG2 would allow investigation into the effect of overexpression of TG2 on ECM deposition and degradation. Through stable transfection both control and IPF cells, it would be possible to generate excessively cross-linked ECM. This with the addition of radio labelled proline for incorporation into deposited collagen as previously described in 4.2.8 and 4.2.9, would allow the determination of the contribution of TG2 to ECM proteolytic resistance. Another addition to the work of TG2 inhibition and subsequent reduction in the proliferative effect of IPF ECM would be to analyse the phenotype of seeded cell populations to assess whether reduced ECM cross linking can

revert the phenotype of IPF fibroblasts towards a normal fibroblast phenotype by multiple techniques such as immunofluorescence to assess the actin cytoskeletal structure, and PCR to analyse the relative levels of collagen synthesis.

#### 6.2.4 Proteomic analysis of ECM turnover and the effect of TG2 inhibition

Proteomic analysis of ECM component turnover would prove to be a highly useful technique; through which we could identify the relative ECM turnover rates through quantification of ECM fragments. This could be applied to both cell culture and murine experiments. Furthermore, it would allow the quantitation of the TG2 mediated cross links in ECM preparations and tissue samples. Also, utilising methods such as mass spectroscopy, it would be possible to investigate the effect of TG2 cross links on specific protein fragments when digested with recombinant proteases. This would allow us to determine the exact effect of either increasing or reducing TG2 mediated cross links on specific protease mediated proteolysis.

## 7 References

- AGUSTI, A. G., ROCA, J., GEA, J., WAGNER, P. D., XAUBET, A. & RODRIGUEZ-ROISIN, R. 1991. Mechanisms of gas-exchange impairment in idiopathic pulmonary fibrosis. *Am Rev Respir Dis*, 143, 219-25.
- ALLEN, J. L., COOKE, M. E. & ALLISTON, T. 2012. ECM stiffness primes the TGFbeta pathway to promote chondrocyte differentiation. *Mol Biol Cell*, 23, 3731-42.
- ALTMAN, D. G. & BLAND, J. M. 2009. Parametric v non-parametric methods for data analysis. *BMJ*, 338, a3167.
- ANNES, J. P., MUNGER, J. S. & RIFKIN, D. B. 2003. Making sense of latent TGFbeta activation. *J Cell Sci*, 116, 217-24.
- AWADALLA, N. J., HEGAZY, A., ELMETWALLY, R. A. & WAHBY, I. 2012. Occupational and environmental risk factors for idiopathic pulmonary fibrosis in Egypt: a multicenter case-control study. *Int J Occup Environ Med*, 3, 107-16.
- AZUMA, A. 2012. Pirfenidone treatment of idiopathic pulmonary fibrosis. *Therapeutic Advances in Respiratory Disease*, 6, 107-114.
- BARBARIN, V., NIHOUL, A., MISSON, P., ARRAS, M., DELOS, M., LECLERCQ, I., LISON, D. & HUAUX, F. 2005. The role of pro- and anti-inflammatory responses in silica-induced lung fibrosis. *Respir Res*, 6, 112.
- BARNES, P. J. 2008. A blood test for lung fibrosis. *PLoS Med*, 5, e98.
- BARON, V. & SCHWARTZ, M. 2000. Cell adhesion regulates ubiquitin-mediated degradation of the platelet-derived growth factor receptor beta. *Journal of Biological Chemistry*, 275, 39318-39323.
- BARRY-HAMILTON, V., SPANGLER, R., MARSHALL, D., MCCAULEY, S., RODRIGUEZ, H. M., OYASU, M., MIKELS, A., VAYSBERG, M., GHERMAZIEN, H., WAI, C., GARCIA, C. A., VELAYO, A. C., JORGENSEN, B., BIERMANN, D., TSAI, D., GREEN, J., ZAFFRYAR-EILOT, S., HOLZER, A., OGG, S., THAI,

- D., NEUFELD, G., VAN VLASSELAER, P. & SMITH, V. 2010. Allosteric inhibition of lysyl oxidase-like-2 impedes the development of a pathologic microenvironment. *Nature Medicine*, 16, 1009-U107.
- BAUMGARTNER, K. B., SAMET, J. M., COULTAS, D. B., STIDLEY, C. A., HUNT, W. C., COLBY, T. V. & WALDRON, J. A. 2000. Occupational and environmental risk factors for idiopathic pulmonary fibrosis: a multicenter case-control study. Collaborating Centers. *Am J Epidemiol*, 152, 307-15.
- BENAZET, J. D. & ZELLER, R. 2009. Vertebrate limb development: moving from classical morphogen gradients to an integrated 4-dimensional patterning system. *Cold Spring Harb Perspect Biol*, 1, a001339.
- BENINGO, K. A. & WANG, Y. L. 2002. Flexible substrata for the detection of cellular traction forces. *Trends Cell Biol*, 12, 79-84.
- BERGERON, A., SOLER, P., KAMBOUCHNER, M., LOISEAU, P., MILLERON, B., VALEYRE, D., HANCE, A. J. & TAZI, A. 2003. Cytokine profiles in idiopathic pulmonary fibrosis suggest an important role for TGF-beta and IL-10. *Eur Respir J*, 22, 69-76.
- BIENKOWSKI, R. S. & GOTKIN, M. G. 1995. Control of collagen deposition in mammalian lung. *Proc Soc Exp Biol Med*, 209, 118-40.
- BLAISDELL, R. J. & GIRI, S. N. 1995. Mechanism of antifibrotic effect of taurine and niacin in the multidose bleomycin-hamster model of lung fibrosis: inhibition of lysyl oxidase and collagenase. *J Biochem Toxicol*, 10, 203-10.
- BONDAREVA, A., DOWNEY, C. M., AYRES, F., LIU, W., BOYD, S. K., HALLGRIMSSON, B. & JIRIK, F. R. 2009. The lysyl oxidase inhibitor, beta-aminopropionitrile, diminishes the metastatic colonization potential of circulating breast cancer cells. *PLoS One*, 4, e5620.
- BONNANS, C., CHOU, J. & WERB, Z. 2014. Remodelling the extracellular matrix in development and disease. *Nat Rev Mol Cell Biol*, 15, 786-801.

- BONNER, J. C., BADGETT, A., OSORNIOVARGAS, A. R., HOFFMAN, M. & BRODY, A. R. 1990. Pdgf-Stimulated Fibroblast Proliferation Is Enhanced Synergistically by Receptor-Recognized Alpha-2-Macroglobulin. *Journal of Cellular Physiology*, 145, 1-8.
- BRADFORD, M. M. 1976. A rapid and sensitive method for the quantitation of microgram quantities of protein utilizing the principle of protein-dye binding. *Analytical Biochemistry*, 72, 248-254.
- BRUEL, A., ORTOFT, G. & OXLUND, H. 1998. Inhibition of cross-links in collagen is associated with reduced stiffness of the aorta in young rats. *Atherosclerosis*, 140, 135-145.
- BURGESS, J. K. 2009. The role of the extracellular matrix and specific growth factors in the regulation of inflammation and remodelling in asthma. *Pharmacol Ther*, 122, 19-29.
- BUTTNER, C., SKUPIN, A. & RIEBER, E. P. 2004. Transcriptional activation of the type I collagen genes COL1A1 and COL1A2 in fibroblasts by interleukin-4: analysis of the functional collagen promoter sequences. *J Cell Physiol*, 198, 248-58.
- CAO, B., GUO, Z., ZHU, Y. & XU, W. 2000. The potential role of PDGF, IGF-1, TGF-beta expression in idiopathic pulmonary fibrosis. *Chin Med J (Engl)*, 113, 776-82.
- CHAPMAN, H. A., RIESE, R. J. & SHI, G. P. 1997. Emerging roles for cysteine proteases in human biology. *Annual Review of Physiology*, 59, 63-88.
- CHAU, D. Y., COLLIGHAN, R. J., VERDERIO, E. A., ADDY, V. L. & GRIFFIN, M. 2005. The cellular response to transglutaminase-cross-linked collagen. *Biomaterials*, 26, 6518-29.
- CHAUDHURI, O., KOSHY, S. T., BRANCO DA CUNHA, C., SHIN, J. W., VERBEKE, C. S., ALLISON, K. H. & MOONEY, D. J. 2014. Extracellular matrix stiffness

and composition jointly regulate the induction of malignant phenotypes in mammary epithelium. *Nat Mater*, 13, 970-8.

CHEN, J., GHORAI, M. K., KENNEY, G. & STUBBE, J. 2008. Mechanistic studies on bleomycin-mediated DNA damage: multiple binding modes can result in double-stranded DNA cleavage. *Nucleic Acids Res*, 36, 3781-90.

CHEN, L. J., LI, W. D., LI, S. F., SU, X. W., LIN, G. Y., HUANG, Y. J. & YAN, G. M. 2010. Bleomycin induces upregulation of lysyl oxidase in cultured human fetal lung fibroblasts. *Acta Pharmacol Sin*, 31, 554-9.

CHEN, W. L. K. & SIMMONS, C. A. 2011. Mesenchymal Stem Cell Mechanobiology. *Mechanobiology Handbook*, 457-476.

CHIEN, J. W., RICHARDS, T. J., GIBSON, K. F., ZHANG, Y., LINDELL, K. O., SHAO, L., LYMAN, S. K., ADAMKEWICZ, J. I., SMITH, V., KAMINSKI, N. & O'RIORDAN, T. 2014. Serum lysyl oxidase-like 2 levels and idiopathic pulmonary fibrosis disease progression. *Eur Respir J*, 43, 1430-8.

CHILOSI, M., ZAMO, A., DOGLIONI, C., REGHELLIN, D., LESTANI, M., MONTAGNA, L., PEDRON, S., ENNAS, M. G., CANCELLIERI, A., MURER, B. & POLETTI, V. 2006. Migratory marker expression in fibroblast foci of idiopathic pulmonary fibrosis. *Respir Res*, 7, 95.

CHUNG, M. P., MONICK, M. M., HAMZEH, N. Y., BUTLER, N. S., POWERS, L. S. & HUNNINGHAKE, G. W. 2003. Role of repeated lung injury and genetic background in bleomycin-induced fibrosis. *Am J Respir Cell Mol Biol*, 29, 375-80.

CLAESSON-WELSH, L. 1996. Mechanism of action of platelet-derived growth factor. *Int J Biochem Cell Biol*, 28, 373-85.

CLARKE, D. L., CARRUTHERS, A. M., MUSTELIN, T. & MURRAY, L. A. 2013. Matrix regulation of idiopathic pulmonary fibrosis: the role of enzymes. *Fibrogenesis Tissue Repair*, 6, 20.

- CLAUSSEN, C. A. & LONG, E. C. 1999. Nucleic Acid recognition by metal complexes of bleomycin. *Chem Rev*, 99, 2797-816.
- COLIGE, A., SIERON, A. L., LI, S. W., SCHWARZE, U., PETTY, E., WERTELECKI, W., WILCOX, W., KRAKOW, D., COHN, D. H., REARDON, W., BYERS, P. H., LAPIERE, C. M., PROCKOP, D. J. & NUSGENS, B. V. 1999. Human Ehlers-Danlos syndrome type VII C and bovine dermatosparaxis are caused by mutations in the procollagen I N-proteinase gene. *Am J Hum Genet*, 65, 308-17.
- COTTIN, V. 2013. The role of pirfenidone in the treatment of idiopathic pulmonary fibrosis. *Respiratory Research*, 14.
- CRAIG, V. J., ZHANG, L., HAGOOD, J. S. & OWEN, C. A. 2015. Matrix metalloproteinases as therapeutic targets for idiopathic pulmonary fibrosis. *Am J Respir Cell Mol Biol*, 53, 585-600.
- CRAPO, J. D., BARRY, B. E., GEHR, P., BACHOFEN, M. & WEIBEL, E. R. 1982. Cell Number and Cell Characteristics of the Normal Human-Lung. *American Review of Respiratory Disease*, 126, 332-337.
- DANCER, R. C., WOOD, A. M. & THICKETT, D. R. 2011. Metalloproteinases in idiopathic pulmonary fibrosis. *Eur Respir J*, 38, 1461-7.
- DAVIS, G. S., LESLIE, K. O. & HEMENWAY, D. R. 1998. Silicosis in mice: effects of dose, time, and genetic strain. *J Environ Pathol Toxicol Oncol*, 17, 81-97.
- DAYKIN, K., WIDDOP, S. & HALL, I. P. 1993. Control of Histamine-Induced Inositol Phospholipid Hydrolysis in Cultured Human Tracheal Smooth-Muscle Cells. *European Journal of Pharmacology-Molecular Pharmacology Section*, 246, 135-140.
- DEBACQ-CHAINIAUX, F., ERUSALIMSKY, J. D., CAMPISI, J. & TOUSSAINT, O. 2009. Protocols to detect senescence-associated beta-galactosidase (SA-

- betagal) activity, a biomarker of senescent cells in culture and in vivo. *Nat Protoc*, 4, 1798-806.
- DECARIS, M. L., GATMAITAN, M., FLORCRUZ, S., LUO, F., LI, K., HOLMES, W. E., HELLERSTEIN, M. K., TURNER, S. M. & EMSON, C. L. 2014. Proteomic analysis of altered extracellular matrix turnover in bleomycin-induced pulmonary fibrosis. *Mol Cell Proteomics*, 13, 1741-52.
- DEDEOGLU, A., KUBILUS, J. K., JEITNER, T. M., MATSON, S. A., BOGDANOV, M., KOWALL, N. W., MATSON, W. R., COOPER, A. J., RATAN, R. R., BEAL, M. F., HERSCH, S. M. & FERRANTE, R. J. 2002. Therapeutic effects of cystamine in a murine model of Huntington's disease. *J Neurosci*, 22, 8942-50.
- DEGRYSE, A. L. & LAWSON, W. E. 2011. PROGRESS TOWARD IMPROVING ANIMAL MODELS FOR IPF. *The American journal of the medical sciences*, 341, 444-449.
- DELON, I. & BROWN, N. H. 2007. Integrins and the actin cytoskeleton. *Curr Opin Cell Biol*, 19, 43-50.
- DEMPSEY, O. J. 2006. Clinical review: Idiopathic pulmonary fibrosis—Past, present and future. *Respir Med*, 100, 1871-1885.
- DI LULLO, G. A., SWEENEY, S. M., KORKKO, J., ALA-KOKKO, L. & SAN ANTONIO, J. D. 2002. Mapping the ligand-binding sites and disease-associated mutations on the most abundant protein in the human, type I collagen. *J Biol Chem*, 277, 4223-31.
- DISCHER, D. E., JANMEY, P. & WANG, Y. L. 2005. Tissue cells feel and respond to the stiffness of their substrate. *Science*, 310, 1139-1143.
- DMITRI, V. P., CORY, M. H., ERIC, Y., NASREEN, K., MOISES, S. & DARRYL, A. K. 2012. Fibroblast Senescence In UIP/IPF: A Contributing Factor Or Consequence Of The Disease? C109. *EFFECTS OF SENESCENCE AND MANIFESTATIONS OF AGING IN THE LUNG*. American Thoracic Society.

- DUPONT, W. D. & PLUMMER, W. D., JR. 1990. Power and sample size calculations. A review and computer program. *Control Clin Trials*, 11, 116-28.
- ERLER, J. T., BENNEWITH, K. L., NICOLAU, M., DORNHOFER, N., KONG, C., LE, Q. T., CHI, J. T., JEFFREY, S. S. & GIACCIA, A. J. 2006. Lysyl oxidase is essential for hypoxia-induced metastasis. *Nature*, 440, 1222-6.
- FERNANDEZ, I. E. & EICKELBERG, O. 2012. New cellular and molecular mechanisms of lung injury and fibrosis in idiopathic pulmonary fibrosis. *Lancet*, 380, 680-8.
- FESTING, M. F. 2002. The design and statistical analysis of animal experiments. *ILAR J*, 43, 191-3.
- FUKUDA, Y., ISHIZAKI, M., KUDOH, S., KITAICHI, M. & YAMANAKA, N. 1998. Localization of matrix metalloproteinases-1, -2, and -9 and tissue inhibitor of metalloproteinase-2 in interstitial lung diseases. *Laboratory Investigation*, 78, 687-698.
- FULMER, J. D., BIENKOWSKI, R. S., COWAN, M. J., BREUL, S. D., BRADLEY, K. M., FERRANS, V. J., ROBERTS, W. C. & CRYSTAL, R. G. 1980. Collagen concentration and rates of synthesis in idiopathic pulmonary fibrosis. *Am Rev Respir Dis*, 122, 289-301.
- GADEK, J. E., KELMAN, J. A., FELS, G., WEINBERGER, S. E., HORWITZ, A. L., REYNOLDS, H. Y., FULMER, J. D. & CRYSTAL, R. G. 1979. Collagenase in the lower respiratory tract of patients with idiopathic pulmonary fibrosis. *N Engl J Med*, 301, 737-42.
- GAO, Y., XIAO, Q., MA, H., LI, L., LIU, J., FENG, Y., FANG, Z., WU, J., HAN, X., ZHANG, J., SUN, Y., WU, G., PADERA, R., CHEN, H., WONG, K. K., GE, G. & JI, H. 2010. LKB1 inhibits lung cancer progression through lysyl oxidase and extracellular matrix remodeling. *Proc Natl Acad Sci U S A*, 107, 18892-7.

- GEORGE, M. D., VOLLBERG, T. M., FLOYD, E. E., STEIN, J. P. & JETTEN, A. M. 1990. Regulation of transglutaminase type II by transforming growth factor-beta 1 in normal and transformed human epidermal keratinocytes. *J Biol Chem*, 265, 11098-104.
- GHOBADI, G., BARTELD, B., VAN DER VEEN, S. J., DICKINSON, M. G., BRANDENBURG, S., BERGER, R. M., LANGENDIJK, J. A., COPPES, R. P. & VAN LUIJK, P. 2012. Lung irradiation induces pulmonary vascular remodelling resembling pulmonary arterial hypertension. *Thorax*, 67, 334-41.
- GIBRAT, C. & CICCHETTI, F. 2011. Potential of cystamine and cysteamine in the treatment of neurodegenerative diseases. *Prog Neuropsychopharmacol Biol Psychiatry*, 35, 380-9.
- GOODMAN, R. B., PUGIN, J., LEE, J. S. & MATTHAY, M. A. 2003. Cytokine-mediated inflammation in acute lung injury. *Cytokine Growth Factor Rev*, 14, 523-35.
- GREENBERG, C. S., BIRCKBICHLER, P. J. & RICE, R. H. 1991. Transglutaminases - Multifunctional Cross-Linking Enzymes That Stabilize Tissues. *Faseb Journal*, 5, 3071-3077.
- GRIFFIN, M., CASADIO, R. & BERGAMINI, C. M. 2002. Transglutaminases: nature's biological glues. *Biochem J*, 368, 377-96.
- GROSS, T. J. & HUNNINGHAKE, G. W. 2001. Idiopathic pulmonary fibrosis. *N Engl J Med*, 345, 517-25.
- GUILAK, F., COHEN, D. M., ESTES, B. T., GIMBLE, J. M., LIEDTKE, W. & CHEN, C. S. 2009. Control of stem cell fate by physical interactions with the extracellular matrix. *Cell Stem Cell*, 5, 17-26.
- GURDON, J. B. & BOURILLOT, P. Y. 2001. Morphogen gradient interpretation. *Nature*, 413, 797-803.

- HABIEL, D. M. & HOGABOAM, C. 2014. Heterogeneity in fibroblast proliferation and survival in idiopathic pulmonary fibrosis. *Front Pharmacol*, 5, 2.
- HADJIPANAYI, E., MUDERA, V. & BROWN, R. A. 2009. Close dependence of fibroblast proliferation on collagen scaffold matrix stiffness. *J Tissue Eng Regen Med*, 3, 77-84.
- HAROON, Z. A., AMIN, K., SAITO, W., WILSON, W., GREENBERG, C. S. & DEWHIRST, M. W. 2002. SU5416 delays wound healing through inhibition of TGF-beta 1 activation. *Cancer Biol Ther*, 1, 121-6.
- HARTIGAN, N., GARRIGUE-ANTAR, L. & KADLER, K. E. 2003. Bone morphogenetic protein-1 (BMP-1). Identification of the minimal domain structure for procollagen C-proteinase activity. *J Biol Chem*, 278, 18045-9.
- HAYASHI, T., STETLER-STEVENSON, W. G., FLEMING, M. V., FISHBACK, N., KOSS, M. N., LIOTTA, L. A., FERRANS, V. J. & TRAVIS, W. D. 1996. Immunohistochemical study of metalloproteinases and their tissue inhibitors in the lungs of patients with diffuse alveolar damage and idiopathic pulmonary fibrosis. *Am J Pathol*, 149, 1241-56.
- HEDRICH, H. J. & BULLOCK, G. R. 2004. *The laboratory mouse*, Amsterdam ; Boston, Elsevier Academic Press.
- HELDIN, C. H. & WESTERMARK, B. 1999. Mechanism of action and in vivo role of platelet-derived growth factor. *Physiol Rev*, 79, 1283-316.
- HOPFER, U., JACOBBERGER, J. W., GRUENERT, D. C., ECKERT, R. L., JAT, P. S. & WHITSETT, J. A. 1996. Immortalization of epithelial cells. *Am J Physiol*, 270, C1-11.
- HUANG, L., HAYLOR, J. L., HAU, Z., JONES, R. A., VICKERS, M. E., WAGNER, B., GRIFFIN, M., SAINT, R. E., COUTTS, I. G., EL NAHAS, A. M. & JOHNSON, T. S. 2009. Transglutaminase inhibition ameliorates experimental diabetic nephropathy. *Kidney Int*, 76, 383-94.

- HUANG, L. H., HAYLOR, J. L., FISHER, M., HAU, Z., EL NAHAS, A. M., GRIFFIN, M. & JOHNSON, T. S. 2010. Do changes in transglutaminase activity alter latent transforming growth factor beta activation in experimental diabetic nephropathy? *Nephrology Dialysis Transplantation*, 25, 3897-3910.
- HUGHES, P. 2008. The costs of using unauthenticated, over-passaged cell lines: how much more data do we need? (vol 43, pg 575, 2007). *Biotechniques*, 44, 47-47.
- HUMPHREYS, B. D., LIN, S. L., KOBAYASHI, A., HUDSON, T. E., NOWLIN, B. T., BONVENTRE, J. V., VALERIUS, M. T., MCMAHON, A. P. & DUFFIELD, J. S. 2010. Fate tracing reveals the pericyte and not epithelial origin of myofibroblasts in kidney fibrosis. *Am J Pathol*, 176, 85-97.
- HYNES, M., SAKANI, O., SPIEGEL, P. & CORNIER, N. 2012. A study of refugee maternal mortality in 10 countries, 2008-2010. *Int Perspect Sex Reprod Health*, 38, 205-13.
- HYNES, R. O. & NABA, A. 2012. Overview of the Matrisome-An Inventory of Extracellular Matrix Constituents and Functions. *Cold Spring Harbor Perspectives in Biology*, 4.
- IISMAA, S. E., MEARNS, B. M., LORAND, L. & GRAHAM, R. M. 2009. Transglutaminases and disease: lessons from genetically engineered mouse models and inherited disorders. *Physiol Rev*, 89, 991-1023.
- IOANNIDIS, J. P. A. 2008. Why most discovered true associations are inflated. *Epidemiology*, 19, 640-648.
- IVASKA, J., NISSINEN, L., IMMONEN, N., ERIKSSON, J. E., KAHARI, V. M. & HEINO, J. 2002. Integrin alpha 2 beta 1 promotes activation of protein phosphatase 2A and dephosphorylation of Akt and glycogen synthase kinase 3 beta. *Molecular and Cellular Biology*, 22, 1352-1359.
- IWATA, F., KUEHL, E. M., REED, G. F., MCCAIN, L. M., GAHL, W. A. & KAISER-KUPFER, M. I. 1998. A randomized clinical trial of topical cysteamine

- disulfide (cystamine) versus free thiol (cysteamine) in the treatment of corneal cystine crystals in cystinosis. *Mol Genet Metab*, 64, 237-42.
- IYER, S. N., GURUJEYALAKSHMI, G. & GIRI, S. N. 1999a. Effects of pirfenidone on procollagen gene expression at the transcriptional level in bleomycin hamster model of lung fibrosis. *J Pharmacol Exp Ther*, 289, 211-8.
- IYER, S. N., GURUJEYALAKSHMI, G. & GIRI, S. N. 1999b. Effects of pirfenidone on transforming growth factor-beta gene expression at the transcriptional level in bleomycin hamster model of lung fibrosis. *J Pharmacol Exp Ther*, 291, 367-73.
- IZBICKI, G., SEGEL, M. J., CHRISTENSEN, T. G., CONNER, M. W. & BREUER, R. 2002. Time course of bleomycin-induced lung fibrosis. *Int J Exp Pathol*, 83, 111-9.
- JANG, G. Y., JEON, J. H., CHO, S. Y., SHIN, D. M., KIM, C. W., JEONG, E. M., BAE, H. C., KIM, T. W., LEE, S. H., CHOI, Y., LEE, D. S., PARK, S. C. & KIM, I. G. 2010. Transglutaminase 2 suppresses apoptosis by modulating caspase 3 and NF-kappaB activity in hypoxic tumor cells. *Oncogene*, 29, 356-67.
- JEITNER, T. M., DELIKATNY, E. J., AHLQVIST, J., CAPPER, H. & COOPER, A. J. 2005. Mechanism for the inhibition of transglutaminase 2 by cystamine. *Biochem Pharmacol*, 69, 961-70.
- JOHN, A. E., LUCKETT, J. C., TATLER, A. L., AWAIS, R. O., DESAI, A., HABGOOD, A., LUDBROOK, S., BLANCHARD, A. D., PERKINS, A. C., JENKINS, R. G. & MARSHALL, J. F. 2013. Preclinical SPECT/CT imaging of alphavbeta6 integrins for molecular stratification of idiopathic pulmonary fibrosis. *J Nucl Med*, 54, 2146-52.
- JOHNSON, T. S., EL-KORAIE, A. F., SKILL, N. J., BADDOUR, N. M., EL NAHAS, A. M., NJLOMA, M., ADAM, A. G. & GRIFFIN, M. 2003. Tissue transglutaminase and the progression of human renal scarring. *J Am Soc Nephrol*, 14, 2052-62.

- JOHNSON, T. S., FISHER, M., HAYLOR, J. L., HAU, Z., SKILL, N. J., JONES, R., SAINT, R., COUTTS, I., VICKERS, M. E., EL NAHAS, A. M. & GRIFFIN, M. 2007. Transglutaminase inhibition reduces fibrosis and preserves function in experimental chronic kidney disease. *J Am Soc Nephrol*, 18, 3078-88.
- JORDANA, M., SCHULMAN, J., MCSHARRY, C., IRVING, L. B., NEWHOUSE, M. T., JORDANA, G. & GAULDIE, J. 1988. Heterogeneous proliferative characteristics of human adult lung fibroblast lines and clonally derived fibroblasts from control and fibrotic tissue. *Am Rev Respir Dis*, 137, 579-84.
- JOURDAN-LE SAUX, C., TOMSCHE, A., UJFALUSI, A., JIA, L. & CSISZAR, K. 2001. Central nervous system, uterus, heart, and leukocyte expression of the LOXL3 gene, encoding a novel lysyl oxidase-like protein. *Genomics*, 74, 211-8.
- JUNG, S. A., LEE, H. K., YOON, J. S., KIM, S. J., KIM, C. Y., SONG, H., HWANG, K. C., LEE, J. B. & LEE, J. H. 2007. Upregulation of TGF-beta-induced tissue transglutaminase expression by PI3K-Akt pathway activation in human subconjunctival fibroblasts. *Investigative Ophthalmology & Visual Science*, 48, 1952-1958.
- JUNG, S. M., JANDU, S., STEPPAN, J., BELKIN, A., AN, S. S., PAK, A., CHOI, E. Y., NYHAN, D., BUTLIN, M., VIEGAS, K., AVOLIO, A., BERKOWITZ, D. E. & SANTHANAM, L. 2013. Increased tissue transglutaminase activity contributes to central vascular stiffness in eNOS knockout mice. *Am J Physiol Heart Circ Physiol*, 305, H803-10.
- KAGAN, H. M. & LI, W. 2003. Lysyl oxidase: properties, specificity, and biological roles inside and outside of the cell. *J Cell Biochem*, 88, 660-72.
- KAGE, H. & BOROK, Z. 2012. EMT and interstitial lung disease: a mysterious relationship. *Curr Opin Pulm Med*, 18, 517-23.

- KARLINSKY, J. B. & GOLDSTEIN, R. H. 1980. Fibrotic lung disease--a perspective. *J Lab Clin Med*, 96, 939-42.
- KATZENSTEIN, A. L. A. & FIORELLI, R. F. 1994. Nonspecific Interstitial Pneumonia/Fibrosis - Histologic Features and Clinical-Significance. *American Journal of Surgical Pathology*, 18, 136-147.
- KHALIL, N. & GREENBERG, A. H. 1991. The role of TGF-beta in pulmonary fibrosis. *Ciba Found Symp*, 157, 194-207; discussion 207-11.
- KIM, K. K., KUGLER, M. C., WOLTERS, P. J., ROBILLARD, L., GALVEZ, M. G., BRUMWELL, A. N., SHEPPARD, D. & CHAPMAN, H. A. 2006. Alveolar epithelial cell mesenchymal transition develops in vivo during pulmonary fibrosis and is regulated by the extracellular matrix. *Proceedings of the National Academy of Sciences of the United States of America*, 103, 13180-13185.
- KIM, Y., ROH, S., PARK, J. Y., KIM, Y., CHO, D. H. & KIM, J. C. 2009. Differential expression of the LOX family genes in human colorectal adenocarcinomas. *Oncol Rep*, 22, 799-804.
- KING, T. E. J., BRADFORD, W. Z., CASTRO-BERNARDINI, S., FAGAN, E. A., GLASPOLE, I., GLASSBERG, M. K., GORINA, E., HOPKINS, P. M., KARDATZKE, D., LANCASTER, L., LEDERER, D. J., NATHAN, S. D., PEREIRA, C. A., SAHN, S. A., SUSSMAN, R., SWIGRIS, J. J. & NOBLE, P. W. 2014. A Phase 3 Trial of Pirfenidone in Patients with Idiopathic Pulmonary Fibrosis. *New England Journal of Medicine*, 370, 2083-2092.
- KLEINMAN, H. K., PHILP, D. & HOFFMAN, M. P. 2003. Role of the extracellular matrix in morphogenesis. *Current Opinion in Biotechnology*, 14, 526-532.
- KOJIMA, S., NARA, K. & RIFKIN, D. B. 1993. Requirement for transglutaminase in the activation of latent transforming growth factor-beta in bovine endothelial cells. *J Cell Biol*, 121, 439-48.

- KORFEI, M., RUPPERT, C., MAHAVADI, P., HENNEKE, I., MARKART, P., KOCH, M., LANG, G., FINK, L., BOHLE, R. M., SEEGER, W., WEAVER, T. E. & GUENTHER, A. 2008. Epithelial endoplasmic reticulum stress and apoptosis in sporadic idiopathic pulmonary fibrosis. *Am J Respir Crit Care Med*, 178, 838-46.
- KRIZHANOVSKY, V., YON, M., DICKINS, R. A., HEARN, S., SIMON, J., MIETHING, C., YEE, H., ZENDER, L. & LOWE, S. W. 2008. Senescence of activated stellate cells limits liver fibrosis. *Cell*, 134, 657-67.
- KROPSKI, J. A., LAWSON, W. E., YOUNG, L. R. & BLACKWELL, T. S. 2013. Genetic studies provide clues on the pathogenesis of idiopathic pulmonary fibrosis. *Dis Model Mech*, 6, 9-17.
- KSHITIZ, PARK, J., KIM, P., HELEN, W., ENGLER, A. J., LEVCHENKO, A. & KIM, D. H. 2012. Control of stem cell fate and function by engineering physical microenvironments. *Integr Biol (Camb)*, 4, 1008-18.
- KUHN, C. & MCDONALD, J. A. 1991. The roles of the myofibroblast in idiopathic pulmonary fibrosis. Ultrastructural and immunohistochemical features of sites of active extracellular matrix synthesis. *Am J Pathol*, 138, 1257-65.
- LACOUTURE, M. E., MORRIS, J. C., LAWRENCE, D. P., TAN, A. R., OLENCKI, T. E., SHAPIRO, G. I., DEZUBE, B. J., BERZOFSKY, J. A., HSU, F. J. & GUITART, J. 2015. Cutaneous keratoacanthomas/squamous cell carcinomas associated with neutralization of transforming growth factor beta by the monoclonal antibody fresolimumab (GC1008). *Cancer Immunol Immunother*, 64, 437-46.
- LAGARES, D. & KAPOOR, M. 2013. Targeting focal adhesion kinase in fibrotic diseases. *BioDrugs*, 27, 15-23.
- LAI, T. S. & GREENBERG, C. S. 2013. TGM2 and implications for human disease: role of alternative splicing. *Front Biosci*, 18, 504-19.

- LAKATOS, H. F., BURGESS, H. A., THATCHER, T. H., REDONNET, M. R., HERNADY, E., WILLIAMS, J. P. & SIME, P. J. 2006. Oropharyngeal aspiration of a silica suspension produces a superior model of silicosis in the mouse when compared to intratracheal instillation. *Exp Lung Res*, 32, 181-99.
- LARDOT, C. G., HUAUX, F. A., BROECKAERT, F. R., DECLERCK, P. J., DELOS, M., FUBINI, B. & LISON, D. F. 1998. Role of urokinase in the fibrogenic response of the lung to mineral particles. *Am J Respir Crit Care Med*, 157, 617-28.
- LARRETA-GARDE, V. & BERRY, H. 2002. Modeling extracellular matrix degradation balance with proteinase/transglutaminase cycle. *J Theor Biol*, 217, 105-24.
- LAWSON, W. E., CROSSNO, P. F., POLOSUKHIN, V. V., ROLDAN, J., CHENG, D. S., LANE, K. B., BLACKWELL, T. R., XU, C., MARKIN, C., WARE, L. B., MILLER, G. G., LOYD, J. E. & BLACKWELL, T. S. 2008. Endoplasmic reticulum stress in alveolar epithelial cells is prominent in IPF: association with altered surfactant protein processing and herpesvirus infection. *American Journal of Physiology-Lung Cellular and Molecular Physiology*, 294, L1119-L1126.
- LAWSON, W. E., POLOSUKHIN, V. V., STATHOPOULOS, G. T., ZOIA, O., HAN, W., LANE, K. B., LI, B., DONNELLY, E. F., HOLBURN, G. E., LEWIS, K. G., COLLINS, R. D., HULL, W. M., GLASSER, S. W., WHITSETT, J. A. & BLACKWELL, T. S. 2005. Increased and prolonged pulmonary fibrosis in surfactant protein C-deficient mice following intratracheal bleomycin. *Am J Pathol*, 167, 1267-77.
- LAZARUS, H. M., CRUIKSHANK, W. W., NARASIMHAN, N., KAGAN, H. M. & CENTER, D. M. 1995. Induction of human monocyte motility by lysyl oxidase. *Matrix Biol*, 14, 727-31.

- LE, M., GOHR, C. M. & ROSENTHAL, A. K. 2001. Transglutaminase participates in the incorporation of latent TGFbeta into the extracellular matrix of aging articular chondrocytes. *Connect Tissue Res*, 42, 245-53.
- LEASK, A. & ABRAHAM, D. J. 2004. TGF-beta signaling and the fibrotic response. *FASEB J*, 18, 816-27.
- LEE, D. A., KNIGHT, M. M., CAMPBELL, J. J. & BADER, D. L. 2011. Stem Cell Mechanobiology. *Journal of Cellular Biochemistry*, 112, 1-9.
- LEE, J. S., IM, J. G., AHN, J. M., KIM, Y. M. & HAN, M. C. 1992. Fibrosing alveolitis: prognostic implication of ground-glass attenuation at high-resolution CT. *Radiology*, 184, 451-4.
- LEIGHT, J. L., WOZNIAK, M. A., CHEN, S., LYNCH, M. L. & CHEN, C. S. 2012. Matrix rigidity regulates a switch between TGF-beta1-induced apoptosis and epithelial-mesenchymal transition. *Mol Biol Cell*, 23, 781-91.
- LEVENTAL, K. R., YU, H., KASS, L., LAKINS, J. N., EGEBLAD, M., ERLER, J. T., FONG, S. F., CSISZAR, K., GIACCIA, A., WENINGER, W., YAMAUCHI, M., GASSER, D. L. & WEAVER, V. M. 2009. Matrix crosslinking forces tumor progression by enhancing integrin signaling. *Cell*, 139, 891-906.
- LI, S., YANG, X., LI, W., LI, J., SU, X., CHEN, L. & YAN, G. 2012a. N-acetylcysteine downregulation of lysyl oxidase activity alleviating bleomycin-induced pulmonary fibrosis in rats. *Respiration*, 84, 509-17.
- LI, W., HU, Y., YUAN, W., LI, L. & HUANG, W. 2012b. [Comparison of two mouse models of lung fibrosis induced by intratracheal instillation and intratracheal aerosol administration of bleomycin]. *Nan Fang Yi Ke Da Xue Xue Bao*, 32, 221-5.
- LI, W., LIU, G., CHOU, I. N. & KAGAN, H. M. 2000. Hydrogen peroxide-mediated, lysyl oxidase-dependent chemotaxis of vascular smooth muscle cells. *J Cell Biochem*, 78, 550-7.

- LI, Z., DRANOFF, J. A., CHAN, E. P., UEMURA, M., SÉVIGNY, J. & WELLS, R. G. 2007. Transforming growth factor- $\beta$  and substrate stiffness regulate portal fibroblast activation in culture. *Hepatology*, 46, 1246-1256.
- LIMJUNYAWONG, N., MITZNER, W. & HORTON, M. R. 2014. A mouse model of chronic idiopathic pulmonary fibrosis. *Physiol Rep*, 2, e00249.
- LINDENSCHMIDT, R. C., TRYKA, A. F., GODFREY, G. A., FROME, E. L. & WITSCHI, H. 1986. Intratracheal versus intravenous administration of bleomycin in mice: acute effects. *Toxicol Appl Pharmacol*, 85, 69-77.
- LIU, M., TANSWELL, A. K. & POST, M. 1999. Mechanical force-induced signal transduction in lung cells. *Am J Physiol*, 277, L667-83.
- LIVAK, K. J. & SCHMITTGEN, T. D. 2001. Analysis of relative gene expression data using real-time quantitative PCR and the 2(-Delta Delta C(T)) Method. *Methods*, 25, 402-8.
- LOCK, J. G., WEHRLE-HALLER, B. & STROMBLAD, S. 2008. Cell-matrix adhesion complexes: master control machinery of cell migration. *Semin Cancer Biol*, 18, 65-76.
- LODISH, H. F. 2000. *Molecular cell biology*, New York, W.H. Freeman.
- LU, H., HOSHIBA, T., KAWAZOE, N. & CHEN, G. 2012. Comparison of decellularization techniques for preparation of extracellular matrix scaffolds derived from three-dimensional cell culture. *Journal of Biomedical Materials Research Part A*, 100A, 2507-2516.
- MAICHE, A. G. 1983. Adjuvant Treatment Using Bleomycin in Squamous-Cell Carcinoma of Penis - Study of 19 Cases. *British Journal of Urology*, 55, 542-544.
- MAKI, J. M., SORMUNEN, R., LIPPO, S., KAARTEENAHO-WIIK, R., SOININEN, R. & MYLLYHARJU, J. 2005. Lysyl oxidase is essential for normal development and function of the respiratory system and for the integrity of elastic and collagen fibers in various tissues. *Am J Pathol*, 167, 927-36.

- MAMMOTO, A., MAMMOTO, T., KANAPATHIPILLAI, M., WING YUNG, C., JIANG, E., JIANG, A., LOFGREN, K., GEE, E. P. & INGBER, D. E. 2013. Control of lung vascular permeability and endotoxin-induced pulmonary oedema by changes in extracellular matrix mechanics. *Nat Commun*, 4, 1759.
- MARTINET, Y., BITTERMAN, P. B., MORNEIX, J. F., GROTENDORST, G. R., MARTIN, G. R. & CRYSTAL, R. G. 1986. Activated Human-Monocytes Express the C-Sis Protooncogene and Release a Mediator Showing Pdgf-Like Activity. *Nature*, 319, 158-160.
- MARTINET, Y., MENARD, O., VAILLANT, P., VIGNAUD, J. M. & MARTINET, N. 1996. Cytokines in human lung fibrosis. *Arch Toxicol Suppl*, 18, 127-39.
- MARTINEZ-MARTINEZ, E., RODRIGUEZ, C., GALAN, M., MIANA, M., JURADO-LOPEZ, R., BARTOLOME, M. V., LUACES, M., ISLAS, F., MARTINEZ-GONZALEZ, J., LOPEZ-ANDRES, N. & CACHOFEIRO, V. 2016. The lysyl oxidase inhibitor (beta-aminopropionitrile) reduces leptin profibrotic effects and ameliorates cardiovascular remodeling in diet-induced obesity in rats. *J Mol Cell Cardiol*, 92, 96-104.
- MCDONALD, S., RUBIN, P., CHANG, A. Y., PENNEY, D. P., FINKELSTEIN, J. N., GROSSBERG, S., FEINS, R. & GREGORY, P. K. 1993. Pulmonary changes induced by combined mouse beta-interferon (rMuIFN-beta) and irradiation in normal mice--toxic versus protective effects. *Radiother Oncol*, 26, 212-8.
- MEYER, K. C. & NATHAN, S. D. 2014. Idiopathic Pulmonary Fibrosis A Comprehensive Clinical Guide *Idiopathic Pulmonary Fibrosis: A Comprehensive Clinical Guide*, 9, Vii-Ix.
- MHAOUTY-KODJA, S. 2004. Ghalpha/tissue transglutaminase 2: an emerging G protein in signal transduction. *Biol Cell*, 96, 363-7.

- MOELLER, A., ASK, K., WARBURTON, D., GAULDIE, J. & KOLB, M. 2008. The bleomycin animal model: a useful tool to investigate treatment options for idiopathic pulmonary fibrosis? *Int J Biochem Cell Biol*, 40, 362-82.
- MOHAN, K., PINTO, D. & ISSEKUTZ, T. B. 2003. Identification of tissue transglutaminase as a novel molecule involved in human CD8+ T cell transendothelial migration. *J Immunol*, 171, 3179-86.
- MOORE, B. B. & HOGABOAM, C. M. 2008. Murine models of pulmonary fibrosis. *Am J Physiol Lung Cell Mol Physiol*, 294, L152-60.
- MORGAN, G. W. & BREIT, S. N. 1995. Radiation and the Lung - a Reevaluation of the Mechanisms Mediating Pulmonary Injury. *International Journal of Radiation Oncology Biology Physics*, 31, 361-369.
- MORRIS, J. C., TAN, A. R., OLENCKI, T. E., SHAPIRO, G. I., DEZUBE, B. J., REISS, M., HSU, F. J., BERZOFSKY, J. A. & LAWRENCE, D. P. 2014. Phase I study of GC1008 (fresolimumab): a human anti-transforming growth factor-beta (TGFbeta) monoclonal antibody in patients with advanced malignant melanoma or renal cell carcinoma. *PLoS One*, 9, e90353.
- MOTULSKY, H. 2010. *Intuitive biostatistics : a nonmathematical guide to statistical thinking*, New York, Oxford University Press.
- MU, D., CAMBIER, S., FJELLBIRKELAND, L., BARON, J. L., MUNGER, J. S., KAWAKATSU, H., SHEPPARD, D., BROADDUS, V. C. & NISHIMURA, S. L. 2002. The integrin alpha(v)beta8 mediates epithelial homeostasis through MT1-MMP-dependent activation of TGF-beta1. *J Cell Biol*, 157, 493-507.
- MURAD, S., GROVE, D., LINDBERG, K. A., REYNOLDS, G., SIVARAJAH, A. & PINNELL, S. R. 1981. Regulation of collagen synthesis by ascorbic acid. *Proc Natl Acad Sci U S A*, 78, 2879-82.
- MURRAY, J. F. & MASON, R. J. 2010. *Murray and Nadel's textbook of respiratory medicine*, Philadelphia, PA, Saunders/Elsevier.

- MYLLYHARJU, J. & KIVIRIKKO, K. I. 2004. Collagens, modifying enzymes and their mutations in humans, flies and worms. *Trends Genet*, 20, 33-43.
- NAKANE, H., ISHIDA-YAMAMOTO, A., TAKAHASHI, H. & IIZUKA, H. 2002. Elafin, a secretory protein, is cross-linked into the cornified cell envelopes from the inside of psoriatic keratinocytes. *J Invest Dermatol*, 119, 50-5.
- NALYSNYK, L., CID-RUZAFI, J., ROTELLA, P. & ESSER, D. 2012. Incidence and prevalence of idiopathic pulmonary fibrosis: review of the literature. *Eur Respir Rev*, 21, 355-61.
- NANDA, N., IISMAA, S. E., OWENS, W. A., HUSAIN, A., MACKAY, F. & GRAHAM, R. M. 2001. Targeted inactivation of Gh/tissue transglutaminase II. *J Biol Chem*, 276, 20673-8.
- NATHAN, S. D., NOBLE, P. W. & TUDER, R. M. 2007. Idiopathic pulmonary fibrosis and pulmonary hypertension: connecting the dots. *Am J Respir Crit Care Med*, 175, 875-80.
- NAVARATNAM, V., FOGARTY, A. W., MCKEEVER, T., THOMPSON, N., JENKINS, G., JOHNSON, S. R., DOLAN, G., KUMARAN, M., POINTON, K. & HUBBARD, R. B. 2014. Presence of a prothrombotic state in people with idiopathic pulmonary fibrosis: a population-based case-control study. *Thorax*, 69, 207-15.
- NGOKA, L. C. 2008. Sample prep for proteomics of breast cancer: proteomics and gene ontology reveal dramatic differences in protein solubilization preferences of radioimmunoprecipitation assay and urea lysis buffers. *Proteome Sci*, 6, 30.
- NIEDER, C., ZIMMERMANN, F. B., ADAM, M. & MOLLS, M. 2005. The role of pentoxifylline as a modifier of radiation therapy. *Cancer Treat Rev*, 31, 448-55.

- NIKBAKHS, N., POURHASAN AMIRI, A. & HOSEINZADEH, D. 2011. Bleomycin in the treatment of 50 cases with malignant pleural effusion. *Caspian J Intern Med*, 2, 274-8.
- NKYIMBENG, T., RUPPERT, C., SHIOMI, T., DAHAL, B., LANG, G., SEEGER, W., OKADA, Y., D'ARMIENTO, J. & GUNTHER, A. 2013. Pivotal role of matrix metalloproteinase 13 in extracellular matrix turnover in idiopathic pulmonary fibrosis. *PLoS One*, 8, e73279.
- NOGEE, L. M. 2002. Abnormal expression of surfactant protein C and lung disease. *Am J Respir Cell Mol Biol*, 26, 641-4.
- OBERDORSTER, G. 1996. Significance of particle parameters in the evaluation of exposure-dose-response relationships of inhaled particles. *Inhal Toxicol*, 8 Suppl, 73-89.
- OBRINK, B. 1973. The influence of glycosaminoglycans on the formation of fibers from monomeric tropocollagen in vitro. *Eur J Biochem*, 34, 129-37.
- OH, K., PARK, H.-B., BYOUN, O.-J., SHIN, D.-M., JEONG, E. M., KIM, Y. W., KIM, Y. S., MELINO, G., KIM, I.-G. & LEE, D.-S. 2011. Epithelial transglutaminase 2 is needed for T cell interleukin-17 production and subsequent pulmonary inflammation and fibrosis in bleomycin-treated mice. *The Journal of Experimental Medicine*, 208, 1707-1719.
- OLSEN, K. C., EPA, A. P., KULKARNI, A. A., KOTTMANN, R. M., MCCARTHY, C. E., JOHNSON, G. V., THATCHER, T. H., PHIPPS, R. P. & SIME, P. J. 2014. Inhibition of transglutaminase 2, a novel target for pulmonary fibrosis, by two small electrophilic molecules. *Am J Respir Cell Mol Biol*, 50, 737-47.
- OLSEN, K. C., SAPINORO, R. E., KOTTMANN, R. M., KULKARNI, A. A., IISMAA, S. E., JOHNSON, G. V., THATCHER, T. H., PHIPPS, R. P. & SIME, P. J. 2011. Transglutaminase 2 and its role in pulmonary fibrosis. *Am J Respir Crit Care Med*, 184, 699-707.

- PANTAZIS, P., SARIBAN, E., KUFU, D. & ANTONIADES, H. N. 1986. Induction of C-Sis Gene-Expression and Synthesis of Platelet-Derived Growth-Factor in Human Myeloid-Leukemia Cells during Monocytic Differentiation. *Proceedings of the National Academy of Sciences of the United States of America*, 83, 6455-6459.
- PARDO, A., GIBSON, K., CISNEROS, J., RICHARDS, T. J., YANG, Y., BECERRIL, C., YOUSEM, S., HERRERA, I., RUIZ, V., SELMAN, M. & KAMINSKI, N. 2005. Up-regulation and profibrotic role of osteopontin in human idiopathic pulmonary fibrosis. *PLoS Med*, 2, e251.
- PARDO, A. & SELMAN, M. 2012. Role of matrix metalloproteases in idiopathic pulmonary fibrosis. *Fibrogenesis & Tissue Repair*, 5, 1-5.
- PARKER, M. W., ROSSI, D., PETERSON, M., SMITH, K., SIKSTROM, K., WHITE, E. S., CONNETT, J. E., HENKE, C. A., LARSSON, O. & BITTERMAN, P. B. 2014. Fibrotic extracellular matrix activates a profibrotic positive feedback loop. *J Clin Invest*, 124, 1622-35.
- PAUTIER, P., GUTIERREZ-BONNAIRE, M., REY, A., SILLET-BACH, I., CHEVREAU, C., KERBRAT, P., MORICE, P., DUVILLARD, P. & LHOMME, C. 2008. Combination of bleomycin, etoposide, and cisplatin for the treatment of advanced ovarian granulosa cell tumors. *Int J Gynecol Cancer*, 18, 446-52.
- PELHAM, R. J., JR. & WANG, Y. 1997. Cell locomotion and focal adhesions are regulated by substrate flexibility. *Proc Natl Acad Sci U S A*, 94, 13661-5.
- PENG, R., SRIDHAR, S., TYAGI, G., PHILLIPS, J. E., GARRIDO, R., HARRIS, P., BURNS, L., RENTERIA, L., WOODS, J., CHEN, L., ALLARD, J., RAVINDRAN, P., BITTER, H., LIANG, Z., HOGABOAM, C. M., KITSON, C., BUDD, D. C., FINE, J. S., BAUER, C. M. & STEVENSON, C. S. 2013. Bleomycin induces molecular changes directly relevant to idiopathic pulmonary fibrosis: a model for "active" disease. *PLoS One*, 8, e59348.

- PISCHON, N., BABAKHANLOU-CHASE, H., DARBOIS, L., HO, W. B., BRENNER, M. C., KESSLER, E., PALAMAKUMBURA, A. H. & TRACKMAN, P. C. 2005. A procollagen C-proteinase inhibitor diminishes collagen and lysyl oxidase processing but not collagen cross-linking in osteoblastic cultures. *J Cell Physiol*, 203, 111-7.
- PLATAKI, M., KOUTSOPOULOS, A. V., DARIVIANAKI, K., DELIDES, G., SIAFAKAS, N. M. & BOUROS, D. 2005. Expression of apoptotic and antiapoptotic markers in epithelial cells in idiopathic pulmonary fibrosis. *Chest*, 127, 266-74.
- PORTE, J. & JENKINS, G. 2014. Assessment of the effect of potential antifibrotic compounds on total and alphaVbeta6 integrin-mediated TGF-beta activation. *Pharmacol Res Perspect*, 2, e00030.
- POTTS, J. & YOGARATNAM, D. 2013. Pirfenidone: A Novel Agent for the Treatment of Idiopathic Pulmonary Fibrosis. *Annals of Pharmacotherapy*, 47, 361-367.
- PROCKOP, D. J., SIERON, A. L. & LI, S. W. 1998. Procollagen N-proteinase and procollagen C-proteinase. Two unusual metalloproteinases that are essential for procollagen processing probably have important roles in development and cell signaling. *Matrix Biol*, 16, 399-408.
- QIAO, H., BELL, J., JULIAO, S., LI, L. & MAY, J. M. 2009. Ascorbic acid uptake and regulation of type I collagen synthesis in cultured vascular smooth muscle cells. *J Vasc Res*, 46, 15-24.
- QIU, J. F., ZHANG, Z. Q., CHEN, W. & WU, Z. Y. 2007. Cystamine ameliorates liver fibrosis induced by carbon tetrachloride via inhibition of tissue transglutaminase. *World J Gastroenterol*, 13, 4328-32.
- RAFII, R., JUAREZ, M. M., ALBERTSON, T. E. & CHAN, A. L. 2013. A review of current and novel therapies for idiopathic pulmonary fibrosis. *J Thorac Dis*, 5, 48-73.

- RAGHU, G., CHEN, Y. Y., RUSCH, V. & RABINOVITCH, P. S. 1988. Differential proliferation of fibroblasts cultured from normal and fibrotic human lungs. *Am Rev Respir Dis*, 138, 703-8.
- RAGHU, G., COLLARD, H. R., EGAN, J. J., MARTINEZ, F. J., BEHR, J., BROWN, K. K., COLBY, T. V., CORDIER, J. F., FLAHERTY, K. R., LASKY, J. A., LYNCH, D. A., RYU, J. H., SWIGRIS, J. J., WELLS, A. U., ANCOCHEA, J., BOUROS, D., CARVALHO, C., COSTABEL, U., EBINA, M., HANSELL, D. M., JOHKOH, T., KIM, D. S., KING, T. E., JR., KONDOH, Y., MYERS, J., MULLER, N. L., NICHOLSON, A. G., RICHELDI, L., SELMAN, M., DUDDEN, R. F., GRISS, B. S., PROTZKO, S. L. & SCHUNEMANN, H. J. 2011. An official ATS/ERS/JRS/ALAT statement: idiopathic pulmonary fibrosis: evidence-based guidelines for diagnosis and management. *Am J Respir Crit Care Med*, 183, 788-824.
- RAGHU, G., MASTA, S., MEYERS, D. & NARAYANAN, A. S. 1989. Collagen synthesis by normal and fibrotic human lung fibroblasts and the effect of transforming growth factor-beta. *Am Rev Respir Dis*, 140, 95-100.
- RAGHU, G., WEYCKER, D., EDELSBERG, J., BRADFORD, W. Z. & OSTER, G. 2006. Incidence and Prevalence of Idiopathic Pulmonary Fibrosis. *American Journal of Respiratory and Critical Care Medicine*, 174, 810-816.
- RAMOS, C., MONTANO, M., GARCIA-ALVAREZ, J., RUIZ, V., UHAL, B. D., SELMAN, M. & PARDO, A. 2001a. Fibroblasts from idiopathic pulmonary fibrosis and normal lungs differ in growth rate, apoptosis, and tissue inhibitor of metalloproteinases expression. *Am J Respir Cell Mol Biol*, 24, 591-8.
- RAMOS, C., MONTANO, M., GARCIA-ALVAREZ, J., RUIZ, V., UHAL, B. D., SELMAN, M. & PARDO, A. 2001b. Fibroblasts from idiopathic pulmonary fibrosis and normal lungs differ in growth rate, apoptosis, and tissue inhibitor of metalloproteinases expression. *American Journal of Respiratory Cell and Molecular Biology*, 24, 591-598.

- RAO, X., HUANG, X., ZHOU, Z. & LIN, X. 2013. An improvement of the  $2^{(-\Delta\Delta CT)}$  method for quantitative real-time polymerase chain reaction data analysis. *Biostat Bioinforma Biomath*, 3, 71-85.
- RICHELDI, L., DU BOIS, R. M., RAGHU, G., AZUMA, A., BROWN, K. K., COSTABEL, U., COTTIN, V., FLAHERTY, K. R., HANSELL, D. M., INOUE, Y., KIM, D. S., KOLB, M., NICHOLSON, A. G., NOBLE, P. W., SELMAN, M., TANIGUCHI, H., BRUN, M., LE MAULF, F., GIRARD, M., STOWASSER, S., SCHLENKERHERCEG, R., DISSE, B., COLLARD, H. R. & INVESTIGATORS, I. T. 2014. Efficacy and safety of nintedanib in idiopathic pulmonary fibrosis. *N Engl J Med*, 370, 2071-82.
- RUSSELL, S. B., RUSSELL, J. D. & TRUPIN, K. M. 1981. Collagen synthesis in human fibroblasts: effects of ascorbic acid and regulation by hydrocortisone. *J Cell Physiol*, 109, 121-31.
- SAINI, G., PORTE, J., WEINREB, P. H., VIOLETTE, S. M., WALLACE, W. A., MCKEEVER, T. M. & JENKINS, G. 2015.  $\alpha$ 6 integrin may be a potential prognostic biomarker in interstitial lung disease. *Eur Respir J*, 46, 486-94.
- SARRAZY, V., BILLET, F., MICALLEF, L., COULOMB, B. & DESMOULIERE, A. 2011. Mechanisms of pathological scarring: role of myofibroblasts and current developments. *Wound Repair Regen*, 19 Suppl 1, s10-5.
- SCHONTHAL, A. H. 2012. Endoplasmic reticulum stress: its role in disease and novel prospects for therapy. *Scientifica (Cairo)*, 2012, 857516.
- SCHRADER, J., GORDON-WALKER, T. T., AUCOTT, R. L., VAN DEEMTER, M., QUAAS, A., WALSH, S., BENTEN, D., FORBES, S. J., WELLS, R. G. & IREDALE, J. P. 2011. Matrix stiffness modulates proliferation, chemotherapeutic response, and dormancy in hepatocellular carcinoma cells. *Hepatology*, 53, 1192-205.

- SCOTTON, C. J. & CHAMBERS, R. C. 2007. Molecular targets in pulmonary fibrosis: the myofibroblast in focus. *Chest*, 132, 1311-21.
- SELMAN, M. & PARDO, A. 2006. Role of epithelial cells in idiopathic pulmonary fibrosis: from innocent targets to serial killers. *Proc Am Thorac Soc*, 3, 364-72.
- SELMAN, M., PARDO, A., BARRERA, L., ESTRADA, A., WATSON, S. R., WILSON, K., AZIZ, N., KAMINSKI, N. & ZLOTNIK, A. 2006. Gene Expression Profiles Distinguish Idiopathic Pulmonary Fibrosis from Hypersensitivity Pneumonitis. *American Journal of Respiratory and Critical Care Medicine*, 173, 188-198.
- SELMAN, M., PARDO, A. & KAMINSKI, N. 2008. Idiopathic pulmonary fibrosis: aberrant recapitulation of developmental programs? *PLoS Med*, 5, e62.
- SELMAN, M., PARDO, A., RICHELDI, L. & CERRI, S. 2011. Emerging drugs for idiopathic pulmonary fibrosis. *Expert Opin Emerg Drugs*, 16, 341-62.
- SELMAN, M., RUIZ, V., CABRERA, S., SEGURA, L., RAMIREZ, R., BARRIOS, R. & PARDO, A. 2000. TIMP-1, -2, -3, and -4 in idiopathic pulmonary fibrosis. A prevailing nondegradative lung microenvironment? *Am J Physiol Lung Cell Mol Physiol*, 279, L562-74.
- SEMENZA, G. L. 2001. Hypoxia-inducible factor 1: control of oxygen homeostasis in health and disease. *Pediatr Res*, 49, 614-7.
- SHESKIN, D. 2011. *Handbook of parametric and nonparametric statistical procedures*, Boca Raton, CRC Press.
- SHIN, D. M., JEON, J. H., KIM, C. W., CHO, S. Y., LEE, H. J., JANG, G. Y., JEONG, E. M., LEE, D. S., KANG, J. H., MELINO, G., PARK, S. C. & KIM, I. G. 2008. TGF beta mediates activation of transglutaminase 2 in response to oxidative stress that leads to protein aggregation. *Faseb Journal*, 22, 2498-2507.

- SHWEKE, N., BOULOS, N., JOUANNEAU, C., VANDERMEERSCH, S., MELINO, G., DUSSAULE, J.-C., CHATZIANTONIOU, C., RONCO, P. & BOFFA, J.-J. 2008. Tissue Transglutaminase Contributes to Interstitial Renal Fibrosis by Favoring Accumulation of Fibrillar Collagen through TGF- $\beta$  Activation and Cell Infiltration. *The American Journal of Pathology*, 173, 631-642.
- SIEGEL, M. & KHOSLA, C. 2007. Transglutaminase 2 inhibitors and their therapeutic role in disease states. *Pharmacol Ther*, 115, 232-45.
- SINGH, S. R., BILLINGTON, C. K., SAYERS, I. & HALL, I. P. 2010. Can lineage-specific markers be identified to characterize mesenchyme-derived cell populations in the human airways? *American Journal of Physiology-Lung Cellular and Molecular Physiology*, 299, L169-L183.
- SKILL, N. J., GRIFFIN, M., EL NAHAS, A. M., SANAI, T., HAYLOR, J. L., FISHER, M., JAMIE, M. F., MOULD, N. N. & JOHNSON, T. S. 2001. Increases in renal epsilon-(gamma-glutamyl)-lysine crosslinks result from compartment-specific changes in tissue transglutaminase in early experimental diabetic nephropathy: pathologic implications. *Lab Invest*, 81, 705-16.
- SKILL, N. J., JOHNSON, T. S., COUTTS, I. G., SAINT, R. E., FISHER, M., HUANG, L., EL NAHAS, A. M., COLLIGHAN, R. J. & GRIFFIN, M. 2004. Inhibition of transglutaminase activity reduces extracellular matrix accumulation induced by high glucose levels in proximal tubular epithelial cells. *J Biol Chem*, 279, 47754-62.
- SPENCER, P. S. & SCHAUMBURG, H. H. 1983. Lathyrism: a neurotoxic disease. *Neurobehav Toxicol Teratol*, 5, 625-9.
- STEPPAN, J., SIKKA, G., JANDU, S., BARODKA, V., HALUSHKA, M. K., FLAVAHAN, N. A., BELKIN, A. M., NYHAN, D., BUTLIN, M., AVOLIO, A., BERKOWITZ, D. E. & SANTHANAM, L. 2014. Exercise, vascular stiffness, and tissue transglutaminase. *J Am Heart Assoc*, 3, e000599.

- STEVENSON, J. P., KINDLER, H. L., PAPASAVVAS, E., SUN, J., JACOBS-SMALL, M., HULL, J., SCHWED, D., RANGANATHAN, A., NEWICK, K., HEITJAN, D. F., LANGER, C. J., MCPHERSON, J. M., MONTANER, L. J. & ALBELDA, S. M. 2013. Immunological effects of the TGFbeta-blocking antibody GC1008 in malignant pleural mesothelioma patients. *Oncoimmunology*, 2, e26218.
- STUDER, S. M. & KAMINSKI, N. 2007. Towards systems biology of human pulmonary fibrosis. *Proc Am Thorac Soc*, 4, 85-91.
- SUH, I. B., YOON, D. W., OH, W.-O., LEE, E. J., MIN, K. H., HUR, G. Y., LEE, S. H., LEE, S. Y., LEE, S. Y., SHIN, C., SHIM, J. J., IN, K. H., KANG, K. H. & KIM, J. H. 2014. Effects of Transglutaminase 2 Inhibition on Ventilator-Induced Lung Injury. *Journal of Korean Medical Science*, 29, 556-563.
- SUTO, N., IKURA, K. & SASAKI, R. 1993. Expression induced by interleukin-6 of tissue-type transglutaminase in human hepatoblastoma HepG2 cells. *J Biol Chem*, 268, 7469-73.
- TANJORE, H., BLACKWELL, T. S. & LAWSON, W. E. 2012. Emerging evidence for endoplasmic reticulum stress in the pathogenesis of idiopathic pulmonary fibrosis. *Am J Physiol Lung Cell Mol Physiol*, 302, L721-9.
- TREMBLAY, M.-È., SAINT-PIERRE, M., BOURHIS, E., LÉVESQUE, D., ROUILLARD, C. & CICCHETTI, F. 2006. Neuroprotective effects of cystamine in aged parkinsonian mice. *Neurobiology of Aging*, 27, 862-870.
- TZOUVELEKIS, A., HAROKOPOS, V., PAPAPOUNTAS, T., OIKONOMOU, N., CHATZIOANNOU, A., VILARAS, G., TSIAMBAS, E., KARAMERIS, A., BOUROS, D. & AIDINIS, V. 2007. Comparative expression profiling in pulmonary fibrosis suggests a role of hypoxia-inducible factor-1alpha in disease pathogenesis. *Am J Respir Crit Care Med*, 176, 1108-19.
- UHAL, B. D. 2003. Epithelial apoptosis in the initiation of lung fibrosis. *Eur Respir J Suppl*, 44, 7s-9s.

- VAILLANT, P., MENARD, O., VIGNAUD, J. M., MARTINET, N. & MARTINET, Y. 1996. The role of cytokines in human lung fibrosis. *Monaldi Arch Chest Dis*, 51, 145-52.
- VERDERIO, E. A., JOHNSON, T. & GRIFFIN, M. 2004. Tissue transglutaminase in normal and abnormal wound healing: review article. *Amino Acids*, 26, 387-404.
- VISSCHER, D. W. & MYERS, J. L. 2006. Histologic Spectrum of Idiopathic Interstitial Pneumonias. *Proc Am Thorac Soc*, 3, 322-329.
- WANG, Y. L. & PELHAM, R. J., JR. 1998. Preparation of a flexible, porous polyacrylamide substrate for mechanical studies of cultured cells. *Methods Enzymol*, 298, 489-96.
- WAYNFORTH, H. B. 1980. *Experimental and surgical technique in the rat*, London ; New York, Academic Press.
- WELLS, R. G. 2008. The role of matrix stiffness in regulating cell behavior. *Hepatology*, 47, 1394-1400.
- WILLIS, B. C., LIEBLER, J. M., LUBY-PHELPS, K., NICHOLSON, A. G., CRANDALL, E. D., DU BOIS, R. M. & BOROK, Z. 2005. Induction of Epithelial-Mesenchymal Transition in Alveolar Epithelial Cells by Transforming Growth Factor- $\beta$ 1 : Potential Role in Idiopathic Pulmonary Fibrosis. *The American Journal of Pathology*, 166, 1321-1332.
- WITHANA, N. P., MA, X. W., MCGUIRE, H. M., VERDOES, M., VAN DER LINDEN, W. A., OFORI, L. O., ZHANG, R. P., LI, H., SANMAN, L. E., WEI, K., YAO, S. B., WU, P. L., LI, F., HUANG, H., XU, Z. J., WOLTERS, P. J., ROSEN, G. D., COLLARD, H. R., ZHU, Z. H., CHENG, Z. & BOGYO, M. 2016. Non-invasive Imaging of Idiopathic Pulmonary Fibrosis Using Cathepsin Protease Probes. *Scientific Reports*, 6.
- WOODCOCK, H. V. & MAHER, T. M. 2014. The treatment of idiopathic pulmonary fibrosis. *F1000Prime Rep*, 6, 16.

- WORLD MEDICAL, A. 2013. World medical association declaration of helsinki: Ethical principles for medical research involving human subjects. *JAMA*, 310, 2191-2194.
- WU, C. H., DONOVAN, C. B. & WU, G. Y. 1986. Evidence for pretranslational regulation of collagen synthesis by procollagen propeptides. *J Biol Chem*, 261, 10482-4.
- XIA, H., SEEMAN, J., HONG, J., HERGERT, P., BODEM, V., JESSURUN, J., SMITH, K., NHO, R., KAHM, J., GAILLARD, P. & HENKE, C. 2012. Low alpha(2)beta(1) Integrin Function Enhances the Proliferation of Fibroblasts from Patients with Idiopathic Pulmonary Fibrosis by Activation of the beta-Catenin Pathway. *American Journal of Pathology*, 181, 222-233.
- YAMAGUCHI, Y., TAKIHARA, T., CHAMBERS, R. A., VERALDI, K. L., LARREGINA, A. T. & FEGHALI-BOSTWICK, C. A. 2012. A peptide derived from endostatin ameliorates organ fibrosis. *Sci Transl Med*, 4, 136ra71.
- YANAI, H., SHTEINBERG, A., PORAT, Z., BUDOVSKY, A., BRAIMAN, A., ZIESCHE, R. & FRAIFELD, V. E. 2015. Cellular senescence-like features of lung fibroblasts derived from idiopathic pulmonary fibrosis patients. *Aging (Albany NY)*, 7, 664-72.
- YEAGER, V. L., BURANARUGSA, M. W. & ARUNATUT, O. 1985. Lathyrism: mini-review and a comment on the lack of effect of protease inhibitors on osteolathyrism. *J Exp Pathol*, 2, 1-11.
- YUAN, L., CHOI, K., KHOSLA, C., ZHENG, X., HIGASHIKUBO, R., CHICOINE, M. R. & RICH, K. M. 2005. Tissue transglutaminase 2 inhibition promotes cell death and chemosensitivity in glioblastomas. *Mol Cancer Ther*, 4, 1293-302.
- ZHANG, K. & PHAN, S. H. 1996. Cytokines and pulmonary fibrosis. *Biol Signals*, 5, 232-9.

ZUO, F., KAMINSKI, N., EUGUI, E., ALLARD, J., YAKHINI, Z., BEN-DOR, A.,  
LOLLINI, L., MORRIS, D., KIM, Y., DELUSTRO, B., SHEPPARD, D., PARDO,  
A., SELMAN, M. & HELLER, R. A. 2002. Gene expression analysis reveals  
matrilysin as a key regulator of pulmonary fibrosis in mice and humans.  
*Proc Natl Acad Sci U S A*, 99, 6292-7.